Dynamical Behavior of Photoexcited Carriers in InSb

by

Ken-ichi Fujii

1984

CONTENTS

Abstract

Dynamics of photoexcited carriers in InSb under a strong magnetic field have been studied by means of far-infrared laser cyclotron resonance measurement. Motivation of the study was the confirmation of optical hot electrons through the cyclotron emission measurement. In n-type InSb, presence of electrons in higher Landau subbands of the conduction band that few electrons populate in thermal equilibrium, was confirmed in both cyclotron absorption and emission measurements. Examining the off thermal equilibrium electron cyclotron absorption signals by time resolution, the transient behavior of hot electrons could be investigated. For studying optical hot electrons, employing a p-type material is more convenient since observed electron signals are caused only by off thermal electrons.

In the cyclotron absorption measurement, two electron resonance peaks from the two lowest Landau subbands and one donor electron peak were observed. Based on the study of Matsuda and Otsuka, the effective electron temperature determined by population ratio in the two subbands is found to attain to 50 K just after photoexcitation. On the other hand, another temperature determined from the population ratio between the conduction band and the donor level is nearly equal to the lattice temperature.

The high electron temperature between the two subbands is found to be caused by the small probability in spin flip transition between the two subbands. From the excitation intensity dependence and sample dependence of this temperature, it has been concluded that the spin flip transition is caused mainly

by ionized impurity scatterings. Contributions of neutral impurity scatterings and electron-electron scatterings, however, cannot be neglected.

The spin states of electrons in the conduction subband have an important role in the energy dissipation process of optically excited electrons.

Once electrons are excited to the conduction band by light, they will be kept to donor impurity states for a long time after being transfered within the conduction subbands as well as their attached donor levels. Those electrons bound to donor levels eventually recombine with holes bound to acceptor levels. The energy dissipation of donor electrons due to donor-acceptor recombination is observed from the observation of both donor and acceptor signals. The aspect of decrease in donor signal has been consistent with that in acceptor signal.

According to the theory of Thomas et al., the donor-acceptor recombination is dependent on their binding energy. The larger the binding energy, the smaller the recombination probability. Thus the effect of a magnetic field seems to make the recombination probability smaller. Thus a slower decay curve would be expected. An opposite tendency, however, was obtained in our measurement. This may be explicable by considering carefully the overlap integral between donor electron and acceptor hole wavefunctions.

Acknowledgements

The author is very grateful to Professor E.Otsuka for his continual encouragement and guidance as well as for his kindly reading the thesis throughout.

The author is so much indebted to Professor T.Ohyama for stimulating discussion and suitable advice in this work. It is a great pleasure to thank Dr. H. Nakata for his help in the operation of the optical pumping laser as well as for many fruitful discussions.

It is also a pleasure to acknowledge the contribution of the colleagues of the Otsuka laboratory.

The laborious help of Miss Matsumura, who kindly typed the manuscript for the author, is deeply appreciated.

Finally, the author wishes to thank his parents for their endless encouragement and support.

1. Introduction

Since the first pioneering work by Ulbrich[1] on GaAs, the photoexcited hot carriers have been studied by many authors. In a strict sense, however, an original study of hot electrons goes back to the work of Ryder and Shockley.[2] In their experiment a large deviation from Ohmic relation in I-V characteristics was observed under the application of a strong electric field. The concept of "electron temperature" was introduced by them to explain the electron distribution disturbed from thermal equilibrium. Stimulated by the work of Ryder and Shockley, many more works on the hot electron system due to electric field excitation were reported and even some reviews are available now.[3] The primary object of those works was mainly to survey 1) the effect of external field on electron temperature and 2) the energy dissipation mechanism. InSb offers an appropriate stage to investigate hot carriers, since the hot electron condition is easily achieved because of its small electron effective mass and availability of a high purity sample. Indeed so many works related to the hot carrier phenomena in InSb have been carried out.[4-13] Examples are the observation of cyclotron emission by Kobayashi et al.[4] and Gornik[5,6] the magneto phonon measurement by Shimomae et al.[7], the observation of combined resonance in the magneto phonon measurement by Zawadzki et al.[8], impact ionization effect due to hot carrier by Glicksman and Steele[9] and so on. In all these measurements, electrons excited by d.c. or a.c. electric field were always and naturally studied in n-type materials. In the meantime, studies of hot electrons optically excited have also been

carried out, e.g., the observation of Shubnikov-de Haas oscillation of electrons heated by a CO_2 - laser,[10] the study of optical heating of electrons[11] etc. These works were again carried out in n-type materials and the results were told in the language of electron temperature, determined from the electron distribution within the conduction band. The main channel to dissipate the electron energy was considered to be the electron-phonon (acoustic and optical phonon) interaction.

Intensive studies of the hot electron system due to electric field excitation was carried out by Kobayashi and Otsuka[12], and by Matsuda and Otsuka[13] by means of cyclotron resonance absorption measurement. N-type samples were employed. Matsuda and Otsuka measured two kinds of electron temperature, i.e., intra-subband and inter-subband electron temperatures. The electron distribution described by these two kinds of temperature was discussed on the basis of the theory of Kurosawa,[14] who introduced a geometrical distinction in energy distribution of hot electrons under the presence of magnetic field.

In these measurements employing n-type materials, electrons were already present prior to electric excitation. In n-type InSb, the donor levels are so shallow that a large portion of the donor electrons are released into the conduction band even at liquid helium temperature. Applied an electric field, the donor electrons are ejected into the conduction band and then the density of conduction electrons increases. So the electron distribution function is changed over the conduction band and donor levels.

On the other hand,if one applies a small electric field

to a p-type material, nothing is observed in cyclotron absorption measurement because of the absence of electrons to be excited. But employing the intrinsic light to excite carriers, however, electrons in the valence band are released into the conduction band. So the observation of electron signals in p-type material becomes possible. Of course, the electron excitation is dependent on the wavelength of the excitation source. Even the excitation of donor electrons by means of an extrinsic light is possible using an appropriate light source. This case was treated theoretically by Ridley and Harris[15]. But we restrict ourselves in the intrinsic photoexcitation case. One of the most important characteristics of the intrinsic photoexcitation of p-type material is a possible observation of minority carriers (electrons) being sent into a hot state.

One direct evidence of existence of hot carriers is given by the observation of cyclotron emission. Cyclotron emission is the reverse process of cyclotron absorption. Applied a magnetic field to a sample, the conduction band is bunched into the Landau subbands. The electrons excited by light from the valence band can populate the higher Landau subbands. One of the possible energy dissipation channel is the electron transition from higher to lower subbands emitting light. Confirmation of the cyclotron emission due to photoexcited electrons has already been reported.[16] There is no doubt that the photoexcited electrons can be in an optically hot state. In this paper, we will report the dynamics of photoexcited carriers by means of cyclotron resonance absorption. Three resonance peaks will mainly be examined, two electron absorption peaks arising

from the lowest two Landau subbands in the conduction band and one from the ground state of the donor. From the analysis of the intensities of these three peaks, three kinds of electron temperature were obtained. The first is an effective temperature derived from the intensity ratio between two Landau subbands. The second is derived from that between the sum of two Landau subband and the impurity level. It is found that there exists a great difference between these two electron temperatures. The third electron temperature describes the electron distribution within a single subband. This temperature is found to be nearly constant for any change in the experimental condition as far as our experience is concerned.

One of the important characteristics in our experiment is employment of the time resolution technique to investigate the time variation of the absorption intensities after photoexcitation. From the result of the time variation measurement, it is found that the decay process of the photoexcited electrons has three stages. In the first stage, the absorption intensity decreases rapidly due to the free hole-free electron recombination. This stage appears only in the strong excitation case. In the second stage, electrons are transferred in a complicated manner between the conduction band and donor levels. This stage will be discussed in detail in a later section. In the third stage, one observes a very slow decrease in absorption intensity of the donor electron signal. This slow decay is due to the donor-acceptor recombination. The effect of magnetic field on the behavior of this slow decay will also be discussed later.

To investigate the second stage in particular, the time

variation of the absorption intensities was measured, changing the lattice temperature and excitation intensity as parameters, not to speak of the dependence on samples.

From these measurements, it is found that the spin states of electrons play an important role in the energy relaxation process of electrons.

The energy relaxation of photoexcited carriers has been investigated theoretically by several authors.[15,17-21)]

Typically, the group of Calecki, Lewiner and Pottier[19-21)] has constructed a theory of the energy relaxation of photocarriers in a strong magnetic field. It is based on the treatment in InSb of Kurosawa and showed the time evolution of hot electrons excited by pulsed light.

In the above theory, the inter-subband transition was included. But the spin states were unfortunately not considered. So this theory cannot be applied to explain our experimental results. In future , nevertheless, it may be possible to utilize the theory with some modification to explain our results.

2. Experimental Method

2-1) Far-infrared (FIR) cyclotron resonance measurement

a) FIR-laser

Two types of FIR-laser were employed, complying with a purpose. One was a discharge type pulse laser using H_2O or D_2O vapor. The other was an optical pumping CW-laser which was excited by a CO_2 laser, using CH_3OH, CH_3OD, CD_3OD and so on. The employed wavelengths of the former system ranged from 84 μm to 220 μm and those of the latter from 119 μm to 513 μm. In the study of photoexcited hot electrons, the 84 μm laser line of D_2O laser was mainly employed to attain the best resolution.

b) Excitation source

In optical excitation measurement, two kinds of xenon flash lamp were employed. One (EG & G FX108) had a narrow pulse width, FWHM of which was less than 1 μs and maximum peak power was about 200 J/cm^2, while the other (constructed by Sugawara stroboscorpe PS 240MT-U1 and EG & G FX-193) had a pulse of ~10 μs FWHM and maximum peak power 1 J/cm^2. The latter source was employed to get a quasi steady-state excitation. The intensity of excitation light was controlled by glass or neutral density filters. The glass filter cuts the wavelangths shorter than 0.6 μm.

The photopulse due to xenon flash lamp was synchronized in every other turn with the FIR-laser. Usually, operation of the FIR laser was repeated at 30 Hz and photopulses by 15 Hz.

c) Experimental situation and detecting system

Figure 1 shows the block-diagram of the experimental

apparatus. The sample was mounted in a superconducting magnet which generated a magnetic field of up to 5 T. The geometry between the incident FIR-laser and the magnetic field was always in Faraday configuration (q // B). The transmission light was detected by a Putley type InSb detector. The detector was biased at constant current. The a.c. coupled signal was amplified and then detected by a boxcar integrator. An absorption signal at any delay time after photopulse could thus be obtained. Two methods of boxcar detection were available. One was a system using two analogue boxcar integrators (PAL MODEL 160 and NF BX 530A) (system (a) in Fig. 1). In this case, the signal intensity transmitted through the sample under photoexcitation and that under no excitation were taken in selectively by two boxcar integrators and summed up . The FIR absorption by photoexcited carriers could then be obtained using a logarithmic amplifier.

The other system (shown (b) in Fig. 1) was a multichannel system[22], constituted by a transient memory (RIKEN DENSHI TCJ 2000A), a two channel digital boxcar integrator (NF BX531) and a microcomputer (Sord M243) with several peripheral equipments: two 8-inch double density floppy disk drives, a graphic display (the resolution of which was 640 x 400 dots), a 12 bit A/D converter, a printer and an X - Y plotter. The boxcar integrator was connected with the microcomputer by means of GPIB interface bus. The detected signal was digitized and divided into 2048 points every other microsecond and once stored in the transient memory. The transient memory yielded a desired number of sampling points every other 12.5 μs for the boxcar integrator. Any 16 points of the data (duration 12.5 μs) were taken in and

accumulated at each delay point for an appropriate number of sampling times and then sent to the X-Y plotter or held in a floppy diskette. The strength of the magnetic field was monitored by measuring voltage of shunt resistance in the power supply for the magnet. In system (b), the shunt voltage was converted from analogue to digital and held in the microcomputer.

2-2) Light modulation technique in cyclotron resonance measurement

Figure 2 shows typical absorption curves of n-InSb as a function of magnetic field in the cyclotron resonance measurement, using 119 μm laser line. The curves (a) and (b) express the absorption intensities without and with photoexcitation, respectively. These signals have the form $\ell n(I_0/I_{1,2})$ in which I_1 and I_2 are the transmission intensities of laser beam of intensity I_0 through a sample without and with excitation. These signals were obtained by using a logarithmic amplifier and two boxcars. The modulation signal S_{mod} is to be defined as a remainder taken the intensity in (a) from in (b), i.e.,

$$S_{mod} = \ell n (I_1 / I_2) \ . \qquad (2.1)$$

This signal corresponds to the variation of absorption coefficient $\Delta\alpha$ due to photoexcitation, i.e.,

$$\Delta\alpha = S_{mod} / d = (1 / d) \ell n (I_1 / I_2) , \qquad (2.2)$$

where d is the sample thickness.

Using this modulation technique, the change in absorption coefficient arising from only photoexcited carriers could be obtained and the fluctuation of incident laser beam intensity could be eliminated. This technique was especially helpful for the study of minority carriers.

2-3) Time resolution method

We are interested in the time variation of excess carriers generated by photoexcitation. The signal at any delay time after photopulse could be detected selectively by means of a boxcar-integrator. There were two ways in the usage of the boxcar integrator. In the first usage, the gate of boxcar integrator was opened at any delay time and fixed there with appropriate gatewidth (typical value of which was 0.5 μs) for each laser pulse. Then the variation of absorption intensity with any other parameter, for example magnetic field, was recorded.

The other usage was so-called "gate scan" in which the position of the gate fixed on FIR-laser pulse was moved along the time axis from the photopulse at any speed. This method was suitable for the study of the phenomenon having a long time constant, e.g., donor-acceptor recombination.

2-4) Samples

Two n-type and three p-type InSb were employed. Their characteristics are listed in Table 1. To avoid the interference in the cyclotron absorption measurement, all the samples have wedge shape. The samples had typical dimensions of $4 \times 4 \times d$ mm^3, with d being the thickness. The thickness d was chosen to be suitable for the purpose of the measurement in the range between 0.15 ~ 0.8 mm. These samples had a flat face normal to the <111> crystallographic axis. Both sides of the samples were ground with 3000 emery paper and were etched with CP-4.

Determination of the impurity concentration in each sample was made by the measurement of cyclotron absorption. In the

absence of intrinsic photoexcitation, the electron absorption due to residual impurity is observed in n-type material. The intensity of this absorption is proportional to the excess donor concentration $N_D - N_A$. In two samples, A and B, this excess donor concentrations was found by means of Hall measurement. The relation between the absorption intensity of cyclotron resonance measurement and the impurity concentration is given by

$$\alpha d = K(N_D - N_A) \quad , \tag{2.3}$$

where α is the absorption coefficient and d is the sample thickness. The constant K is defined by this equation with the values of α of samples A and B and will be used as a general constant for other InSb samples. Using eq.(2.3) with the above K, the donor concentration of each sample was obtained by means of the measurement of cyclotron absorption.

3. Theoretical Background

3-1) Conduction band structure under the application of magnetic field

Indium-antimonide is one of the III-V compound semiconductors and is known as a typical narrow-gap semiconductor. It is also a direct gap semiconductor. The bottom of the conduction band is located at Γ_6. The top of the valence band is located at Γ_8 and that of the spin split-off band is located at Γ_7. Kane[23] constructed a three band model based on K. P perturbation in the zero magnetic field. This model, which is constituted by Γ_6, Γ_8, Γ_7 levels, describes the energy diagram near Γ-points with simple form and considarable precision. Bowers and Yafet[24] and Yafet[25] first showed theoretical description of energy levels near Γ point for InSb in the presence of a magnetic field. Treatments of these people are based on the perturbation theory and only a finite number of close-lying bands are considered. So the treatment becomes in effect a three band model. The resulting 8 x 8 set of differential equations for the envelope functions was solved exactly in terms of harmonic oscillator functions. The following assumption is made. The asymmetric Landau gauge is used for the vector potential of external magnetic field and the kinetic energy term of the free electron is naglected because of its small contribution to electron energy itself. The assumption, $\Delta >> \varepsilon_g$, furthermore, is used. The energies of conduction electron Landau subbands are given by

$$E(n, k_z, \pm) = -\varepsilon_g/2 + [(\varepsilon_g/2)^2 + \varepsilon_g D_{n, k_z, \pm}]^{1/2}, \qquad (3.1)$$

where

$$D_{n,k_z,\pm} = \hbar\omega_c (n + 1/2) + (\hbar^2 k_z^2 / 2m_e^*) \mp |g^*| \mu_B H/2 \quad . \qquad (3.2)$$

Here the notations n, k_z, $\pm$ denote Landau quantum number, the momentum along z-axis, which is parallel to the magnetic field, and the effective spin state, respectively. When the spin-orbit interaction is included, the pure spin state is no longer a good quantum number. The quantities m_0^* and g_0^* denote effective mass and effective g-factor at the band edge of the conduction band, respectively, and are given by

$$m_e^* = \frac{3\varepsilon_g}{2K^2} \frac{\Delta + \varepsilon_g}{2\Delta + 3\varepsilon_g} \qquad (3.3)$$

and

$$g_o^* = -\frac{m}{m_e^*} \frac{2\Delta}{2\Delta + 3\varepsilon_g} \quad . \qquad (3.4)$$

It has been found that three band model gives quite a good analytical description of conduction electrons. The model also describes the aspect of the valence bands Γ_8 and Γ_7. When one needs more detailed and precise description about not only conduction band but also degenerate valence band to consider, for example, interband magneto-optical transitions, the contribution from other bands must be included in the theory. Pidgeon and Brown[26] gave a theory including the interaction with higher bands. This model has indeed shows a considerable success in describing the valence and conduction bands systematically. But, in this model, there remains uncertainty of band parameters.

According to the treatment by Zawadzki[27,28], who gave a review of the three band model in InSb type semiconductors,

let us write down the wavefunction and energy levels of conduction electrons in the presence of a magnetic field. The Schrödinger equation in question is

$$\mathcal{H}\Psi = E\Psi \quad , \tag{3.5}$$

where hamiltonian $\mathcal{H}$ is represented by

$$\mathcal{H} = \frac{1}{2m}\vec{P}^2 + V_0(\vec{r}) + \frac{\hbar^2}{4m^2c^2}(\vec{\sigma}\times\vec{\nabla}V_0)\vec{P} + \mu_B\vec{H}\vec{\sigma} \quad . \tag{3.6}$$

Here $\vec{P} = \vec{p} + (e/c)\vec{A}$ is the kinetic momentum in the presence of a magnetic field H_0 along the z-axis. $\vec{A}$ represents the vector potential of the magnetic field and μ_B denotes the Bohr magneton. $V_0(\vec{r})$ denotes the periodic potential of the lattice and $\vec{\sigma}$ is the Pauli spin operator. The 3rd and 4th terms in eq.(3.6) represent the spin-orbit interaction and Pauli term, respectively. A solution of eq.(3.5) is represented in the following form

$$\Psi(\vec{r}) = \sum_j f_j(\vec{r})\, u_j(\vec{r}) \quad , \tag{3.7}$$

where the summation is over the energy band. $U_j(\vec{r})$'s are periodic parts of the Bloch functions at band edges, which are called the Luttinger-Kohn[29] amplitudes. The orthonormality between these functions is established, i.e.,

$$\left(\frac{1}{\Omega}\right)\langle u_{\ell'} | u_\ell \rangle = \delta_{\ell'\ell} \quad , \tag{3.8}$$

where the integration is carried over the volume of the unit cell Ω. The envelop functions $f_j(r)$, being in contrast with $u_j(\vec{r})$, are slowly varying functions so that they are regarded constant within a unit cell. By applying the momentum operator on the product $f_j(\vec{r})u_j(\vec{r})$ and multiplying $u_i(\vec{r})$ from the left,

eq.(3.5) becomes the following set of coupled equations

$$\sum_j \Big[\frac{1}{2m}\vec{P}^2 + \varepsilon_{j,0} + E \Big]\delta_{ij} + \vec{\pi}_{ij}\cdot\vec{P} + \mathcal{H}^{SO}_{ij} + \mu_B \vec{H}\vec{\sigma}_{ij} \Big] f_j(\vec{r}) = 0, \tag{3.9}$$

where

$$\vec{\pi}_{ij} = \frac{1}{m} \langle u_i | \vec{P} + \frac{\hbar}{4mc^2} (\vec{\sigma} \times \vec{\nabla} V_0) | u_j \rangle \quad . \tag{3.10}$$

Here $\varepsilon_{j,0}$ is a eigen-energy of $u_j(\vec{r})$ and $\mathcal{H}^{SO}$ is the spin-orbit interaction term. The result, so far, includes no essential approximation. One proceeds according to the similar approach by Kane.[23] A finite number of close-lying levels are treated by means of the perturbation theory of degenerate or nealy degenerate bands, leaving out the contribution from all other bands in the first approximation. Attention is paid only to Γ_8, Γ_6 and Γ_7 bands. To solve eq.(3.9), the following eight states are chosen as the L.-K. functions[29] $u_i(\vec{r})$,

$$\begin{aligned}
u_1 &= iS\downarrow \,, \\
u_2 &= iS\uparrow \,, \\
u_3 &= R_-\downarrow \,, \\
u_4 &= \sqrt{\tfrac{2}{3}}\, Z\downarrow \; + \sqrt{\tfrac{1}{3}}\, R_-\uparrow \,, \\
u_5 &= \sqrt{\tfrac{2}{3}}\, Z\uparrow \; - \sqrt{\tfrac{1}{3}}\, R_+\downarrow \,, \\
u_6 &= R_+\uparrow \,, \\
u_7 &= \sqrt{\tfrac{1}{3}}\, Z\downarrow \; - \sqrt{\tfrac{2}{3}}\, R_-\uparrow \\
\text{and} \quad u_8 &= \sqrt{\tfrac{1}{3}}\, Z\uparrow \; + \sqrt{\tfrac{2}{3}}\, R_+\downarrow \,,
\end{aligned} \tag{3.11}$$

where $$R_{\pm} = (X \pm iY)/\sqrt{2} \,. \tag{3.12}$$

Here S and X, Y, Z are periodic functions which transform like atomic s and p functions under the operations of the tetrahedral group at the point Γ. The symbol $\uparrow$ means the spin-up function and $\downarrow$ spin-down function. By applying the functions (3.11) to eq.(3.9), the infinite set (3.9) becomes 8 x 8 set and is represented as follows:

$$\begin{bmatrix} & \\ & \mathcal{H}_{ij} \\ & \end{bmatrix} \begin{bmatrix} \\ f_j \\ \\ \end{bmatrix} = 0 \,. \tag{3.13}$$

Here K is defined as follows:

$$K = (-i/m)\langle S | P_z | Z \rangle \,. \tag{3.14}$$

This is called the interband matrix element. Using eq.(3.13), the functions $f_3 \cdots f_8$ can be expressed by f_1 and f_2.[28] Eq. (3.13) is divided into two orthogonal solutions. First solution corresponds to $f_2 = f_6 = 0$ (which is denoted '-') and another solution denoted '+' corresponds to the set including $f_1 = f_3 = 0$. Adopting the Landau gauge for the vector

$$[H_{ij}]\ [f_j] = 0$$

$$\begin{bmatrix}
-E+V & kP_+ & \sqrt{\frac{1}{3}}kP_- & \sqrt{\frac{2}{3}}kP_- & 0 & 0 & \sqrt{\frac{2}{3}}kP_z & \sqrt{\frac{1}{3}}kP_z \\
kP_- & -\varepsilon_g-E+V & 0 & 0 & 0 & 0 & 0 & 0 \\
\sqrt{\frac{1}{3}}kP_+ & 0 & -\varepsilon_g-E+V & 0 & \sqrt{\frac{2}{3}}kP_z & 0 & 0 & 0 \\
-\sqrt{\frac{2}{3}}kP_+ & 0 & 0 & -\varepsilon_g-\Delta-E+V & \sqrt{\frac{1}{3}}kP_z & 0 & 0 & 0 \\
0 & 0 & \sqrt{\frac{2}{3}}kP_z & \sqrt{\frac{1}{3}}kP_z & -E+V & kP_- & -\sqrt{\frac{1}{3}}kP_+ & \sqrt{\frac{2}{3}}kP_+ \\
0 & 0 & 0 & 0 & kP_+ & -\varepsilon_g-E+V & 0 & 0 \\
\sqrt{\frac{2}{3}}kP_z & 0 & 0 & 0 & -\sqrt{\frac{1}{3}}kP_- & 0 & -\varepsilon_g-E+V & 0 \\
\sqrt{\frac{1}{3}}kP_z & 0 & 0 & 0 & \sqrt{\frac{2}{3}}kP_- & 0 & 0 & -\varepsilon_g-\Delta-E+V
\end{bmatrix}
\begin{Bmatrix} f_1 \\ f_3 \\ f_5 \\ f_7 \\ f_2 \\ f_4 \\ f_6 \\ f_8 \end{Bmatrix} = 0$$

(3.13)

potential $\vec{A}$, i.e. $\vec{A} = (-Hy, 0, 0)$, the solution of eq.(3.13) is given as the following form

$$f_{1,2}(\vec{r}) = \exp[i(k_x x + k_z z)]\,\phi_n\left(\frac{y - y_o}{L}\right), \qquad (3.15)$$

where $y_0 = k_x L^2$. Using the above functions, and putting $f_2 = 0$ and solving the remaining equations of (3.13) to get $f_3 \cdots f_8$, the following complete wave function is obtained:

$$\begin{aligned}\psi^{+}_{n,k_x k_z}(\vec{r}) = \exp[i(k_x x + k_z z)] \\ \times \Big\{ [i a_+ \phi_n S - \frac{b_+ - c_+\sqrt{2}}{2}\Big(\frac{\hbar\omega_c(n+1)}{D_{n+}}\Big)^{1/2}\phi_{n+1}R_- \\ - \frac{b_+ - c_+\sqrt{2}}{2}\Big(\frac{\hbar\omega_c n}{D_{n+}}\Big)^{1/2}\phi_{n-1}R_+ + c_+\Big(\frac{\hbar^2 k_z^2/2m_e^*}{D_{n+}}\Big)^{1/2}\phi_n z\,]\uparrow \\ + b_+\Big[\Big(\frac{\hbar^2 k_z^2/2m_e^*}{D_{n+}}\Big)^{1/2}\phi_n R_+ - \Big(\frac{\hbar\omega_c(n+1)}{D_{n+}}\Big)^{1/2}\phi_{n+1} z/\sqrt{2}\,\Big]\downarrow \Big\}.\end{aligned} \qquad (3.16)$$

By a similar procedure, putting $f_1 = 0$, the following function is obtained:

$$\begin{aligned}\psi^{-}_{n\,k_x k_z}(\vec{r}) = \exp[i(k_x x + k_z z)] \\ \times \Big\{ [i a_- \phi_n S + \frac{b_- + c_-\sqrt{2}}{2}\Big(\frac{\hbar\omega_c(n+1)}{D_{n-}}\Big)^{1/2}\phi_{n+1}R_- \\ - \frac{b_- - c_-\sqrt{2}}{2}\Big(\frac{\hbar\omega_c n}{D_{n-}}\Big)^{1/2}\phi_{n-1}R_+ + c_-\Big(\frac{\hbar^2 k_z^2/2m_e^*}{D_{n-}}\Big)^{1/2}\phi_n z\,]\uparrow \\ + b_-\Big[\Big(\frac{\hbar^2 k_z^2/2m_e^*}{D_{n-}}\Big)^{1/2}\phi_n R_- - \Big(\frac{\hbar\omega_c n}{D_{n-1}}\Big)^{1/2}\phi_{n-1} z/\sqrt{2}\,\Big]\downarrow \Big\},\end{aligned} \qquad (3.17)$$

where the coefficients are

$$a_{\pm} = \frac{\varepsilon_g + E_{\pm}}{\varepsilon_g + 2E_{\pm}} \quad , \quad b_{\pm} = \frac{1}{3}\frac{E_{\pm}}{\varepsilon_g + 2E_{\pm}}\beta^2$$

$$\text{and} \qquad c_{\pm} = \frac{2}{3}\cdot\frac{E_{\pm}}{\varepsilon_g + 2E_{\pm}}\gamma^2 \qquad (3.18)$$

with

$$\beta = \frac{\Delta^2}{(\Delta + \varepsilon_g)(\Delta + 3\varepsilon_g/2)} \quad \text{and} \quad \gamma = \frac{\Delta + 3\varepsilon_g/2}{\Delta + \varepsilon_g} \qquad (3.19)$$

3-2) Valence band & acceptor level in the presence of a magnetic field

Valence bands cannot be treated in the manner of treating the conduction band, because of their band degeneracy and warping. InSb is a narrow-gap semiconductor, so that for valence bands a calculation taking account of the contribution of the conduction band and other bands is needed. Pidgeon and Brown[26] gave the total band description of the conduction and valence bands, including the contribution of higher bands. In their theory, several valence band parameters are included. The determination of these parameters has come into question. New parameter sets are given by several authors.[30-34] Some authors proposed modified theories based on Pidgeon and Brown's one.[30,31,35]

Because of the complexity of valnece bands, the determination of the acceptor level in the presence of the magnetic field is so difficult that few authors[36-39] treated the acceptor level theoretically. Only Lin-Chung and Henvis[40]

treated the acceptor levels in InSb theoretically. In this theory, the acceptor levels associated with the light hole band and the donor levels are calculated by a variational method based on the treatment of conduction and valence bands by Pidgeon and Brown.[26] Zawadzki[41,42] however, pointed out that there is a failure in the treatment of Lin-Chung and Henvis for donor levels, so that the observed spin-flip transition of donor electron is missing theoretically. Nevertheless, out of this theory, Seiler et al.[43] achieve a considerable success in the interpretation of hole transition between acceptor levels. In the absence of an appropriate alternative, we will proceed, somewhat tentatively, with the theory of Lin-Chung and Henvis for dealing with our experimental result. Lin-Chung and Henvis treated the following effective mass equation :

$$\left[\mathcal{H}_0 - \frac{2}{(\rho^2+z^2)^{\frac{1}{2}}} \right] F(N,M,\lambda) = E(N,M,\lambda) F(N,M,\lambda) , \qquad (3.20)$$

where $\mathcal{H}_0$ is the Hamiltonian for free carriers in the presence of the external magnetic field. The Schrödinger equation for $\mathcal{H}_0$ is given by

$$\mathcal{H}_0 f(N,M) = E(N,M) f(N,M) . \qquad (3.21)$$

This equation is equivalent to eq.(3.9). Here envelope functions of free carrier, f(N,M) are divided into two parts, that is, a-series and b-series, and written in one column vector form; namely,

$$f_a(N,M) = \begin{pmatrix} A_1 \Phi_{N,M} \\ A_3 \Phi_{N-1,M-1} \\ A_5 \Phi_{NH,M+1} \\ A_7 \Phi_{N+1,M+1} \end{pmatrix} \qquad (3.22)$$

and

$$f_b(N,M) = \begin{pmatrix} A_2\phi_{N,M} \\ A_6\phi_{N-1,M-1} \\ A_4\phi_{N+1,M+1} \\ A_8\phi_{N+1,M+1} \end{pmatrix}, \qquad (3.23)$$

where Φ_{NM} is a harmonic oscillator function ($N \leq M$). The energy levels belonging to Φ_{NM} are labelled by Landau quantum number N and are degenerate for different M (angular momentum). Following Wallis and Bowlden's[44] treatment and using above envelope functions, the variational envelope functions of impurity is give in one column vector form, i.e.,

$$F_{a,b}(N,M,\lambda) = f_{a,b}(N,M)\,P_\lambda(z)\,e^{-\frac{1}{4}\gamma\varepsilon^2 z^2}, \qquad (3.24)$$

where ε is the variational parameter, the variation of which is shown in Fig. 3 against the magnetic field.[40] $P_\lambda(z)$ represents a set of orthogonal polynomials of z of order λ, given by Wallis and Bowlden[44] ; for example,

$$P_0(z) = (\varepsilon^2\gamma/2\pi)^{1/4}, \qquad (3.25)$$

$$P_1(z) = (\varepsilon^6\gamma^3/2\pi)^{1/4} z, \text{ etc.}$$

The exponential factor in eq.(3.24) derived is from the inspection of the similarity to a hydrogenic wave function. This trial function is valid under the high field limit, i.e., $\gamma >> 1$, so the function is appropriate for high-field impurity states associated with light hole Landau subbands.

3-3) Several scattering processes

In this section, the transition probabilities concerned with 0^+ and 0^- Landau subbands and donor levels will be summarized. In InSb, the spin flip transition of electrons due to the electric type perturbation having no spin operator can be possible, because of the spin mixing in the electron wavefunction. Elliott[45] first pointed out this possibility. So this spin flip transition due to electric perturbation is called the Elliott process. In InSb, it has been found that the spin flip transitions play an important role for all scattering modes.[46] The relaxation times for several scattering mechanism with spin flip (for example, ionized impurity scattering, acoustic scattering and so on) are given here after the manner of ref. 47.

When the transition from 0^- subband to 0^+ subband is considered, the relaxation time τ is given by the following equation:

$$\tau = \tau_{temp} + T_1 + \tau_e . \qquad (3.26)$$

The first relaxation time τ_{temp} denotes the time establishing the electron temperature of excited electrons in 0^- subband. Second time T_1 is the spin relaxation time and the third is the momentum relaxation time of deexcited electrons in 0^+ subband. It is reasonable to assume that τ_{temp}, $\tau_e < T_1$. In view of the carrier concentration of $10^{13} \sim 10^{14}$ cm^{-3}, the non-degenerate statistics will be employed, so that T_1 is independent of the electron concentration in 0^- subband.

a) Spin relaxation due to ionized impurity scattering

The potential of ionized impurities in the crystal is written:

$$U(\vec{r}) = \sum_I v(\vec{r} - \vec{R}_I) \quad , \tag{3.27}$$

where the summation runs over impurity atoms situated at Ith lattice site $\vec{R}_I$. The single impurity potential $v(\vec{r})$ is given by a screened Coulomb type one:

$$v(\vec{r}) = -e^2 \exp(-q_s r) / \varepsilon_0 r \quad , \tag{3.28}$$

where ε_0 is the static dielectric constant and q_s is the inverse screening length.

The spin relaxation time T_1 is represented as

$$\frac{1}{T_1} = \frac{2\pi}{\hbar} < |\vec{k}', + |U| \vec{k}, - > |^2 > \delta(E_+ - E_-) \, . \tag{3.29}$$

The calculation of the matrix element of the potential is carried out using electron wave functions (3.16) and (3.17), so that the following expression of T_1 is obtained,

$$\frac{1}{T_1} = \frac{\pi e^4 N_D}{2\hbar \varepsilon_0} \frac{E_z}{(E_g + 2D_-)(E_g + 2D_+)} \frac{\alpha^2}{(k_z^2 + k_s^2)^{1/2}} \sum_{i=1}^{2} I(\zeta_i) \, , \tag{3.30}$$

where

$$I(x) = -1 - (1+x) \exp(x) \, Ei(-x) \, , \tag{3.31}$$

$Ei(x)$ is the exponential integral function

$$Ei(-x) = -\int_x^\infty \frac{e^{-t}}{t} dt \tag{3.32}$$

and $\zeta_{1,2}$ is given by

$$\zeta_{1,2} = (l_H^2/2) \left\{ \left[k_z \pm (k_z^2 + k_s^2)^{1/2} \right]^2 + q_s^2 \right\} \, . \tag{3.33}$$

The quantity α has the following form:

$$\alpha = \frac{\Delta}{\Delta + \varepsilon_g} \frac{\Delta + 2\varepsilon_g}{\Delta + 3\varepsilon_g/2} \quad . \tag{3.34}$$

The expression (3.30) is slightly different from the form of Boguslawski.[47)]

b) Deformation potential interaction with acoustic phonons

The spin relaxation time due to the deformation potential interaction with acoustic phonons will be treated. The form of the interaction potential with acoustic phonons is given by Bir and Pikus[48)] as follows:

$$\delta V_{ac} = \sum_{mn} D_{mn} \varepsilon_{mn} \qquad (m, n = 1, 2, 3) \quad , \tag{3.35}$$

where m,n are Cartesian coordinates. The notation ε_{mn} represents the deformation tensor, having the following form,

$$\varepsilon_{mn} = \frac{1}{2} \left[\partial \xi_m / \partial x_n + \partial \xi_m / \partial x_m \right] \quad , \tag{3.36}$$

where

$$\vec{\xi}(\vec{r}) = \left(\frac{\hbar}{2V\rho\omega_\nu(\vec{q})} \right)^{\frac{1}{2}} \hat{e}^\nu \left[b_{\vec{q}\nu} \exp(i\vec{q}\vec{r}) + H.C. \right] . \tag{3.37}$$

Here ρ is the crystal density, $b_{\vec{q}\nu}$ the annihilation operator of a phonon mode, $\omega_\nu(\vec{q})$ the phonon frequency and $\hat{e}^\nu$ the phonon polarization vector. The vector $\vec{q}$ is the wavevector from the νth phonon branch. H.C. denotes Hermite conjugatate. The deformation potential D_{mn} has a form

$$D_{mn} = - P_m P_n / m_o + V_{mn} \quad , \tag{3.38}$$

where V_{mn} represents the derivative of the crystal potential with respect to strain ε_{mn} and P_m is the momentum operator. To calculate the matrix element of δV_{ac}, the procedure used by Szymanska et al.[46] is taken. The resultant relaxation time is expressed by two terms, i.e. "intraband" term and "interband" term,

$$T_1^{-1} = (T_{ac}^{intra})^{-1} + (1 / T_{ac}^{inter})^{-1} . \tag{3.39}$$

The intraband part is expressed by

$$\frac{1}{T_{ac}^{intra}} = \frac{k_B T}{16\pi P} \frac{m_o^*}{(k_z^2 + k_s^2)^{1/2}} \left(\frac{\omega_c}{\hbar l_H \varepsilon_g} \right)^2 \sum_{\nu} \sum_{i=1}^{2} \frac{1}{\nu_\nu^2} M^{\nu}(z_i) , \tag{3.40}$$

where

$$z_{1,2} = (l_H^2 / 2) [k_z \pm (k_z^2 + k_s^2)^{1/2}]^2 \tag{3.41}$$

and summation of ν runs over three branches of the polarization of phonon, i.e., e^{Tl}, e^{Tl} and e^{L}. $M^{\nu}(z_i)$ are given by

$$\begin{aligned} M^{L}(z) &= [C_1 - 8 C_2 - z(2C_1 + 16 C_2) - z^2 (C_1 + 4C_2)] z \\ &\quad + [-4C_2 - 20 z C_2 - z^2 (20 C_2 + 3 C_1) - z^3 (C_1 + 4 C_2)] F(z) , \\ M^{Tl}(z) &= [C_1 - C_2 - z (C_1 + C_2)] z \\ &\quad + [- C_2 - 2 z C_2 - (C_1 + C_2) z^2] F(z) \end{aligned} \tag{3.42}$$

and

$$\begin{aligned} M^{T2}(z) &= [C_2 + 8 z C_2 + z^2 (C_1 + 16 C_2) + z^3 (C_1 + 4 C_2)] \\ &\quad + [4 C_2 + 10 z C_2 + z^2 (2 C_1 + 20 C_2) + z^3 (C_1 + 4 C_2)] F(z) \end{aligned}$$

with

$$F(z) = - z \exp(z) Ei(-z) . \tag{3.43}$$

The interband part is calculated similarly and is expressed as follows:

$$\frac{1}{T_{ac}^{intra}} = \frac{1}{3\pi\hbar^2} \frac{\beta^2 S^2}{\ell_H^2 \rho \varepsilon_g} \frac{k_B T}{(k_z^2 + k_S^2)^{1/2}} \sum_{\nu} \sum_{i=1}^{2} \frac{1}{\omega_\nu^2} N(z_i) \qquad (3.44)$$

with

$$N^{L} = \frac{1}{8}(1 - 2z - 9z^2) - \frac{1}{8} z (11 + 9z) F(z) \ ,$$

$$N^{T1} = \frac{1}{2}(1 - z) - \frac{3}{2} z F(z) \qquad (3.45)$$

and $$N^{T2} = \frac{3}{2}(1 + 3z) + (5 + \frac{9}{2} z) z F(z) \ .$$

These two parts are divided according to the relationship to the deformation potential constants l, m, n and s. The constants are defined as follows:

$$\begin{aligned} \ell &= \langle X | D_{xx} | X \rangle \ , \\ m &= \langle X | D_{yy} | X \rangle \ , \\ n &= \langle X | D_{xy} | Y \rangle \ , \\ S &= \langle S | D_{xy} | z \rangle \end{aligned} \qquad (3.46)$$

or their cyclic equivalents. X, Y, Z and s are periodic functions of Γ_{15} and Γ_1 symmetries, respectively. The intraband part is related to l, m, n and interband part is related to s interband constant.

c) Piezo-acoustic interaction

The form of the interaction potential is given by

$$\frac{1}{\varepsilon(q)} \delta V_{PA} = -\frac{8\pi e P}{\varepsilon(q)\varepsilon_0} \left(\frac{\hbar}{2V\rho\omega_\nu(q)} \right)^{1/2} \qquad (3.47)$$

$$K_\nu \left[b_{\vec{q}\nu} \exp(i\vec{q}\vec{r}) - b_{\vec{q}\nu}^{\dagger} \exp(-i\vec{q}\vec{r}) \right]$$

for a single phonon mode $\vec{q}\nu$. P is the piezo-electric constant of the crystal, and K describes the angular dependence of the interaction. Considering the screening effect by free carriers, the free carrier dielectric function $\varepsilon(q)$ is included in eq.(3.48).

The resultant spin relaxation time thus becomes

$$\frac{1}{T_{PA}} = 36\pi \left(\frac{Pe\alpha}{\varepsilon_g \varepsilon_0}\right)^2 \frac{k_B T \omega_c k_z^2}{(k_z^2+k_s^2)^{1/2}} \left(\frac{K^2}{\nu^2}\right)_{av} \sum_i P(\xi_i) \quad , \tag{3.48}$$

where

$$(K^2/\nu^2)_{av} = \sum_\nu (K_\nu^2/\nu_\nu^2)_{av} \quad , \tag{3.49}$$

$$P(\xi) = 1 + S + (\xi + S + \xi S)\exp(\xi) E_i(-\xi) \tag{3.50}$$

and

$$S = l_H^2 q_s^2 / 2 \, . \tag{3.51}$$

3-4) Donor-acceptor recombination

Thomas et al.[49] showed that the experimental results of donor-acceptor recombination radiation could be explained clearly in GaP. In their treatment, two cases are considered. One is the situation that donor or acceptor concentration is in excess and all the impurities are initially neutral. The other is the situation that donor and acceptor concentrations are equal and all of them are initially neutral. The former will be called type 1 and the latter will be called type 2. For both situations, the time variation of residual neutral donor (or acceptor) concentration and that of the radiation intensity caused by donor-acceptor pair recombination are given by this

theory. The decay profile does not obey an exponential law. If the distance to the donor is not too small, a hole bound to an acceptor sees an incident electron wave weakly bound to a donor, the wave function of which is denoted by $\psi_1(r_e)$. Giving a full credit to the assumption that the electron wave function $\psi_1(r_e)$ can be replaced by the wave function $\psi_1^*(r_e)$, which is the wave function of the electron at the site of the acceptor in the absence of the acceptor, the optical matrix element is given by

$$M_{cv}(r) = \text{const.} \times \psi_1^*(r) \ , \tag{3.52}$$

where r is the distance between the donor and the acceptor. Furthermore the behavior of $\psi_1(r)$ for large r is given by the following simple equation,

$$\psi_1(r) \propto r^m \exp(-r/a_B) \ , \tag{3.53}$$

where

$$a_B^{-1} = [\, 2 m_h^* E / \hbar^2 \,]^{1/2} \tag{3.54}$$

and

$$m = -1 + (E_H / E_a)^{1/2} \ . \tag{3.55}$$

Here E_H is the binding energy of an ideal hydrogenic donor and E_a is that of a real donor. If the simple hydrogenic donor is considered, there m will be zero and a_B will be the donor Bohr radius. The radiative recombination rate W(r) of an electron bound on a donor with a hole bound on an acceptor at a distance r from the donor will be written

$$W(r) = W_{max} \exp(-2r/a_B) \ . \tag{3.56}$$

Here W_{max} is a constant depending on the impurity levels. Let Q(t) be the probability that the electron populates on the donor at a time t. The quantity to be compared with an experimental value is the ensemble average of Q(t), which we will denote $\langle Q(t) \rangle$. After calculating the ensemble average, the following expression is obtained, for the case of type 1;

$$\langle Q(t) \rangle = \exp\left[4\pi n \int_0^\infty \{\exp[-W(r)t] - 1\} r^2 dr\right] . \qquad (3.57)$$

Here the quantity n denotes the concentration of the majority constituent. In the situation of type 2, in which the compensation is exactly attained, the average probability $\langle Q(t) \rangle_{comp}$ is given by the following equations;

$$\langle Q(t) \rangle_{comp} = \exp\left\{4\pi n \int_0^\infty \exp\left\{-W(r) \int_0^t \langle Q(t') \rangle_{comp} dt'\right\} - 1\right) r^2 dr\right\} \qquad (3.58)$$

and $$\langle Q(t) \rangle_{comp} = \langle Q(\tau) \rangle$$

with $$t = \int_0^\tau \frac{dt'}{\langle Q(t') \rangle} . \qquad (3.59)$$

Here t denotes the true time. In both situations, one parameter W_{max}, that is characterized by material and impurity, has to be included.

4. Experimental Results

4-1) Strong excitation case in n-type InSb

As mentioned in the preceding section, Figure 2 shows the absorption signal of photoexcited carriers just after photoexcitation in n-type sample A at 4.2 K obtained by using 119 μm FIR-laser. In Fig. 2-(a), which is the absorption signal in the absence of intrinsic photoexcitation, there arise the well known double peaks due to electron transitions. The resonance peak at the lower magnetic field is the transition of donor electrons from the ground state $(000)^+$ to the excited state $(010)^+$, i.e., the so-called impurity cyclotron resonance (ICR)[50]. Here the nomenclature of Wallis-Bowlden[44] is employed for donor levels in the strong magnetic field. The other peak is the cyclotron resonance of conduction electrons and corresponds to the transition from 0^+ to 1^+ Landau subband (denoted by C_1), where the number indicates the Landau quantum number and + and - indicate the effective up- and down-spin states.

The absorption signal is due to the carriers in thermal equilibrium. In other words, electrons populate only the 0^+ subband and $(000)^+$ level, while practically no free holes exist, in thermal equilibrium at 4.2 K. On photoexcitation, two new peaks were obtained related to light holes (indicated by ↑ in Fig. 2(b) and (c)). The peak located at B = 1.66 T ($m^* = 0.0184m_0$) corresponds to the transition from -1^- Landau subband of light hole to 0^- subband and the peak located at 4.56 T ($m^* = 0.0505m_0$) corresponds to that from -1^+ to 0^+ subband. In Fig. 4, the Landau-fan for light holes is shown, that is calculated after the manner of Pidgeon and Brown[26] with our valence band

parameters.[33] The cyclotron resonance absorptions with $\omega_c/2\pi$ = 2519 GHz (corresponding to the wavelength 119 μm) are shown by the vertical arrows in Fig. 4. The above assignment is verified from this figure and agrees with that by Button et al.[51] The time variation series of the cyclotron absorption at 4.2 K is shown in Fig. 5 up to the magnetic field of ~3 T with laser wavelength of 84 μm. These are not modulation signals. On the right shoulder of each curve is denoted the delay time after photoexcitation. The resonance peaks of light hole (denoted by ↓ in Fig. 5) disappear at a delay time of 7 μs. From this series, it is found that the time constant of the light hole signal is 1.5 μs. Furthermore the time constant of the light hole signal at 4.56 T in Fig. 5 is also found to be ~1.5 μs. Under the strong excitation in n-InSb, the aspect of the absorption signal associated with electrons is considerably complicated. There appears no obvious resonance peak related to electrons just after the photoexcitation. The disappearence of electron resonance peaks may be explained by Li et al.[52] They have shown that no bound state exists, when the donor impurity concentration is greater than 6×10^{13} cm^{-3} because of the broadening of impurity levels due to the overlapping of bound electron wavefunctions. When the excitation intensity is high enough to neutralize all the donors, the number of free electrons increases with the increase of excitation intensity and then the binding energy decreases. The difference between bound and free states disappears, so that a very broad peak is obtained. The critical impurity concentration may be larger than that predicted by Li et al. Then the measurement of the time variation of the

absorption signal at the resonance magnetic field of the donor electrons yields the information about both free and bound electrons. Figure 6 shows the time variation of the absorption signal at B = 1.66 T corresponding to the resonance field of ICR by means of the gate scan technique. It is found that the decay curve is divided into two stages, the first stage decaying very fast and being observable till about 10 μs and the second decaying very slowly. The fast stage has a time constant of ~1.5 μs, that is independent of temperature (between 1.7 and 4.2 K) and samples so far as n-type samples are concerned. The decay rate of the second stage varies from sample to sample, ranging from several tens of μs to a few ms. The decay curve is not necessarily expressible by a simple exponential. This second stage with a slow decay has proved to be due to the donor-acceptor recombination from its analogy with a similar phenomenon in germanium.[53] A detailed discussion will be given later.

The first stage does not appear in the weak excitation condition. The time constant of the electron signal in this state agrees with that of the light hole signal mentioned before. The first stage is interpreted as the signal due to overflowing free carriers. The photoexcited carriers promptly fill up the ionized impurity states. If the intensity of photoexcitation is strong enough, one should expect a large number of free carriers, which are unable to find a place to neutralize among the impurity centers. The sole channel for these excess carriers is electron-hole recombination. The time constant 1.5 μs is two or three times larger than the value obtained for radiative recombination by Fossum & Ancker-Johnson.[54] More quantitative

study about this stage is difficult, since the response time of the whole detecting system including the Putley detector[55] is equal to or larger than 0.5 μs.

4-2) Weak excitation case

When an n-type sample was subjected to a strong photoexcitation, the absorption signals just after photopulse was very broad and overlap each other even in the highly resolved measurement at 84 μm. This makes a quantitative analysis difficult. Resolution in absorption curves becomes better after about ten microseconds from photopulse, whence the curves can be treated analytically. Instead of waiting for a good resolution after a strong excitation, we may as well treat the signals under a weak excitation. In that case, not all of the impurities are occupied by carriers and there exist no overflowing carriers. In Fig. 7 and Fig. 8, a series of time resolution traces under weak photoexcitation are shown as a function of magnetic field for n-type sample B and p-type sample C, respectively. It is noticed that an additional peak is observed, corresponding to the electron cyclotron resonance of 0^- subband (denoted by C_2). Comparing with the signals without excitation for n- and p-type materials denoted by ∞ in each figure, it is found that there exists a great difference between these signals. In n-type sample, there exist double peaks (C_1 and ICR). On the other hand, no residual signal is observed in p-type material. In other words, all the observed signals are of the transient character in p-type sample, so that it is better to use a p-type sample for studying the time dependent behavior of the photoexcited electrons.

Meanwhile, in p-type InSb, small changes in peak position, half width and linehsape can be recognized for each peak, the peak shift could not be observed within experimental error. The changes of the half width is less than those in n-type. Though asymmetry of lineshape due to k_z-broadening[13] is recognizable at the beginning of photoexcitation in n-type sample, the lineshape of each peak in p-type sample can be fitted by a simple symmetrical Lorentzian.

For these reasons, we studied the behavior of photoexcited carriers in p-type material. The integrated intensities of resonance peaks ICR, C_1, C_2 are proportional to the densities of electrons populated in $(000)^+$ level, 0^+ and 0^- subbands, respectively. These integrated intensities of ICR, C_1, C_2 will be denoted by I_D, I_1, I_2, respectively. By tracing the variation of each intensity, the variation of the electron density populating each level can be obtained. In Fig. 9, we plot the time variation of each integrated intensity derived from the absorption signals in the p-type sample C. The intensities I_D, I_1, I_2 and their total $I_{tot} = I_D + I_1 + I_2$ vary over the time scale of several tens of microseconds. The intensity I_D first rises, then reaches a maximum and starts decaying. The first rise reflects the progressive neutralization of the donor centers at the initial stage. In the time variation of I_1, a similar first rise can be slightly recognized. After 1 μs, the variation is regarded as an exponential decay. The time variation of I_2 is also exponential. The time constants of I_1 and I_2 are 12 μs and 2.7 μs, respectively. If the time variation of I_D after reaching the maximum at 3 μs is regarded as exponential, its

time constant is found to be 23 μs.

Discussion of electron density in each level needs a detailed knowledge about electron transfer processes in these levels. Before stepping into this, we shall recall the concept of electron temperature. In each level, the momentum relaxation time is as small as 10^{-11} sec for sample C at 4.2 K, so that the establishment of quasithermal state can be attained. The introduction of electron temperature is not so strange and is convenient to describe the nonequilibrium carriers. We will introduce two kinds of electron temperature, i.e., intersubband electron temperature T_E^{CC} and the electron temperature established between donor level and 0^+ subband, T_E^{DC}. These effective temperatures will be described in the next section.

4-3) Electron temperature

To describe a transient behavior of a photoexcited electron system, two kinds of electron temperature are introduced. We assume that the electron distribution between 0^+- subband and $(000)^+$ donor level and that between 0^+- and 0^--subbands are described by Maxwell-Boltzmann statistics. These two distributions, however, will correspond to different electron temperatures, i.e., T_E^{CC}, T_E^{DC}, respectively. This treatment is according to the manner of Kobayashi et al.[12] and Matsuda and Otsuka.[13]

First intersubband temperature T_E^{CC} is defined by the equation,

$$\frac{n_d}{n_u} = \exp\left[-\frac{\Delta E}{k_B T_E^{CC}}\right], \tag{4.1}$$

where n_u and n_d are densities of electrons populating 0^+- and 0^-- subbands, respectively, and ΔE is the energy difference between these two subbands, that is ~5 meV at 2 T. The electron densities are proportional to the integrated absorption intensities, so that the ratio of electron densities between 0^+ and 0^- subband is equal to that of absorption intensities, that is, $(n_d/n_u) = (I_2/I_1)$. By measuring the intensity ratio (I_2/I_1), the electron temperature T_E^{CC} is determined by the equation,

$$T_E^{CC} = -\frac{\Delta E}{k_B}\left[\ln\left(\frac{I_2}{I_1}\right)\right]^{-1} . \qquad (4.2)$$

Another electron temperature T_E^{DC} is determined by the population ratio between $(000)^+$ donor level and 0^+ subband, so that the relation between this ratio and temperature obtained by Matsuda and Otsuka[13] is used. They have measured the cyclotron resonance absorption by varying the lattice temperature from 4.2 K to 90 K in n-InSb (Fig. 10). In thermal equilibrium, by considering an n-type material having densities N_D and N_A of donors and acceptors, respectively, the electron density occupying to 0^+- subband, n_u, is determined by the following equations;

$$\frac{n_u(N_D - N_D^0)}{N_D^0} = \frac{1}{2} N_c^* \exp\left[-\frac{\varepsilon_d}{k_B T_E^{DC}}\right] \qquad (4.3)$$

and

$$n_u = N_D - N_A - N_D^0 , \qquad (4.4)$$

where N_c^* is the effective density of states in the presence of a magnetic field; ε_d is the ionization energy of $(000)^+$ ground

donor level; and N_D^0 is the density of neutral donors (Here the factor 1/2 is different from the corresponding equation of Matsuda and Otsuka[13]). By fitting the data obtained by Matsuda and Otsuka to eq.(4.3) (Fig. 11), N_c^* and ε_d are obtained as follows:

$$N_c^* = 5.5 \times 10^{15}\ cm^{-3} \quad and \quad \varepsilon_d = 1.4\ meV . \tag{4.5}$$

The effective density of states N_c^* is given by

$$N_c^* = (1/2\pi^2)(2\pi m_c^* k_B T/\hbar^2)^{1/2}(eB/c\hbar) . \tag{4.6}$$

By taking appropriate values of parameters to fit the experimental conditions, we obtain 3.25×10^{15} cm^{-3} as N_c^*. The binding energy of $(000)^+$ state at 2 T is ~2.3 meV[40,56]. The agreement of N_c^* between above two values is fairly good but ionization energies have a considarable gap. We will employ the value (4.5) to obtain the effective temperature T_E^{DC} in the study of photoexcited carriers by means of the following equation,

$$T_E^{DC} = -\frac{\varepsilon_d}{k_B}\left\{\ln\left[2\left(\frac{n_u}{N_D^0}\right)\left(\frac{N_D - N_D^0}{N_c^*}\right)\right]\right\}^{-1} . \tag{4.7}$$

Under weak excitation, the condition $N_D >> N_D^0$ is established ; so that eq.(7) is rewritten

$$T_E^{DC} = -\frac{\varepsilon_d}{k_B}\left\{\ln\left[2\left(\frac{n_u}{N_D^0}\right)\left(\frac{N_D}{N_c^*}\right)\right]\right\}^{-1} . \tag{4.8}$$

Here the ratio n_u/N_D^0 must be determined from experiment. From the measurement of impact ionization due to electric field, Kobayashi[12] has found that the oscillator strength of donor electron transition is nearly equal to that of conduction

electron transition. The ratio n_u/N_D^0 in eq.(4.8), therefore, can be replaced by I_1/I_D.

4-4) Expression of experimental data by electron temperature

Figure 12 shows the two kinds of electron temperature derived from the time variation of absorption intensities at $T_L = 4.2$ K and 1.6 K (Fig. 8). It is found that there exists a great difference between the behavior of T_E^{DC} and T_E^{CC}. T_E^{CC} for $T_L = 4.2$ K attains to 40 K at the just end of the photopulse and cools down to 10 K at 12 μs, while the maximum value of T_E^{DC} is only 5 K and it does not vary very much with delay time. Moreover, T_E^{DC} becomes even lower than lattice temperature $T_L = 4.2$ K after ~5 μs. The determination of T_E^{DC} depends on the choice of the ε_d value. If we choose as ε_d not 1.4 meV but 2.3 meV,[40,56] T_E^{DC} attains 8 K just after photopulse. The lattice temperature seems not to affect the electron temperatures between 1.6 K and 4.2 K. It should be remembered that, in p-type, all the observed signals are due to transient carriers. It may not be too strange then that the effective temperature is less than the lattice temperature. In this time variation of the absorption, there exists the following characters. The existence of C_2 peak determines the effective temperature T_E^{CC} and indicates for the electron system to be in non-equilibrium; in other words, in an optically "hot" state. The low value of T_E^{DC} shows that the hot electron state is not derived from the rising of the lattice temperature, T_L. If T_L were high enough for the peak C_2 to appear, the disappearence of ICR would be accompanied with (see Fig. 10). The low value of T_E^{DC}, therefore, proves that

the lattice temperature has not increased.

If T_E^{CC} decreases to the lattice temperature T_L according to an exponential curve with time constant τ_c, the description of the time variation of T_E^{CC} is given by

$$\frac{dT_E^{cc}}{dt} = \frac{T_E^{cc} - T_L}{\tau_c} \quad . \tag{4.9}$$

When this equation is applied to the experimental result, τ_c becomes 6 μs. That seems to be a considerably large value.

Let us take the Shockley mechanism[3] to explain the large τ_c . Then, τ_c is defined in the form

$$\tau_c = \tau (k_B T_L / m_e^* S^2) \; ; \tag{4.10}$$

where τ is the electron-phonon scattering time which depends both on T_E^{CC} and on T_L, m_e^* the effective mass of electron and S the sound velocity. Putting $T_E^{CC} = 40$ K and $T_L = 4.2$ K, one obtains $\tau_c = 1.3 \times 10^{-7}$ s, that is much shorter than the experimental value.

Here one may add another temperature, i.e., intrasubband electron temperature, T_e^{intra}. This temperature has been defined by Matsuda and Otsuka[13] and discussed in the electric field excitation. In InSb, one of the hot electron effects is shown in the deviation of momentum k_z in a subband. This effect induces a tail on the high field side of the resonance peak and the shape of resonance peak becomes aysmmetrical (called "k_z-broadening"[13]). Figure 13 shows the ratio between the right and left half widths of half maximum of C_1, which are denoted by $\Delta\ell$ and Δr, respectively. It is found that the ratio ($\Delta r/\Delta\ell$) is nearly equal to 1 and is much smaller than the ratio in the

electric field excitation (denoted by a bar at 0 μs). And the ratio seems to be independent of delay time. This means that almost all the electrons populate the bottom of 0^+ subband, so that the intrasubband temperature is not much higher than T_L. This fact holds true also for the C_2 peak. By studying the line shapes of C_1 and C_2, T_E^{intra} seems to be independent of the excitation intensity and the lattice temperature (up to ~15 K). And T_E^{intra} seems to be independent of samples. The time-variation of T_E^{CC} can be determined by that of the ratio (I_2/I_1) directly. Let us consider what determines the time variation of the ratio. The ratio (I_2/I_1) seems to decrease exponentially, having 3.6 μs as the time constant. This time constant is much shorter than that of the total electron density ($\tau_{tot} = 19$ μs). As far as considering the decay of the ratio (I_2/I_1), the assumption that the total electron density is constant is reasonable. Under this assumption, let us consider the following simplest rate equations:

$$\dot{n}_d = -n_d/\tau_{21} - n_d/\tau_3 \quad , \tag{4.11}$$

$$\dot{n}_u = n_d/\tau_{21} - n_u/\tau_2 \quad , \tag{4.12}$$

$$\dot{N}_u = n_u/\tau_2 \tag{4.13}$$

and

$$\dot{N}_d = n_d/\tau_3 \quad ; \tag{4.14}$$

where n_d and n_u as well as N_u and N_d are the electron densities belonging to the 0^-- and 0^+- subbands as well as to $(000)^+$ and $(000)^-$ donor levels, respectively. The schematic diagram of possible electron transition between these levels is shown in

Fig. 14. τ_{21} is the characteristic time constant of the transition between 0^- and 0^+ subbands. This transition is associated with a flip of electron spin. τ_2 and τ_3 represent the time constants of transitions from subbands 0^+ and 0^- to associated donor states $(000)^+$ and $(000)^-$, respectively. By solving the coupled rate equations, each electron density is represented as a function of delay time with the form,

$$n_d(t) = n_d^\circ \exp\left[-\frac{t}{\tau'}\right] , \tag{4.15}$$

$$n_u(t) = n_u^\circ \exp\left[-\frac{t}{\tau_2}\right] + n_d^\circ\left(\frac{\tau''}{\tau}\right)\left\{\exp\left[-\frac{t}{\tau_2}\right] - \exp\left[-\frac{t}{\tau'}\right]\right\} \tag{4.16}$$

and

$$N_u(t) = \frac{n_d^\circ \tau'}{\tau_{21}(\tau_2-\tau')}\left(\tau' \exp\left[-\frac{t}{\tau'}\right] - \tau_2 \exp\left[-\frac{t}{\tau_2}\right]\right) - n_u^\circ \exp\left(-\frac{t}{\tau_2}\right) + N_u^\infty ; \tag{4.17}$$

where

$$\frac{1}{\tau'} = \frac{1}{\tau_{21}} + \frac{1}{\tau_3} , \tag{4.18}$$

$$\frac{1}{\tau''} = \frac{1}{\tau_{21}} + \frac{1}{\tau_3} - \frac{1}{\tau_2} \tag{4.19}$$

and

$$N_u^\infty = N_u^\circ + n_d^\circ\left(\frac{\tau'}{\tau_{21}}\right) + n_u^\circ . \tag{4.20}$$

Here n_d°, n_u° and N_u° denote the densities of carriers just at the end of photopulse in 0^--, 0^+- subbands and $(000)^+$ donor level, respectively. From eqs.(4.15) and (4.16), the ratio (n_d/n_u) is given by the form,

$$\frac{n_d}{n_u} = \left\{\frac{\tau''}{\tau_{21}}\left(\exp\left[-\frac{t}{\tau''}\right] - 1\right) + \frac{n_u^\circ}{n_d^\circ}\exp\left[-\frac{t}{\tau''}\right]\right\}^{-1} . \tag{4.21}$$

In the experiment, the ratio (n_d/n_u) decreases as the delay time increases, so that it is found that $\tau' < \tau_2$ from eq.(4.18). τ_2 and τ_3 are the time constants of the transitions from 0-Landau subband to (000) donor level having opposite spin states, so that one may assume that τ_2 is nearly equal to τ_3.

Under the approximation, we will consider the donor density $N_u(t)$ in two cases.

a) If $\tau' << \tau_2$, (4.17) is transformed as follows:

$$N_u(t) \approx N_u^\circ + n_u \left(1 - \exp\left[-\frac{t}{\tau_2}\right]\right). \qquad (4.22)$$

b) While, if $\tau' \lesssim \tau_2$, (4.17) becomes

$$N_u(t) \approx (N_u^\circ - N_u^\infty) \exp\left[-\frac{t}{\tau_2}\right] + N_u^\infty . \qquad (4.23)$$

In both cases, the time variation of $N_u(t)$ depends on τ_2. From the time variation of N_u in Fig. 9, one obtains $\tau_2 \sim 10$ μs using either eq.(4.22) or (4.23), assuming an exponential decay. By measuring the slope of the time variation of I_2, one obtains 2.7 μs as the value of τ' from eq.(4.15). Under such a circumstance, it is not so bad an approximation to put $\tau' << \tau_2$. By utilizing the assumption $\tau_2 = \tau_3$, τ' is found nearly equal to τ_1 and also $\tau' \approx \tau_{21}$. From the experimental result in Fig. 9, n_u° being much larger than n_d°, eq.(4.21) is approximately given by

$$\frac{n_d}{n_u} = \frac{n_d^\circ}{n_u^\circ} \exp\left[-\frac{t}{\tau_{21}}\right] . \qquad (4.24)$$

It is found that the time variation of T_E^{CC} (i.e. (n_d/n_u)) is determined by τ_{21} which is the time constant of the transition

from 0^-- to 0^+- subbands, in other words, the life time of electrons in 0^-- subband. Gornik[57] has observed the transition from 1^+ to 0^+ subband by means of saturation measurment of cyclotron radiation with FIR-laser (wavelength 90.6 μm and 66.0 μm) at 2 K. He showed the value of 0.1 ns as the electron lifetime at 1^+ subband for this transition. This value was determined by electron-electron scatterings. In his case, there existed electrons having a concentration of 10^{13} cm^{-3}. The experimental conditions (for example, temperature, resonance field etc.) were similar to ours. The only difference was that he observed 1^+ subband electrons, while we observe 0^-- subband electrons. With all that, there is a big difference between observed lifetimes. The transition from 0^- to 0^+ is accompanied with electron spin flip, while that from 1^+ to 0^+ is not. The observed long lifetime of electrons in 0^-- subband may thus be due to spin-flip.

As mentioned in Section 3, the spin flip transition is possible even by an electric perturbation with no spin operator. The spin flip transition in the presnece of a magnetic field due to various scattering potentials has been investigated extensibly by Boguslawski and Zawadzki[47]. They showed that at low temperatures below 20 K, the dominant scattering mechanism for spin flip transition is the ionized impurity scattering, supposing donor concentration is ~10^{15} cm^{-3}.

Let us calculate the life time of electrons in 0^- subband, i.e., relaxation time of spin flip transition, using the appropriate value of parameters to fit the experimental conditions. The following values are chosen: effective mass of electrons

$m_e^* = 0.016 m_0$, effective g-value $g^* = -50$, static dielectric constant $\varepsilon = 17.8$, impurity concentration $N_D = 10^{14}$ cm^{-3} and Debye-Hükel type screening length ~500 Å. The unquantized part of energy $\hbar k_z$ is assumed to be

$$\frac{(\hbar k_z)^2}{2m_e^*} = \frac{1}{2} k_B T_e^{intra} \qquad (4.25)$$

where T_e^{intra} is the intrasubband electron temperature. After calculating eq.(3.30) with these parameters, we obtained the spin relaxation time T_1, as a function of intrasubband electron temperature T_E^{intra} as plotted in Fig. 15. A fairly good agreement between the calculated value at $T_E^{intra} = 20$ K and experimental data was attained. The observed slow decay of the ratio (I_2/I_1) thus seems to be caused by spin flip transition of 0^- subband electrons. The dominant scattering channel seems to be due to ionized impurities. But other scattering centers have also to be considered. With our experimental conditions, electron-neutral impurity scatterings and electron-electron scatterings have a possibility of contributing to the spin-flip transition.

First treating the neutral impurity scattering, the form proposed by Otsuka[58] was taken as the scattering potential. The form is given as follows;

$$V(r) = -\frac{e^2}{\varepsilon_0}\left(\frac{1}{r} + \frac{1}{a_B^*}\right) \exp\left[-\frac{r}{a_B^*}\right], \qquad (4.26)$$

where a_B^* is the effective Bohr radius. Using the Fourier transform of V(r) and calculating after the manner of Boguslawski,

the spin flip time due to neutral impurity scattering is given by

$$\frac{1}{T_1^{neu}} = \frac{\pi e^4 N_D^0}{2\hbar\varepsilon_0^2} \frac{E_z}{(\varepsilon_g+2D_-)(\varepsilon_g+2D_+)} \frac{\alpha^2}{(k_z^2+k_s^2)^{1/2}} \sum_{i=1}^{2} J(\xi_i) , \tag{4.27}$$

where (4.28)

$$J(x) = (g_s l_H)^4 \frac{1}{6}\left[-1+\frac{1}{x^3}+(1+x)e^x E_i(-x)\right] + \frac{1}{2}(g_s l_H)^2\left[1+\frac{1}{x}-x e^x E_i(-x)\right] + \left[-1-(1+x)e^x E_i(-x)\right] .$$

While the T_1 due to ionized impurity scatterings will be written as T_1^{ion}. The notations in each equation were already given in 3-4. The obtained relaxation time T_1^{neu} is shown in Fig. 16. It is found that T_1^{neu} is nearly equal to but somewhat smaller than T_1^{ion}. It may be noted here that the extent of a single neutral donor (the order of a_B^*) is nearly the same with that of an ionized donor (the order of the screening length). The contribution of neutral donors, accordingly, may not be neglected, so far as their density is comparable with that of ionized donors.

Second, the spin flip relaxation time due to electron-electron scattering has been given by Boguslawski [59]. The expression was given in no magnetic field as follows;

$$\frac{1}{T_1^{ee}} = \frac{5}{4} m_c \left(\frac{e^2\alpha}{\varepsilon_0\varepsilon_g}\right)\left(\frac{\pi k_B T}{m_e^*}\right)^{1/2} J(s), \tag{4.29}$$

where $$J(x) = -1-(1+x)\exp(x)E_i(-x) \tag{4.30}$$

and $S = \beta\hbar^2 q_s^2/2m_e^*$. Here q_s is the inverse screening radius of

Debye-Hückel type and other parameters are as before. A different point from the ionized impurity scattering is the existence of the exchange channel included in the factor $\frac{5}{4}$. To compare this relaxation time with that due to ionized impurity scatterings, the following expression is readily obtained.

$$\frac{T_1^{ee}}{T_1^{ion}} = \frac{4\sqrt{2}}{5} \frac{J(5/4)}{J(s)} \frac{N_D^+}{n_c} \tag{4.31}$$

One may note $J(s) \to -\ell n\ s$ as $s \to 0$. Then in the limit of high temperature, we have

$$\frac{T_1^{ee}}{T_1^{ion}} \longrightarrow 1.13 \frac{N_D^+}{n_c} \tag{4.32}$$

It is found that the spin relaxation time due to electron-electron scatterings becomes nearly the same as that due to ionized impurity scatterings, supposing that the density of conduction electrons is nearly equal to that of ionized donors. The form of eq.(4.31) can be applied to general cases. With appropriate parameters, one obtains 8 μs as the relaxation time T_1^{ee}.

These two additional scattering mechanisms, neutral impurity scatterings and electron-electron scatterings, have the same physical origin as ionized impurity scatterings, namely the electron scattering by an electric potential of the screened Coulomb type or similar, in a crystal with non-negligible spin-orbit interaction.

4-5) Excitation intensity variation of spin relaxation

To study the contribution of these three scattering mechanisms on spin relaxation time, the effect of excitation intensity on spin relaxation time was studied. By increasing the excitation intensity, the density of free electrons and that of neutral donors will be increased, while the density of ionized donors will be decreased. The measurement of the excitation intensity dependence of the time constant τ_{21} of the ratio (I_2/I_1) will then show what the main scattering center is.

To obtain the relaxation time T_1, a series of time variation data with other physical parameters being fixed was needed. The versatile multichannel time resolution system was full used to get such on dependence of spin relaxation time on some physical parameters (for example, excitation intensity, lattice temperature etc.) under the same conditions.

Figure 17 shows a series of time variation of sample C under a medium excitation intensity, obtained by means of a single scanning of the magnetic field. The series consists of 15 absorption curves with their time interval being 1 μs between adjacent traces. To survey the effect of excitation intensity, this series of the absorption curves was obtained under several excitation intensities between 0.025 mW/cm^2 and 0.2 mW/cm^2 measured at just before a sample.

By obtaining the integrated absorption intensities I_D, I_1 and I_2 for each curve of trace, time constants for I_D, I_1 and I_2, as well as that of the ratio (I_2/I_1), or the assumed spin relaxation time T_1, were determined. We notice the relaxation time τ_{21} of the ratio (I_2/I_1) to be a function of excitation

intensity. Figure 18 shows the excitation intencity (I_{ex}) dependence of τ_{21} as well as that of the absorption intensities I_D, I_1 and I_2. τ_{21} first increases with excitation intensity I_{ex}, reaches a maximum at $I_{ex} \simeq 0.13$ mW/cm^2 and then slowly decreases.

As seen in eq.(3.30), the spin relaxation time T_1 due to ionized impurity scattering is inversly proportional to the density of ionized impurities N_D^+. If only the ionized impurity scattering were contributing to the determination of T_1, that is, determination of τ_{21}, the observed relaxation time τ_{21} would be longer as neutral impurities increased. In other words, the intensification of the photopulse would reduce τ_{21}. This is not the case of the experimental result. In the calculation of Boguslawski,[47,59] the scattering originated from Coulomb potential was based on one electron approximation, so that spin relaxation time due to electron-electron scattering is also inversly proportional to the density of conduction electrons n_c. If the potential form (4.26) is taken as the potential due to neutral impurity scattering, the corresponding relaxation time should also be inversly proportional to the density of neutral donors N_D°. When the spin relaxation times T_1^{neu} given by eq.(4.27) and T_1^{ee} given by eq.(4.29) are calculated with appropriate parameters, it is found that $T_1^{neu} = 2$ μs and $T_1^{ee} = 8$ μs. These values are comparable with $T_1^{ion} = 6$ μs due to ionized impurity scatterings. Under such a circumstance one might as well make an overall treatment for three different kinds of scattering centers rather than treating them separately. So the following effective density of scattering centers N is

introduced;

$$N = aN_D^{\circ} + bN_D^{+} + cn_c \quad , \tag{4.33}$$

where the constants a,b and c denote relative scattering probabilities due to a single neutral donor, an ionized donor and a conduction electron, respectively. As far as one assumes the one electron approximation to hold, the variation of N agrees with that of relaxation time T_1 (that is, τ_{21}). In the lower part of Fig. 18, dependence of densities of conduction electrons and donor electrons on excitation intensity is shown. The densities are derived from the absorption intensities $(I_1 + I_2)$ and I_D at 2 μs after the photopulse, respectively. The density of neutral donors shows a tendency to saturate at the total donor density of 1×10^{14} cm^{-3} as excitation intensity is increased. The observed absorption intensity I_D as a function of excitation intensity I_{ex} is extrapolated to the limit of the strongest excitation, where I_D converges to the maximum value I_D^{max}, that corresponds to the absorption intensity due to all the donors, the concentration of which is 1.0×10^{14} cm^{-3}. By measuring the absorption intensities I_D and $(I_1 + I_2)$ with I_D^{max} as a calibration standard, the relative electron densities N_D° and n_c can be obtained. These are shown in Fig. 18 and the position of the N_D (corresponding to I_D^{max}) is denoted by a horizontal dot-dashed line. The relative density of ionized donors N_D^{+} could be determined from the relation

$$N_D^{+} = N_D - N_D^{\circ} \quad . \tag{4.34}$$

The resultant ionized impurity density N_D^{+} is shown by a broken

line in Fig. 18. Using these densities, N can be determined by choosing appropriate values of a, b and c to fit the experimental result shown in Fig. 18. The chosen values of a, b and c are 0.9, 1 and 0.8, respectively. The resultant curve of N is shown in Fig. 19 as a function of I_{ex}. Though these parameter values have a considerable uncertainity, the experimental result that there exists a maximum in τ_{21} at 0.13 mW/cm^2 may be explained. In InSb, the binding energy of a donor electron is very small (~0.6 meV at zero magnetic field), so that the neutral donor impurity has a large Bohr radius(that is even larger than the screening length of ionized donor calculated from the Debye-Hückel model in our experimental condition). The scattering cross-section of a neutral donor is thus comparable with that of an ionized impurity. Considering that a neutral impurity has so large an extent as an ionized impurity, it is not surprising that the contribution of neutral impurity scatterings to τ_{21} is comparable with that of ionized impurity scatterings. If eq.(4.31) holds in our experimental condition, the contribution of electron-electron scatterings may be about 90 % of that of ionized impurity scatterings. This value seems to be reasonable in view of the ratio c/b = 0.8 that is predicted from eq.(4.32).

From the measurement of the excitation dependence of τ_{21}, it is found that the contributions from these three kinds of scattering centers to τ_{21} have more or less the same importance.

4-6) Sample dependence of spin relaxation time

Figures 20 and 21 show the absorption curves of samples D and E, respectively. The experimental conditions (excitation

intensity, lattice temperature and so on) were the same as those for the data of sample C shown in Fig. 8. Comparing the three absorption curves, it is found that the intensity of C_2 of sample E just after the photopulse is much smaller than those of samples C and D. The maximum electron temperature in sample E is 30 K, while that attains to 40 K in sample C. In sample D, it becomes as high as 54 K.

In Fig. 22 the time variations of the ratio (I_2/I_1) of these samples are shown. It is obvious that difference is seen not only in the magnitude but also in the decay behavior between samples C and D and sample E. The ratio I_2/I_1 in sample E is much smaller than those in sample C and D. This means the electron temperature T_E^{inter} in sample E is lower than those in samples C and D. The slope of decay curve of I_2/I_1 in sample E is larger than those of sample C and D. The time constants τ_{21} of these three samples are plotted against the inverse donor concentration $(1/N_D)$ in Fig. 23. Here the solid line indicates the calculated value T_1^{ion} ty the theory of Boguslawski[47], with appropriate parameters, in which the spin relaxation time T_1^{ion} is considered to be inversely proportional to the ionized donor densities N_D^-. Assuming $N_D^\circ \ll N_D$, the relation $N_D \approx N_D^+$ is realized, so $T_1^{ion} \propto (1/N_D)$. The donor concentration of sample E is about twice as large as those of samples C and D, the donor densities of which are 1.0×10^{14} cm^{-3} and 1.3×10^{14} cm^{-3}, respectively. This result seems to indicate that the dominant scattering channel of the spin relaxation of 0^-- subband electrons is due to the impurity scattering and this seems to support our previous conclusion.

4-7) Lattice temperature dependence

To explore the phonon effect on the spin relaxation time T_1, the lattice temperature dependence of τ_{21} (i.e., T_1) was measured. The temperature range was from 4.2 K to 15 K, and the multichannel time resolution system was utilized as before. In Fig. 24, the time constants τ_D, τ_1, τ_2 and τ_{tot} of I_D, I_1, I_2 and total absorption intensity I_{tot} are shown as a function of lattice temperature at a medium excitation intensity. It is noticed that the time constant τ_{tot} of the total absorption intensity I_{tot} shows a considerable large change against temperature T_L. It has been assumed that the total electron density n_{tot} (i.e. I_{tot}) is constant and independent of any physical parameter changes till the discussions in the last section. This assumption no longer holds true. The time constant of I_1 now decreases with increasing temperature in the same manner as I_D and I_{tot}. Of particular interest is that the time constant of I_2 is almost independent of lattice temperature. The large lattice temperature dependence of τ_{tot} means that the electron disappearance from the conduction band is accelerated by electron-phonon scatterings. In our experimental condition, all the holes are populating the acceptor levels, as evidenced of the small time constant of free holes. So there are two possible channels for electrons to disappear. One is the donor-acceptor recombination and the other is the conduction electron-acceptor hole recombination. In the donor-acceptor recombination, the recombination probability is governed by the extent of the overlapping between donor and acceptor wavefunctions. No doubt this overlapping is independent of lattice temperature. So the observed temperature

dependence of τ_{tot} seems due mainly to the conduction electron-acceptor hole recombination.

The acceptor level in InSb has been studied extensively by several authors.[60-63] The binding energy of the lowest acceptor level is said to be ~8 meV[63] at zero magnetic field. There are, however, two types of acceptor levels reflecting the complexity of the valence bands. On is the light hole like acceptor level and the other the heavy hole like level. The heavy hole like acceptor level has a small γ-value even at a considerably high magnetic field, so that this level can be treated under the weak magnetic field condition. The light hole like acceptor level, on the other hands, easily attains the high magnetic field condition. It is, therefore, natural to consider that the lowest acceptor level has mainly heavy-hole like character in the magnetic field. In our experimental condition (B = 2 T), the light hole like acceptor level is located shallower than the heavy hole like acceptor level. A free hole is first captured at a light hole like acceptor level and then falls to a heavy hole like levels in a cascade like process.[64] So we treat the condiction electron-light hole like acceptor recombination.

The decay channels of 0^- subband electrons are considered to consist of the following: the first channel is the transition to the 0^+ subband, the second the conduction electron-acceptor hole transition and the third is the transfer to $(000)^-$ donor level. In our experiment, practically no magneto-optical absorption associated with $(000)^-$ donor level is obvious, so that its reverse process, or the third channel mentioned above, would not be very important. The first channel is not expected

to show a large change due to phonon scatterings from the calculation of Boguslawski using eq.(3.40),(3.45) and (3.48) below 20K. Then the main decay channel of C_2 will also be due to the conduction electron-light hole like acceptor recombination. If the time constants τ_1 and τ_2, corresponding to the decays of I_1 and I_2, respectively, are determined by the same origin, why such a big difference is observed between them. There are two possibilities to explain the difference. One is the difference in hole distribution function and the other is the difference in transition probability. The selection rule for conduction electron-acceptor hole recombination is similar to that for interband transition in the theory of Lin-Chung and Henvis,[40], corresponding to $\Delta n = 0$, where n is the Landau quantum number, spin being conserved. First, the transition probability of interband transitions 0^+ conduction subband to the acceptor level associated with 0^+ light hole band 0^- subband to the acceptor level attached to 0^- subband, after the manner of Lin-Chung and Henvis.

The matrix element for electric dipole transition is given by[65]

$$M = \langle \Psi_I | \vec{\pi} \cdot \vec{\varepsilon} | \Psi_F \rangle \quad , \tag{4.35}$$

where ϕ_I and ϕ_F are the initial and final state wavefunctions, respectively, the form of which is given by eq.(3.7), $\vec{\Pi}$ is the modified matrix, the element of which is given by eq.(3.10) and $\vec{\varepsilon}$ is the polarization vector of light. Using the wavefunction (3.7), the matrix element becomes

$$M = \sum_{jj'} [\vec{\pi}_{jj'} \cdot \vec{\varepsilon}] \langle f_j^I | f_{j'}^F \rangle + \sum_{jj'} \vec{\varepsilon} \left[\sum \frac{\vec{\pi}_{ji} \vec{\pi}_{ij'}}{\varepsilon_g - \varepsilon_i} + \sum \frac{\vec{\pi}_{ij'} \vec{\pi}_{ji}}{\varepsilon_g - \varepsilon_i} \right] \langle f_i^I | \vec{K} | f_{j'}^F \rangle , \quad (4.36)$$

where ε_i is the electron eigenvalue at the i th band and $\vec{K} = \vec{p} + e\vec{A}/c$. The first term in eq.(4.36) is the allowed transition while the second the forbidden transition. Since the contribution from the second term is much less than that from the first term, attention will be paid only to the first term. This part of the matrix element M_{all} is calculated, employing the wavefunctions (3.7) and (3.24) for the conduction band and the acceptor level, respectively. Here the envelope functions of both wavefunctions are denoted by the following vector forms;

$$f^c_{a,m} = \begin{pmatrix} A_1^c \phi_m \\ A_3^c \phi_{m-1} \\ A_5^c \phi_{m+1} \\ A_7^c \phi_{m+1} \end{pmatrix} \text{ and } f^c_{b,m} = \begin{pmatrix} A_2^c \phi_m \\ A_6^c \phi_{m-1} \\ A_4^c \phi_{m+1} \\ A_8^c \phi_{m-1} \end{pmatrix} \quad (4.37)$$

for the n-th spin-up and -down conduction subbands, respectively[40], while

$$F_a(N,M,\lambda) = f^{lh}_{a,N} P_\lambda(z) e^{-\frac{1}{4}\gamma\varepsilon^2 z^2}$$

and

$$F_b(N,M,\lambda) = f^{lh}_{b,N} P_\lambda(z) e^{-\frac{1}{4}\gamma\varepsilon^2 z^2} \quad (4.38)$$

with

$$f_{a,N}^{lh} = \begin{pmatrix} A_1^{lh}\phi_N \\ A_3^{lh}\phi_{N-1} \\ A_5^{lh}\phi_{N+1} \\ A_7^{lh}\phi_{N+1} \end{pmatrix} \text{ and } f_{b,N}^{lh} = \begin{pmatrix} A_2^{lh}\phi \\ A_6^{lh}\phi_{N-1} \\ A_4^{lh}\phi_{N+1} \\ A_8^{lh}\phi_{N-1} \end{pmatrix} \tag{4.39}$$

for the spin-up and down acceptor levels attached to the Nth light hole subbands, respectively. Assuming that the conduction electrons only populate the lowest two subbands, namely 0^+ and 0^-, the matrix elements are calculated. Four levels of the acceptor are considered; namely, (N. M. λ) = ($\bar{1}\bar{1}0$), ($0\bar{1}0$) with two spin states. The matrix elements M_{all} is given, using the orthonormality of the harmonic oscillator functions ϕ_M, by

$$\begin{aligned} M_{all} &= \sum_{jj'=1}^{8} [\pi_{jj'} \cdot \varepsilon] < f_{s,o}^{c} \mid F_{s,(N,M,0)} > \\ &= \sum_{jj'} [\pi_{jj'} \cdot \varepsilon] \int f_{s,o}^{c*} f_{s,N}^{lh} P_\lambda(z) e^{-\frac{1}{4}\gamma\varepsilon^2 z^2} d^3r \\ &= \sum_{jj'} [\pi_{jj'} \cdot \varepsilon] (f_{s,o}^{c*} f_{s,N}^{lh}) \int P_\lambda(z) e^{-\frac{1}{4}\gamma\varepsilon^2 z^2} d^3r \ . \end{aligned} \tag{4.40}$$

It should be noted that the factor $\int P_\lambda(z) e^{-\frac{1}{4}\gamma\varepsilon^2 z^2} d^3r$ is a nearly common value as far as the transitions considered above are concerned ($\lambda = 0$). If the factor $[\Pi_{jj} \cdot \varepsilon]$ is not sensitive to the values j and j', the transition probability is determined only by $f_{a0}^{c*} f_{aN}^{lh}$. The quantity $f_{s0}^{c*} f_{sN}^{lh}$ will be calculated for several transitions. The value of f is given in Tables 2 and 3 for both conduction band and light hole band. These sets of values were calculated by Pidgeon and Brown(P B), and by Lin-Chung and Henvis(LH). The latter set (Table 3) was obtained at 5 T.

The result is given in Table 4. It is interesting that $f_{b0}^{c*} f_{bo}^{lh}$ of the transition $0^- \rightarrow (0\bar{1}0)^-$ is exactly zero, while $f_{a0}^{c*} f_{a0}^{lh}$ has a small finite value. If holes from the valence bands populate not $(\bar{1}\bar{1}0)$ acceptor level but $(0\bar{1}0)$ level, the conduction electrons in 0^- subband cannot recombine with holes. The probability of recombination is not zero for electrons in 0^+ subband, however. If this situation is the case, our experimental data can be explained. Because of the violation of the assumption that the electron number is conserved, the simple rate equations in Section 4-4 cannot be employed. All in all the lifetime of I_2, so that the spin relaxation time T_1, seems to be independent of lattice temperature. This result agrees with the prediction of Boguslawski[47].

In this experiment of temperature dependence, some peak shifts of C_1 and C_2 were observed. Figure 25 shows the temperature variation of effective masses of 0^+ and 0^- electrons due to their peak shifts. For the temperature range investigated, the change in effective mass was about 2 %. The effective mass increases slightly with temperature. This agrees with the result of Matsuda and Otsuka[13] and is explained in terms of the change in band gap ε_g due to thermal expansion.

4-8) Steady state photoexcitation

So far, the variation of the electron distribution after photoexcitation has been discussed. The electron system generated by photopulse decays through several channels. So the process is very complicated. In order to make analysis easier, a wide pulse xenon flash lamp was employed with the aim of achieving

a steady state excitation condition. Under the steady state condition, the coupled rate equations (4.11)-(4.14), describing the electron transfer, become easy to consider. Under the condition that total electron number does not conserve, a more precise set of rate equations is required. The following coupled rate equations will be considered:

$$\dot{n}_u = G - \left(\frac{1}{\tau_1} + \frac{1}{\tau_6}\right) n_u + \frac{1}{\tau_0} n_d + \frac{1}{\tau_5} N_u = 0, \tag{4.41}$$

$$\dot{n}_d = G - \left(\frac{1}{\tau_0} + \frac{1}{\tau_2} + \frac{1}{\tau_8}\right) n_d + \frac{1}{\tau_7} N_d = 0, \tag{4.42}$$

$$\dot{N}_u = -\left(\frac{1}{\tau_3} + \frac{1}{\tau_5}\right) N_u + \frac{1}{\tau_6} n_u = 0 \tag{4.43}$$

and

$$\dot{N}_d = -\left(\frac{1}{\tau_4} + \frac{1}{\tau_7}\right) N_d + \frac{1}{\tau_8} n_d = 0, \tag{4.44}$$

where n_u and n_d are the electron densities in 0^+- and 0^-- subbands of the conduction band, respectively; G and G' denote the generation rates of elections in unit time at the 0^+ and 0^--subbands, respectively; N_u and N_D are the densities of electrons populating $(000)^+$ and $(000)^-$ donor levels, respectively. The time constants characterize the relevant transitions and their roles are indicated in the schematic diagram of conduction subbands and donor levels (Fig. 26). If the intensity of excitation light is too weak to neutralize all of the acceptors by holes, photoexcited holes mainly populate the acceptor levels and few free holes populate the valence band. The lifetimes τ_1 and τ_2 are determined by the conduction electron-acceptor hole

recombination. The time constant of donor-acceptor recombination is so large that we may put τ_5, $\tau_7 << \tau_3$, τ_4. The terms including τ_3 and τ_4, therefore, can be neglected and eqs.(4.43) and (4.44) are rewritten

$$\dot{N}_u = -\frac{N_u}{\tau_5} + \frac{n_u}{\tau_6} = 0 \tag{4.45}$$

and

$$\dot{N}_d = -\frac{N_d}{\tau_7} + \frac{n_d}{\tau_8} = 0 \quad . \tag{4.46}$$

Then we have

$$\frac{n_u}{N_u} = \frac{\tau_6}{\tau_5} \tag{4.47}$$

and

$$\frac{n_d}{N_d} = \frac{\tau_8}{\tau_7} \quad . \tag{4.48}$$

Substituting eqs.(4.47) and (4.48) to eqs.(4.41) and (4.42), respectively, one obtains

$$\dot{n}_u = G - \frac{n_d}{\tau_1} + \frac{n_u}{\tau_0} = 0 \tag{4.49}$$

and

$$\dot{n}_d = G' - \left(\frac{1}{\tau_0} + \frac{1}{\tau_2}\right) n_d = 0 \quad . \tag{4.50}$$

From eq.(4.50), n_d has the following expression,

$$n_d = \tau^* G' \tag{4.51}$$

with

$$\frac{1}{\tau^*} = \frac{1}{\tau_0} + \frac{1}{\tau_2} \tag{4.52}$$

Substituting eq.(4.59) to eq.(4.49), we get

$$n_u = \left(G + \frac{\tau^*}{\tau_0} G' \right) \tau_1 \quad . \tag{4.53}$$

From eqs.(4.51) and (4.53), the population ratio can be written

$$\frac{n_d}{n_u} = \frac{G'}{\tau_1 (G/\tau^* + G'/\tau_0)} \quad . \tag{4.54}$$

Assuming that the electron number generated by light is equal in both subbands, i.e., $G = G'$, eq.(4.54) becomes

$$\frac{n_d}{n_u} = \left[\tau_1 \left(\frac{1}{\tau^*} + \frac{1}{\tau_0} \right) \right]^{-1} \quad . \tag{4.55}$$

The ratio n_d/n_u does not depend on the excitation intensity. From the result of the measurement of temperature dependence, the inequality $\tau_1, \tau_0 << \tau_2$ is found to hold, so that $\tau^* \approx \tau_0$; one thus arrives at the relation

$$\frac{n_d}{n_u} = \frac{\tau_0}{2\tau_1} \quad . \tag{4.56}$$

The population ratio n_d/n_u is derived from the ratio of the absorption intensity I_2/I_1. In the steady state condition, the measurement of the ratio I_2/I_1 gives the ratio of the time constant $\tau_0/2\tau_1$.

Before entering in the discussion of the absorption intensity at the steady state excitation, it should be confirmed that the steady state for the photoexcited electron system is actually established by means of a wide width xenon flash lamp with 10 μs FWHM. Figure 27 shows the time variation of the absorption intentisies I_D, I_1 and I_2. The delay time is measured from the

start of the photopulse. By taking the FWHM of a photopulse over the range of delay time between 2 μs and 11 μs, effectively steady state is realized. It is noted that I_2 is nearly constant over this time range. This behavior is quite different from the time variation of I_2 obtained out of the shorter excitation pulse (see Fig. 9). The absorption intensities I_D and I_1 are also considered constant approximately. So the steady state excitation seems to be practically established during the photopulse. From now on, the absorption in steady state will be meant by the absorption signal at 8 μs after the beginning of the wide photopulse.

In Fig. 28, the excitation intensity dependence of the absorption intensity is shown for I_D, I_1 and I_2. Under weak excitation, these three intensities are found to be linear functions of the excitation intensity. The linearity of these intensities is deduced from eqs.(4.51) and (4.53). If one photon absorption is the main generation channel of electrons, the generation rates G and G' are proportional to the excitation intensity I_{ex}. The relation between G and I_{ex} is written down as[66]

$$G = \frac{1}{\hbar\omega} [K_1 (1 - R) I_{ex}] , \qquad (4.57)$$

where R is the reflectivity of the material (0.36 for InSb) and K_1 is the coefficient for the one photon magneto-absorption and $\hbar\omega$ is the photon energy of the xenon flash lamp. The xenon lamp has a continuous spectrum and several line spectra. The 1.06 μm line is most effective to generate electrons in InSb, so that we may take $\hbar\omega = 1.17$ eV. Littler et al[66]. obtained

the value $K_1 = 1.3 \times 10^{-3}$ cm^{-1} from the two photon resonant photo-Hall measurement. Taking these parameter values, the relation (4.57) between G and I_{ex} becomes

$$G = 4.44 \times 10^{8} \; I_{ex} \; . \tag{4.58}$$

Now using the relation (4.58) to eqs.(4.51) and (4.53) with obtained values of n_d and n_u, the relation of τ^*, τ_1 and τ_0 can be obtained. One should keep it in mind, however, that a considerable uncertainty exists in the estimate of $n_{u,d}$ and I_{ex}.

Then we will treat the ratio (n_d/n_u) and (n_u/N_u). The linear dependence of n_d, n_u and N_u on I_{ex} yields

$$\frac{n_d}{n_u} = \frac{I_2}{I_1} = 0.27 \tag{4.59}$$

and

$$\frac{n_u}{N_u} = \frac{I_1}{I_D} = 1.3 \tag{4.60}$$

Here the numerals are constants derived from the ratio of slopes in Fig. 28. Using eqs.(4.47) and (4.55), the following relations are obtained;

$$\tau_6 = 1.3 \, \tau_5 \tag{4.61}$$

and

$$\tau_0 = 0.54 \, \tau_1 \; . \tag{4.62}$$

The time constant τ_0 is nothing but the spin relaxation time T_1. Substituting 3.5 μs (obtained in the preceding section) to τ_0, τ_1 is found to be = 6.5 μs. It has been obtained by Littler et al.

that $\tau_5 \sim 14$ μs by means of thermal excitation. Applying those values summarized in Table 5 to the rate equations (4.41)-(4.44), we tried to predict the experimental decay curves. The result is shown in Fig. 29. Here we have put $\tau_9 = 10$ μs. This shows fairly good agreement to the experimental result shown in Fig. 8. Here we assumed that $\tau_5 = \tau_7$ and $\tau_6 \simeq \tau_8$. Furthermore, it is noticed that the first rising of I_D can be reproduced.

4-9) Donor-acceptor recombination

We have mentioned the magnetooptical absorption of donor electron(ICR). The absorption peak ICR can be observed for a long period in samples A and C once the sample is illuminated. If the decay curve of the absorption signal due to donor electrons is assumed to be exponential, the time constant amounts to several milliseconds. This slow decay process can be interpreted in terms of the donor-acceptor recombination. The absorption signal of ICR does not always have such a long time constant. The long tail in time of ICR was mainly observed in sample A.

A resonance signal having a long time constant was also observed in sample C as shown in Fig. 30 by an arrow. Here we employed 172 μm laser line as the prove of cyclotron resonance. The signal is shown till only 200 μs after the photopulse. The time variation of this peak is traced in Fig. 31 for longer period by means of the gate scan technique (shown by solid circle). The decay process initially is not exponential. After 1 millisecond, however, regarding it as exponential (shown by solid line in Fig. 31) is fairly good approximation. The time constant there is found to be 7.0 milliseconds. This value is quite the

same as that of the donor electron system observed in sample A (see Fig. 6).

It is true that this absorption peak is caused by photo-excitation but cannot be considered due to free carriers. Then, to survey the magnetic field dependence of the peak positions, we took the absorption signals employing eight laser lines having their wavelengths between 84 and 220 μm. The obtained resonance peaks are shown in Fig. 32. Here open triangles are the peaks associated with free and bound electrons (that is ICR and C_1) while open circles are considered as the resonance of free holes. The solid circles are new peaks that appear only in p-type samples, having long lifetimes. These peaks are considered to originate from holes bound to acceptors. Several authors[60-63] have studied the acceptor levels and observed transitions having energy between 5 and 9 meV. They are considered the transitions from the acceptor ground level to higher excited levels. Kaplan[60] obtained the optical excitation spectra of Zn, Cd and Ag acceptors in p-InSb by means of the Fourier transform spectroscopic technique. This result is shown in Fig. 33 with schematic diagram of acceptor levels. Here observed resonance positions are indicated by dots as a function of magnetic field. These peaks are divided into three series. They are called C, D and G according to the Ge nomenclature[67], which correspond to the transitions from the ground state $1S_{3/2}$ to the excited states $2P_{5/2}\Gamma_7$, $2P_{5/2}\Gamma_8$ and $2P_{3/2}$, respectively (shown the diagram in Fig. 33 as an inset). The open triangles α, β and γ indicate the resonance points for 171, 163 and 146 μm laser lines, respectively. It is strongly suggested that these points correspond

to the transitions C or D series. So they are expected to yield the information of the acceptor ground state.

Observation of the bound hole signals corresponds to the study of the donor-acceptor pair recombination from the acceptor side. So it is not strange that the time constant of this signal agrees with that of the donor electron. The absorption signal of acceptors in p-type material is a convenient tool since the donor signal in n-type is strongly overlapped by the conduction electron signal just after the photopulse under strong photo-excitation (mentioned in Section 4-1). In Fig. 34, the calculated decay curves of the neutral impurity density are shown for several values of W_{max}. These are derived from eqs.(3.58) and (3.59), using the parameter values of $N_A = N_D = 1 \times 10^{14}$ cm^{-3} and $a_B = 500$ Å. The calculated curves are appropriate for samples with large compensation rates, say for samples C and A. The solid circles show the experimental values for sample C (shown in Fig. 34). They show a fairly good agreement with a calculated curve if its W_{max} value is taken 7.5×10^4 s^{-1}. For the decay curve of donor electron in sample A (shown in Fig. 6), the theory of Thomas et al.[49] cannot be applied to fit the whole observed time range because of the intervention of the conduction electron contribution. Choosing the signal at 0.1 ms for the standard of intensity, however, the decay curve of sample A agrees with that of sample C (solid circles in Fig. 31). The donor concentration of sample A is twice as large as that of sample C. It thus seems that the decay curve does not very strongly depend on the impurity concentration.

The quantity W_{max} is the sole adjustable parameter in the

theory of Thomas et al.[49] It shows the strength of the recombination probability, and is a characteristic value for each material. It is expected to depend on the impurity state but is seemingly independent of the impurity concentration. For GaP, Thomas et al. have chosen 5×10^5 s^{-1} for W_{max} from the fitting of the time resolved luminescence data. Ohyama[68] obtained 5×10^7 s^{-1} as the W_{max} for GaAs in the cyclotron absorption measurement. Our value $\sim 8 \times 10^4$ s^{-1} for InSb is smaller than those for GaP and GaAs. From eq.(3.56), one can see that W_{max} means the recombination probability for unit time at $r = 0$, i.e., the probability on the acceptor impurity which is thought to be a point in the theory by Thomas et al. The binding energy of the donor electron for the three materials, GaP, GaAs and InSb, are 40, 5 and 1 meV, respectively, so that the extent of the donor electron in InSb is the largest of all. Taking a normalized wave function in InSb at a given point r must be the smallest in the three materials. The strength of the recombination probability on the acceptor, W_{max}, is proportional to the squared modulus of the donor wave function (see eq.(3.52)) at that point. This is the reason why W_{max} of InSb is smaller than other two materials.

The recombination probability W(r) depends on the binding energy of the impurity (see eq.(3.56)). It seems that the behavior of the time variation of donor or acceptor absorption signal depends on the binding energy of impurity. In InSb, it is well known that the effect of the magnetic freeze-out occurs at a relatively weak magnetic field.[69] In other words, a large variation in donor binding energy occurs as a magnetic field

is applied. It is accordingly expected that a large variation may be observed in the decay profile of the donor electron (or acceptor hole) signal, if one changes the resonance magnetic field in the cyclotron absorption measurement. In Fig. 35, the cyclotron absorption traces of sample C are demonstrated using 146, 163 and 171 μm laser lines. The three resonance peaks denoted by α, β and γ correspond to the same transition peaks between acceptor levels in Figs. 32 and 33. The resonance fields of the peaks α, β and γ are ~0, 2.74 and 3.36 T, respectively. The time variations of the intensities of α, β and γ peaks are shown in Fig. 36. The difference in the initial intensities between α and β, γ is not important.

The relative variation in each absorption intensity vs. delay time curve should be noted. After an appropriate delay time (~400 μs), each absorption intensity can be considered to decrease exponentially. Fitting these three decay curves with exponentials, the following values are obtained as the time constants; namely, $\tau_1 = 2.09$ ms (for 171 μm), $\tau_2 = 1.52$ ms (for 163 μm), and $\tau_3 = 1.41$ ms (146 μm). These time constants are plotted against the parameter γ in Fig. 37. Here γ is the ratio between the zero point energy due to magnetic field ($\hbar\omega_c/2$) and the donor binding energy. This figure, therefore, shows the dependence of the decay constant on the donor binding energy. It is found that the time constant decreases linearly as γ increases. To explain the behavior of the time constant, we also consider the form of the recombination rate (given by eq.(3.56)) more accurately for an individual donor-acceptor pair. According to the Adams et al.[70], the recombination rate W(r) is

written with the following form:

$$W(r) = \frac{4e^2 n \hbar\omega}{m_e^{*2}\hbar^2 c^3} |M_{cv}|^2 I^2 , \qquad (4.63)$$

where r denotes the separation between a donor and an acceptor, n the refractive index and I the overlap integral between donor and acceptor wavefunctions that is calculated by Kamiya and Wagner.[71] The expression of I is given by

$$I = [\pi(a_A a_D)^{3/2}]^{-1} \int \exp\left(-\frac{x}{a_A} - \frac{|\vec{x}-\vec{r}|}{a_D}\right) d^3x$$

$$= \frac{8\alpha^{3/2}}{(\alpha^2-1)^3 \rho} \left\{ \exp(-\alpha\rho)[\rho(\alpha^2-1)+4\alpha \right.$$

$$\left. + \exp(-\rho)[\rho\alpha(\alpha^2-1)-4\alpha] \right\} \qquad (4.64)$$

with

$$\alpha = (a_A/a_D) \quad \text{and} \quad \rho = (R/a_A) . \qquad (4.65)$$

Here a_A and a_D are the effective Bohr radii of the acceptor and the donor, respectively. Using this expression of W(R), we will estimate the effect of magnetic field on W(r). In W(r), the treatment of the optical matrix element factor $|M|^2$ in magnetic field is difficult. If the treatment of Thomas et al. still holds, however, M is proportional to the donor wavefunction $\psi(r)$. As $\psi(r)$ is considered to shrink by application of magnetic field, M(r) becomes smaller with increasing magnetic field. The diminishing of M(r) due to the magnetic field makes the

recombination rate W(R) smaller. Then one is apt to think that the time constant gets larger. Obviously the experimental result is in the reverse direction. We have to treat the case more carefully.

Let us consider the effect of magnetic field on the overlap integral I. In InSb, it is accepted that the binding energy of the acceptor ground state is 8 - 9 meV from the top of the valence band. It is reasonable to assume that this binding energy is independent of magnetic field, since the hole mass is so heavy that the condition $\gamma << 1$ is realized. The overlap integral I is considered as a function of R and a_D. In Fig. 38, I is plotted against $\alpha = (a_A/a_D)$ for several values of ρ. Here the acceptor binding energy is fixed at 8 meV ($a_A \simeq 55$ Å). Out of the four curves of I, three with $\rho \leq 5$ increase first with increasing α. The curve for $\rho = 1$ increases monotonically in the shown range of α, while the two curves with $\rho = 3$ and 5 have maxima. The last curve with $\rho = 10$ is a monotonically decreasing function of α. The increase of the overlap integral I means that the recombination probability becomes larger, so that the time constant is diminished. Increasing the magnetic dield up to 5 T, the binding energy of the donor electron increases and reaches ~3 meV at 5 T. So, if ρ is equal or less than about 3, I is regarded as an increasing function of magnetic field and may explain our experimental data. Assuming the homogeneous spatial distribution of impurities, one obtains a value of order ten for α, by employing the relation

$$R = \left\{ \frac{3}{4\pi} \frac{1}{N_{min}} \right\}^{1/3} \quad \text{with} \quad N_{min} = \min(N_A, N_D) \tag{4.66}$$

where N_A and N_D are the densities of donors and acceptors, respectively. Putting $N_A = N_D \sim 1 \times 10^{14}$ cm^{-3}, one obtains 1.3×10^{-5} cm as r and then ρ attains to about 20. By taking this value of ρ, W(r) becomes a decreasing function of magnetic field. This is a contradiction to the experimental result. There may exist such clustering as to make the average pairing distance between donor-acceptor pair is so small that ρ becomes less than ~5. If we are observing the contribution from such a region, the time constant would become smaller with increasing magnetic field.

5. Discussions

In Table 6, the spin relaxation times T_1 obtained from previous experiments are shown. The data denoted by A was obtained by Nguyen et al.[72] by measuring the saturation of the four-wave mixing process. B is the results of Pascher et al.[73] by measuring the spin flip Raman intensity with two Q-switched CO laser pulse. The results denoted C were deduced from a time-resolved observation of electrical conductivity following a stimulated spin-flip Raman pulse by Grisar et al.[74] The value of D was obtained by Brueck and Mooradian[75] with using a double pulse spin-flip laser technique.

All the obtained values as T_1 are smaller than ours by one or two orders. It should be noted in Table 6 that all the results except ours were obtained from n-type materials and impurity concentrations of these samples are larger than 10^{15} cm^{-3}. These values are the excess donor concentrations, i.e., $N_D - N_A$ the absolute donor concentrations being larger than them. The impurity concentration of our sample C (1×10^{14} cm^{-3}) is by one or two orders smaller than the concentrations of samples employed in previous experiments. This is the main reason why our resultant spin relaxation time is much larger than the previous experimental values. Let us then compare the previous results with ours for the same impurity concentration. Remebering that T_1 is inversely proportionally to donor concentration N_D and putting $N_D = 1 \times 10^{14}$ cm^{-3} for all the previous works, we will calculate T_1 due to ionized impurity scatterings. For example, T_1 of Pascher et al. (denoted B) is 30 times as large as the original value. The new value of ~3 μs agrees well with our

result. In previous works (A - D) it was stated that the spin flip transition is caused by ionized impurity scatterings. No authors, however, estimated the absolute impurity concentration. So there remained an ambiguity in determining what the main contribution is to the spin flip transition. In our experiments, on the other hand, the absolute donor concentration could be estimated from the absorption measurement with varying photo-excitation intensity. The excitation dependence of T_1 was also deduced.

From Fig. 23, one can see that T_1 has quite the same values for samples C and D. The acceptor concentration of sample D is twice as large as that of sample C. So the effect of acceptors seems to be much less than that of donors. This result agrees with the prediction of Blatt.[76)]

The main contribution to the spin relaxation is considered to be ionized impurity scatterings and our results show a fairly good agreement with the theory of Boguslawski.[47)] We employ the Debye Hückel screening length for the ionized impurity scattering. This may cause an overestimate because of the shrinking of the impurity wavefunction due to the presence of magnetic field. But, employing the shrinking donor wavefunction, the screening length becomes smaller and T_1 becomes longer than the value shown in the previous calculation (6 μs). This makes a difference between the experimental and theoretical values larger, and suggests some problem to be improved.

In the preceeding section, we estimated ~7 μs as τ_1, that is, the time constant of the transition between 0^+ subband and the

acceptor level by the experiment of steady state excitation. The time constant of this transition was given by Dumke[77] in the absence of magnetic field; namely,

$$\frac{1}{\tau_1} = \left(\frac{1}{\tau_1^0}\right) \Gamma(T)$$

with

$$\frac{1}{\tau_1^0} = 64\sqrt{2}\pi n \frac{e^2\hbar^2\omega |K|_{av}^2}{c^3 m_e^{*2} (m_A E_A)^{3/2}} N_A ,$$

where $\Gamma(T)$ is a temperature dependent numerical factor that is of the order of unity at helium temperatures, K is a momentum matrix element and n is a refractive index. m_A, E_A and N_A are the hole effective mass, binding energy and concentration of acceptor impurities. To fit our experimental condition, these parameters are chosen as follows:

$$m_A = 0.186\, m_0 \quad , \quad E_A = 8\, meV$$

and

$$\frac{2m}{\hbar^2} |K|^2 = 22\, eV .$$

One obtains 0.3 μs in the temperature range between 4 - 20 K as τ_1. This is about ten times smaller than our experimental value. Such a big difference is considered to be due to the shrinking of wavefunctions caused by magnetic field.

For other time constants characterized in each transition (see Fig. 27), no other experimental values to compare with ours are available.

6. Conclusions

We have observed the time variation of the photoexcited cyclotron absorption in the wide range between several microseconds and several milliseconds for InSb. The signals of electrons in p-type have been observed with emphasis. The decay of photoexcited electrons is, roughly speaking, divided into three stages. In first stage, a rapid decrease in absorption signal due to the direct recombination of conduction electrons with free holes is observed after a strong excitation. In second stage, transitions of electrons are affected strongly by their spin states. Especially, depopulation of electrons in 0^- subband is strongly curbed, since their spin flippings are the bottle neck of the relaxation process to lower energy levels. The spin flip transition from 0^- to 0^+ subband is mainly caused by ionized impurity scatterings. But the contribution of electron-electron scatterings and neutral impurity scatterings cannot be neglected. In contrast with of the reasonably fast recombination from 0^+ subband to acceptor level, the recombination from 0^- subband to acceptor level seems to be nearly forbidden.

For other transitions within the system consisting of 0^+ and 0^- subbands with attached donor levels, the time constants are determined by numerical calculation.

In the final stage, the donor-acceptor recombination plays the main role. This recombination could be observed either from the donor or from the acceptor side. The time variation of this recombination is affected by a magnetic field. This influence is probably caused by the effect of magnetic field on the overlap integral part in the recombination probability.

References

1) R. Ulbrich: Phys. Rev. B8 5719 (1973).

2) E.J. Ryder and W. Shockley: Phys. Rev. 81 139 (1951).

3) E.J. Ryder: Phys. Rev. 90 766 (1953).

3) E.M. Conwell: High Field Transport in Semiconductors
Academic press, 1967, New York.
C.Jacoboni and L. Reggiani: Adv. Phys. 28 493 (1979).
G. Bauer: Linear and Nonlinear Transport in Solids
edited by J.T. Devreese and V.E. Van Doren
(Plenum, New York, 1976).

4) K.L.I. Kobayashi, K.F. Komatsubara and E. Otsuka:
Phys. Rev. Lett. 30 702 (1973).

5) E. Gornik: Phys. Rev. Lett. 29 595 (1972).

6) W. Müller, F. Kohl, H. Partl and E. Gornik:
Solid State Electron. 21 235 (1978).

7) K. Shimomae, Y. Hirose and C. Hamaguchi:
J. Phys. C Solid State Phys. 14 5151 (1981).

8) W. Zawadzki, G. Bauer, W. Racek and H. Kahlert:
Phys. Rev. Lett. 35 1098 (1975).

9) M. Glicksman and M.C. Steele: Phys. Rev. 110 1204 (1958).

10) B.T. Moore, D.G. Seiler and H. Kahlert:
Solid State Electron 21 247 (1978).

11) M.S. Bresler, O.B. Gusev and A.O. Stepanov:
Fiz. Tekh. Poluprovodn. 17 1195 (1983);
translation Sov. Phys. Semicond. 17 755 (1983).

12) K.L.I. Kobayashi and E. Otsuka: J. Phys. Chem. Solids
35 839 (1974).

13) O. Matsuda and E. Otsuka: J. Phys. Chem. Solids 40 809 (1979); J. Phys. Chem. Solids 40 819 (1979).

14) T. Kurosawa: J. Phys. Soc. Jpn. 20 937 (1965)
E. Yamada and T. Kurosawa: J. Phys. Soc. Jpn. 36 603 (1973).

15) B.K. Ridley and J.J. Harris: J. Phys. C Solid State Phys. 9 991 (1976).

16) E. Otsuka, T.Ohyama and K.Fujii: J.de Phys. C7 393 (1981)

17) Y.B. Levinson: Solid State Electron. 21 923 (1978).

18) L.I. Glazman: Zh. Eksp. Teor. Fiz. 80 349 (1981); translation Sov. Phys. JETP 53 178 (1981).

19) C. Lewiner, D. Calecki and N. Pottier: Phys. Rev. B18 6348 (1978).

20) D. Calecki and N. Pottier: Solid State Electron. 22 999 (1979).

21) N. Pottier and D. Calecki: Phys. Rev. B22 3949 (1980).

22) H. Nakata and E. Otsuka: Appl. Phys. B27 2105 (1982).

23) E.O. Kane: J. Phys. Chem. Solids 1 249 (1957).

24) R. Bowers and Y. Yafet: Phys. Rev. 115 1165 (1959).

25) Y. Yafet: Phys. Rev. 115 1172 (1959).

26) C.R. Pidgeon and R.N. Brown: Phys. Rev. 146 575 (1975).

27) P. Kackman and W. Zawadzki: Phys. Stat. Sol. (b) 47 629 (1971).

28) W. Zawadzki: New Developments in Semiconductors edited by P. Wallice, R. Harris and M.J. Zuckermann (Noordhoff International Publishing Leyden p441, 1973).

29) J.M. Luttinger and W. Kohn: Phys. Rev. 97 869 (1955).

30) R. Ranvaud, H.R. Trebin, V. Roessler and F.M. Pollak: Phys. Rev. B20 701 (1979).

31) R. Grisar: Solid State Commun. 25 1023 (1978).

32) Al.L. Efros, L.M. Kanskaya, S.I. Kokhanovskii and R.P. Seysyan: Solid State Commun. 43 613 (1982).

33) T. Ohyama, K. Fujii and E. Otsuka: Jpn. J. Appl. Phys. 21 865 (1982).

34) M.W. Goodwin and D.G. Seiler: Phys. Rev. B27 3451 (1983).

35) M.H. Weiler: J. Magn. Magn. Materials 11 131 (1979).

36) K. Suzuki, M. Okazaki and H. Hasegawa: J. Phys. Soc. Jpn. 19 930 (1964).

37) N.O. Lipari and A. Baldereschi: Phys. Rev. Lett. 25 1660 (1970).

38) A. Baldereschi and N.O. Lipari: Phys. Rev. B8 2697 (1973).

39) A. Baldereschi and N.O. Lipari: Phys. Rev. B9 1525 (1974).

40) P.J. Lin-Chung and B.W. Henvis: Phys. Rev. B12 630 (1975).

41) W. Zawadzki and J. Wlasak: Proc. Int. Conf. on Applic of High Magn. Field in Semicond. Phys. ed. J.F. Ryan, Oxford, 1978 p384

42) W. Zawadzki and J. Wlasak: Theoretical Aspects and New Developments in Magneto-Optics (NATO Adv. Study inst. B60 p347, 1979) ed. J.T. Devreese (Plenum Press New York).

43) C.L. Littler, D.G. Seiler, R. Kaplan and R.J. Wagner: Phys. Rev. B27 7474 (1983).

44) R.F. Wallis and H.J. Bowlden: J. Phys. Chem. Solids 7 78 (1958).

45) R.J. Eliott: Phys. Rev. 96 266 (1954).

46) W. Szymánska, P. Boguslawski and W. Zawadzki: Phys. State. Sol. (b) 65 641 (1974).

47) P. Boguslawski and W. Zawadzki: J. Phys. C: Solid State 13 3933 (1980).

48) G.L. Bir and G.E. Pikus: Fiz. Tverd. Tela 2 2287 (1960) Translated Symmetry and Deformation Effects in Semiconductors (Moscow; Nauka) 1972.

49) D.G. Thomas, J.J. Hopfield and W.M. Augustyniak: Phys. Rev. 140 A202 (1965).

50) R. Kaplan: Proc. VIII Int. Conf. Phys. Semicond., Kyoto, J. Phys. Soc. Jpn. 21 Supplement, 249 (1966).

51) K.J. Button, B. Lax and C.C. Bradley: Phys. Rev. Lett. 21 350 (1968).

52) S.P. Li, W.F. Love and S.C. Miller: Phys. Rev. 162 728 (1967).

53) T. Sanada, K. Matsushita, T. Ohyama and E. Otsuka: J. Phys. Soc. Jpn. 45 501 (1978).

54) H.J. Fossum and B. Ancker-Johnson: Phys. Rev. B8 2850 (1973).

55) E.H. Putley: InSb Submillimeter Photoconductive Detector (Semiconductors and Semimetals 12 143 (1977) ed. R.K. Willardson and A.C. Beer, Academic Press).

56) A. Raymond, J.L. Robert, W. Zawadzki and J. Wlasak: J. Phys. C: Solid State Phys. 17 2381 (1984).

57) E. Gornik, T.Y. Chang, T.J. Bridges, V.T. Nguyen and J.D. McGee: Phys. Rev. Lett. 40 1151 (1978).

58) E. Otsuka: J. Phys. Soc. Jpn. 50 2631 (1981)

59) P. Boguslawski: Solid State Commun. 33 389 (1980).

60) R. Kaplan: Solid State Commun. 12 191 (1973).

61) V.N. Murzin, A.I. Demeshina and L.M. Uwarov: Fiz. Tekh. Poluprov. 6 488 (1972); translation Sov.Phys. Semicond. 6 419 (1972).

62) R. Meisels and F. Kuchar: Phys. Stat. Sol. (b) 116 557 (1983).

63) G. Bauer: in Springer Tracts in Modern Physics (Springer, New York, 1974) vol.74, p12.

64) M. Lax: J. Phys. Chem. Solids 8 66 (1959).

65) L.M. Roth, B. Lax and S. Zwerdling: Phys. Rev. 114 90 (1959).

66) C.L. Littler, D.G. Seiler and S.W. McClure: Solid State Commun. 50 565 (1984).

67) R.L. Jones and R.P. Fisher: J. Phys. Chem. Solids 26 1125 (1965).

68) T. Ohyama: J. Phys. Soc. Jpn. 51 1431 (1982).

69) Y. Yafet, R.W. Keyes and E.N. Adams: J. Phys. Chem. Solids 1 137 (1956).

70) M.J. Adams and P.T. Landsberg in Gallium Arsenide Lasers, ed. C.H. Gooch (Wiley-Interscience, London, 1969), p5.

71) T. Kamiya and E. Wagner: J. Appl. Phys. 48 1928 (1977).

72) V.T. Nguyen, E.G. Burkhardt and P.A. Wolff: Opt. Commun. 16 145 (1976).

73) H. Pascher, G. Appold, R. Ebert and H.G. Häfele: Opt. Commun. 19 104 (1976)

74) R. Grisar, H. Wachering, G. Bauer and W. Zawadzki: Infrared Phys. 16 149 (1976).

75) S.R.J. Brueck and A. Mooradian: Opt. Commun. 18 539 (1976).

76) F.J. Blatt: J. Phys. Chem. Solids 1 262 (1957).

77) W.P.Dumke: Phys. Rev. 132 1998 (1963).

Figure Captions

Fig. 1 Block diagram of the experimental set-up. Crudely, the system is divided into four parts, i.e., an FIR-laser, a cryostat containing a superconducting magnet, an excitation light source and a detecting system. Two kinds of detecting system are employed alternatively. One consists of two conventional boxcar integrators (a) and the other a novel multi-channel system using a digital boxcar and transient memory (b).

Fig. 2 Typical absorption signals for sample A in the cyclotron resonance measurement. To illustrate the optical modulation technique, an absorption signal in the thermal equilibrium, that in the photoexcitation and the modulation signal are shown in (a), (b) and (c), respectively.

Fig. 3 Variational parameter ε as a function of $\gamma = \hbar\omega_c/(2R_y^*)$ for the high field impurity states associated with the light-hole of Landau subband series in InSb. These were calculated in ref. 40. For the impurity states associated with the b-series, a quite similar result has been obtained.

Fig. 4 Landau fan for the light hole band vs magnetic field obtained by a calculation based on the manner of Pidgeon and Brown with our valence band parameters in ref. 33 . The numeral with + or - sign on each curve denotes the quantum state for each subband.

The numbers denote the Landau quantum numbers obtained in the coupled band scheme and the symbols $\pm$ indicate the spin states. The vertical arrows indicate the resonance fields for 119 μm laser line.

Fig. 5 Variation of the absorption signals of sample B at the use of 84 μm laser line under a strong excitation. The absorption peak of light hole appears just after photoexcitation. The peak denoted by ICR corresponds to the donor electron transition. C_1 and C_2 denote the resonance peaks of the transitions from the two lowest Landau subbands with opposite spin states.

Fig. 6 Decrease of the absorption intensity at the resonance field of ICR (1.66 T for 119 μm laser line) is plotted against delay time after photoexcitation. The decay curve can crudely be divided into two exponential curves having 1.5 μs and 2.4 ms as time constants.

Fig. 7 A series of time resolution traces for sample B under weak excitation.

Fig. 8 A series of time resolution traces for sample C under weak excitation.

Fig. 9 Time variation of each integrated absorption intensity derived from the series of time variation traces for sample C shown in Fig. 8. I_D, I_1 and I_2 indicate the intensities of ICR, C_1 and C_2 resonance peaks, respectively.

Fig. 10 Lattice temperature variation of absorption signals in thermal equilibrium obtained by Matsuda and Otsuka. This set of traces was employed to estimate of effective temperature T_E^{DC} for the photoexcited case.

Fig. 11 The quantity $n_u(N_D - N_D^0)/N_D^0$ derived from the absorption signals shown in Fig. 10 is plotted against the inverse lattice temperature (shown as open circle). The broken line indicates the best fit of experimental data to eq.(4.3). From the fitting, values of N_c^* and ε_d are obtained.

Fig. 12 The effective electron temperatures T_E^{CC} and T_E^{DC} in sample C vs delay time after photoexcitation determined from eqs.(4.2) and (4.8).

Fig. 13 Ratio of the right to the left half widths at the half maximum for C_1 peak of illuminated sample C is plotted as a function of delay time. The solid bar in the upper part at 0 μs denotes the range of the same ratio of C_1 in the electric field excitation case.

Fig. 14 A simple schematic diagram of the Landau subbands in the conduction band with attached donor levels under the assumption that electrons are conserved above the donor level. τ_1, τ_2 and τ_3 denote the time constants of the transition from 0^- to 0^+ subbands, and those from the Landau subbands 0^+ and 0^- to donor levels $(000)^+$ and $(000)^-$, respectively.

Fig. 15 Spin relaxation time due to ionized impurity scatterings is plotted as a function of inverse intrasubband electron temperature calculated by Boguslawski with appropriate parameters.

Fig. 16 Spin relaxation time due to neutral impurity scatterings as calculated with eq.(4.27).

Fig. 17 A series of absorption curves in the cyclotron resonance measurement of sample C under a medium excitation by means of a multichannel time resolution system. The time interval between adjacent absorption curves is 1 μs.

Fig. 18 The time constant τ_{21} of the absorption intensity ratio (I_2/I_1) is plotted as a function of excitation intensity I_{ex} at delay time 2 μs (in upper half). This I_{ex} is the value just before light entering the sample. In the lower half, the absorption intensity I_D of ICR is denoted by open triangles and the intensity of the sum of I_1 and I_2 by open circles. The intensity I_D of ICR saturates with the increase of I_{ex}. The extrapolated value corresponds to the absorption intensity contributed by all the donor impurities and is denoted by I_D°. The donor density in sample C is 1×10^{14} cm^{-3}, so I_D° corresponds to the donor density 1×10^{14} cm^{-3}. The ionized donor intensity I_D^+ is deduced from the relation $I_D^+ = I_D^\circ - I_D$ (shown as dotted line).

Fig. 19 Inverse effective density of scattering centers N is plotted against excitation intensity. This quantity is proportional to the spin relaxation time T_1. Choosing appropriate values for a, b and c, we find that there appears a maximum.

Fig. 20 A series of absorption curves for sample D under the same excitation condition as for sample C in Fig. 9.

Fig. 21 A series of absorption curves for sample E under the same excitation condition for sample C in Fig. 9. Even at just after photoexcitation, the intensity I_2 for C_2 is very small.

Fig. 22 Time variations of the intensity ratio (I_2/I_1) for samples C, D and E. The behavior of the ratio for sample E differs from that for other two samples.

Fig. 23 The time constant τ_{21} of the ratio (I_2/I_1) is plotted against inverse donor concentration. The solid line is deduced from the calculation of spin relaxation time due to ionized impurity scatterings based on the theory of Boguslawski.

Fig. 24 The temperature dependence of the time constans τ_{tot}, τ_D, τ_1 and τ_2 of the absorption intensities I_{tot}, I_D, I_1 and I_2, respectively. I_{tot} is given by the relation $I_{tot} = I_D + I_1 + I_2$.

Fig. 25 Temperature dependence of the effective masses of the electrons belonging to the 0^+- and 0^-- subbands.

Both effective masses increase slightly as temperature increases.

Fig. 26 Schematic diagram of the conduction band and associated donor levels. In contrast with the diagram shown in Fig. 14, all the possible transitions are described in terms of their characteristic time constants.

Fig. 27 Time variation of each absorption intensity of sample C under excitation by a wide width lightpulse. The shape of the photopulse is shown in the upper side. In this pulse, the absorption intensities I_D, I_1 and I_2 may be regarded constant.

Fig. 28 Absorption intensities I_D, I_1 and I_2 under quasi-steady state excitation are plotted against excitation intensity. Under weak excitation, these intensities increase linearly with increasing excitation intensity.

Fig. 29 Result of the numerical calculation for the decay of intensities I_1, I_2 and I_D obtained by solving the coupled rate equations (4.21 - 4.44) with the parameters given in Table 5.

Fig. 30 The cyclotron absorption signals of sample C using 172 μm laser line. A new absorption peak appears as denoted by a vertical arrow, in addition to the usual electron peaks. The decay of this peak is very slow. Its presence can be confirmed even at several milliseconds after photopulse.

Fig. 31 Time variation of the new peak in Fig. 30. After ~100 μs, the decay curve can be fitted by exponential. The time constant is as large as 7 ms.

Fig. 32 Transition energy plotted against resonant magnetic field. Open triangles are related to the conduction electron transitions, while open circles to the light hole transitions. Solid circles indicate the transitions corresponding to the unknown peak that appeared in p-type material (sample C).

Fig. 33 The experimental results of Kaplan are shown by dots. The inset shows the energy diagram of acceptor levels. The series of resonance peaks C, D and G correspond to the transitions shown in the inset. The open triangles α, β and γ are the resonance peaks obtained in our experiment, corresponding to the transition energies of 7.2, 7.6 and 8.5 meV, respectively.

Fig. 34 Time variation of the intensity due to the transition denoted by α in Fig. 33 (solid circles). The series of solid lines are the result of the calculation by Thomas et al. with various values of W_{max}. The line with 7.5×10^4 as W_{max} is in a fairly good agreement with the experimental data.

Fig. 35 Absorption signals for 146, 163 and 171 μm laser lines. A new peak is denoted α, β and γ with arrow for each laser wavelength.

Fig. 36 Time variation of the intensities for α, β and γ peaks shown in Fig. 35. Assuming the decay curves after 250 μs as exponential, the time constant for each curve is obtained as to be shown in Fig. 37.

Fig. 37 The resultant time constant for the acceptor associated transitions α, β and γ is plotted against the parameter $\gamma = \hbar\omega_c/2R_y^*$. This time constant decreases as γ increases, in other words, with increasing magnetic field.

Fig. 38 The overlap integral I between donor and acceptor wavefunctions is plotted against the ratio of the Bohr radii of acceptor to donor. The parameter ρ is defined to be the ratio of the mean distance between donor-acceptor pair to the Bohr radius of acceptor.

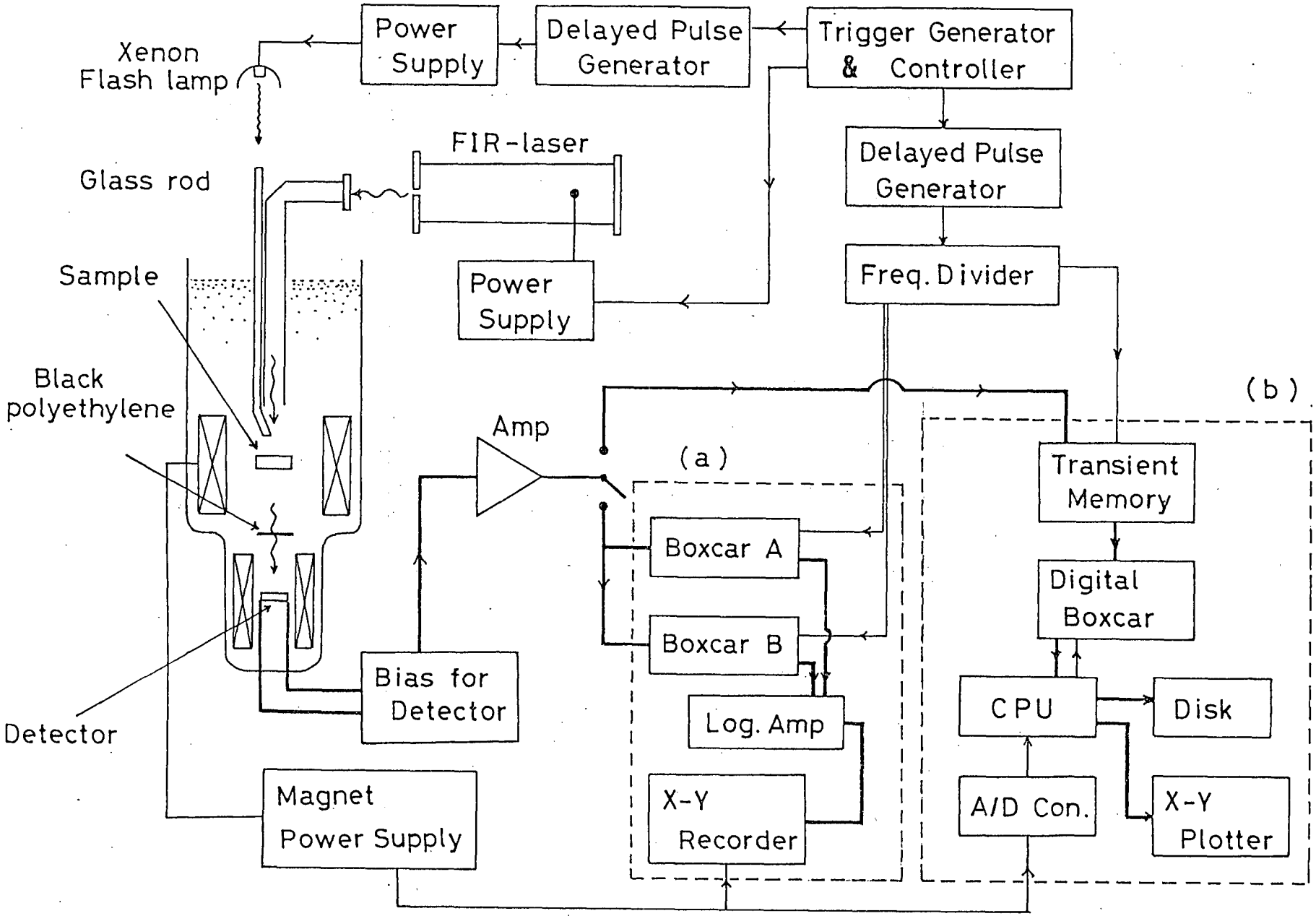
Xenon
Flash lamp
Power
Supply
Delayed Pulse
Generator
Trigger Generator
& Controller
FIR-laser
Glass rod
Delayed Pulse
Generator
Sample
Power
Supply
Freq. Divider
Black
polyethylene
Amp
(a)
(b)
Transient
Memory
Boxcar A
Digital
Boxcar
Boxcar B
Bias for
Detector
CPU
Disk
Log. Amp
Detector
Magnet
Power Supply
X-Y
Recorder
A/D Con.
X-Y
Plotter

Fig.1

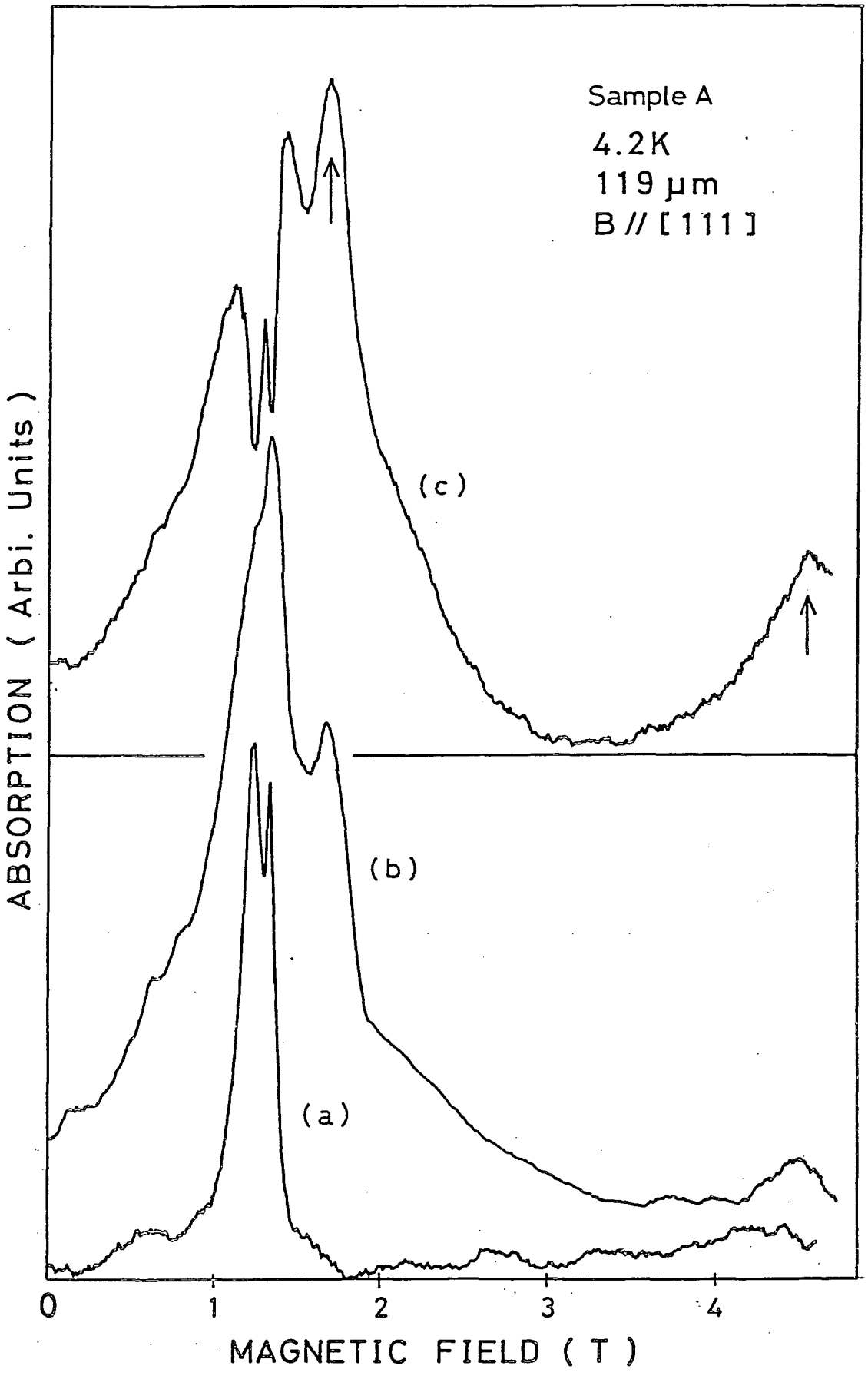
Sample A
4.2K
119 μm
B // [111]
(c)
(b)
(a)
ABSORPTION (Arbi. Units)
0
1
2
3
4
MAGNETIC FIELD (T)

Fig.2

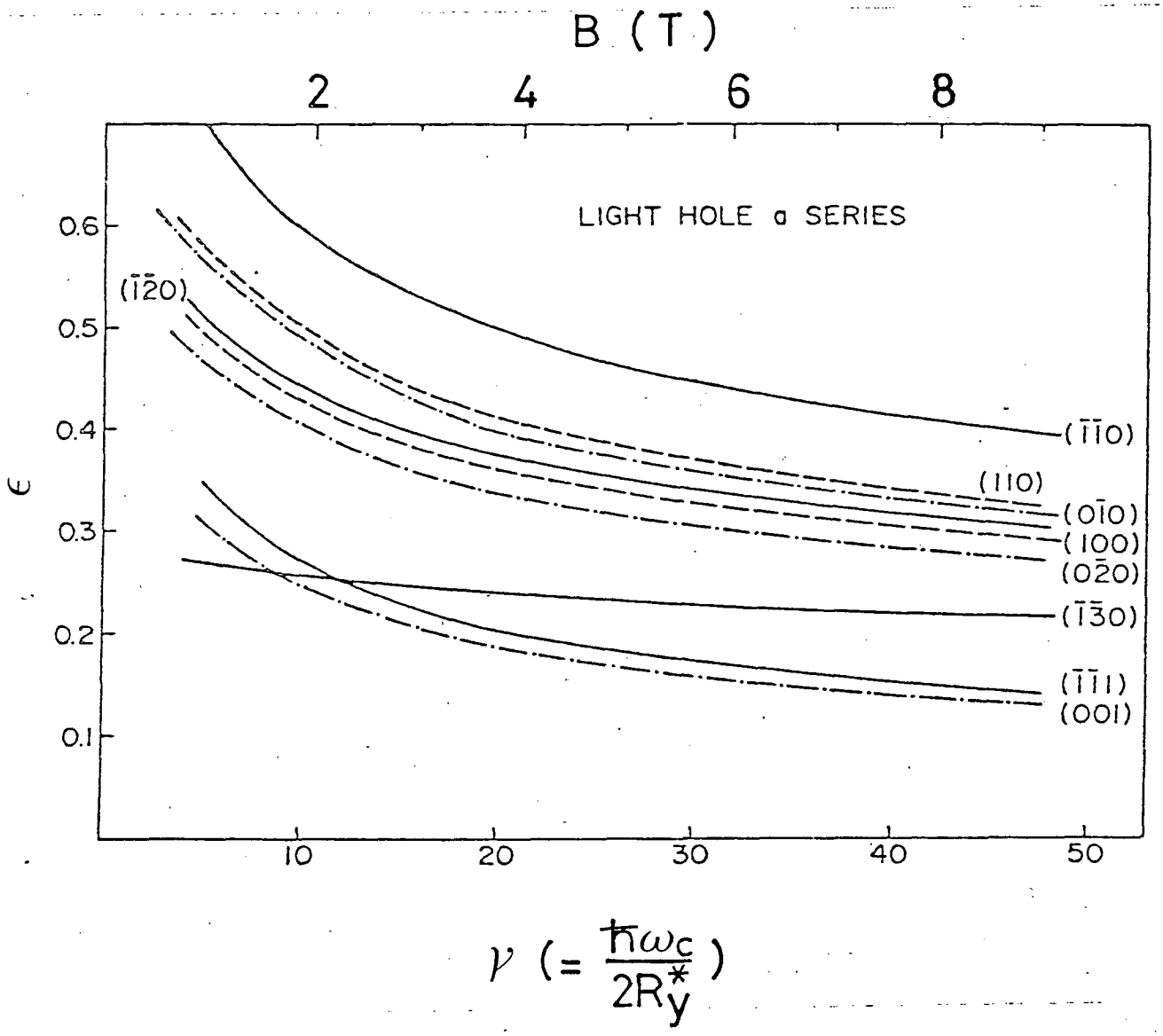
B (T)
2
4
6
8
LIGHT HOLE a SERIES
0.6
0.5
0.4
0.3
0.2
0.1
ε
(1̄2̄0)
(1̄1̄0)
(110)
(01̄0)
(100)
(02̄0)
(1̄3̄0)
(1̄1̄1)
(001)
10
20
30
40
50
ν (= ħω_c / 2R*_y)

Fig.3

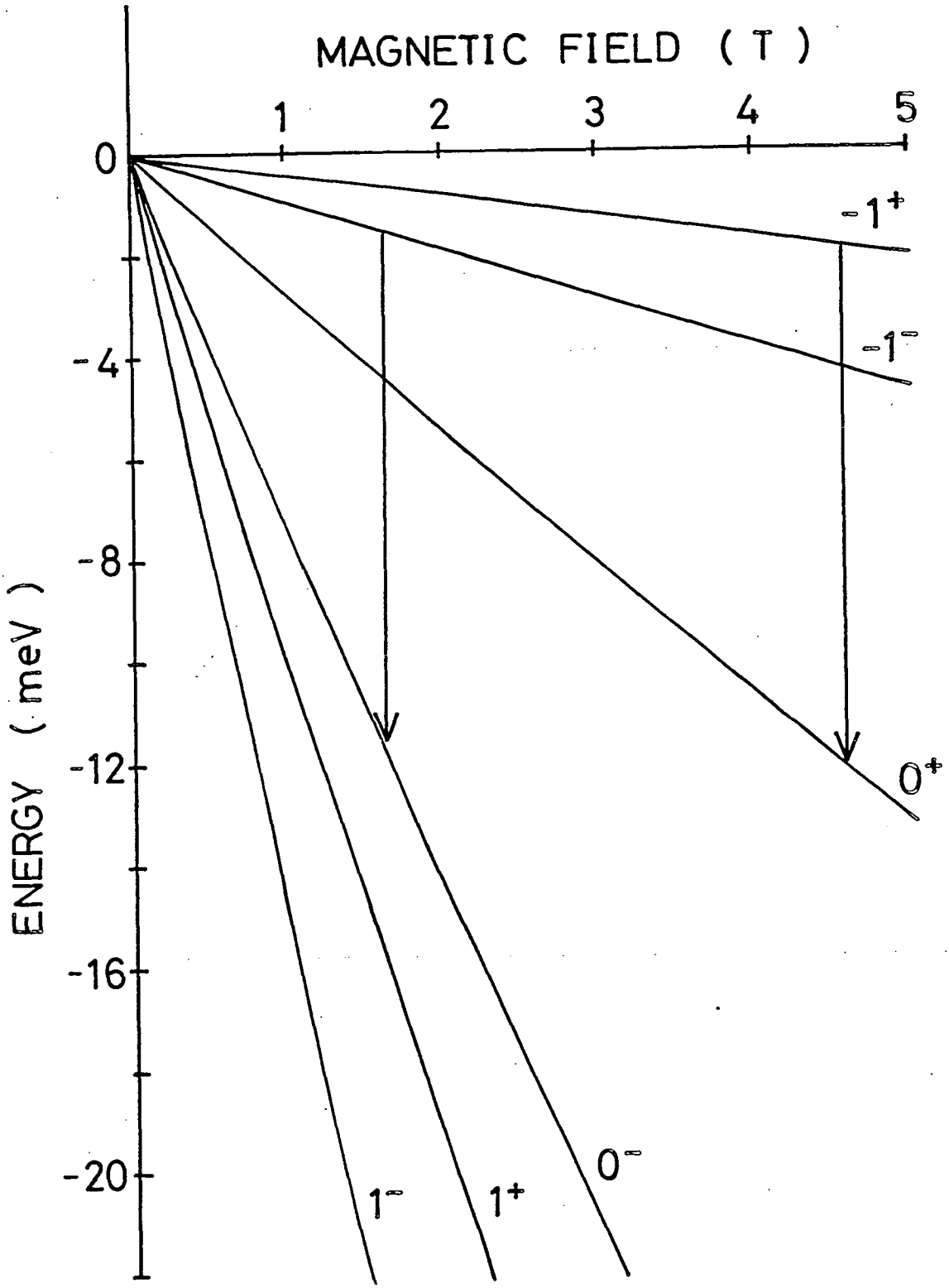

Fig.4

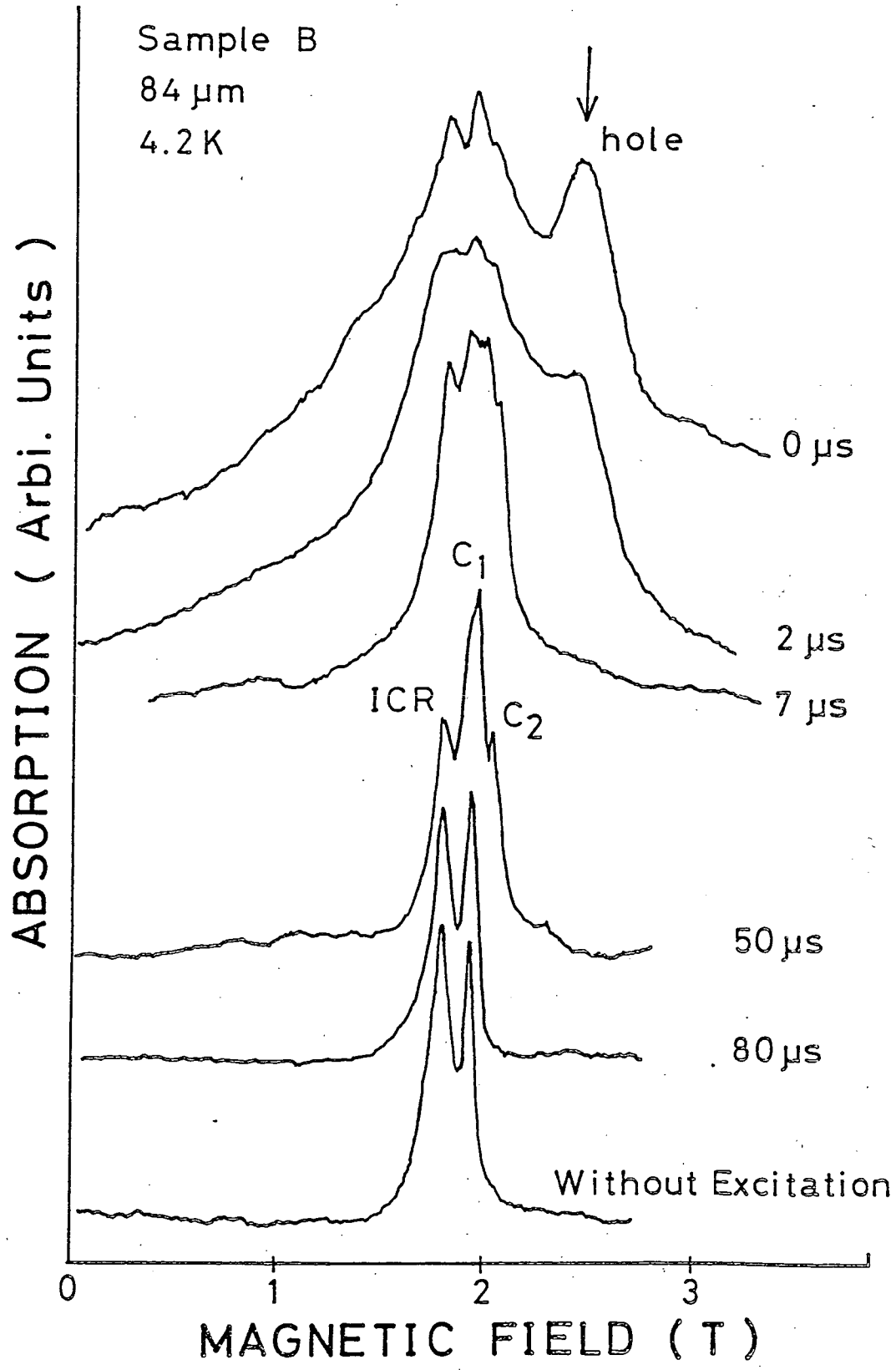
Sample B
84 μm
4.2 K
hole
0 μs
2 μs
7 μs
50 μs
80 μs
Without Excitation
C1
C2
ICR
ABSORPTION (Arbi. Units)
0
1
2
3
MAGNETIC FIELD (T)

Fig.5

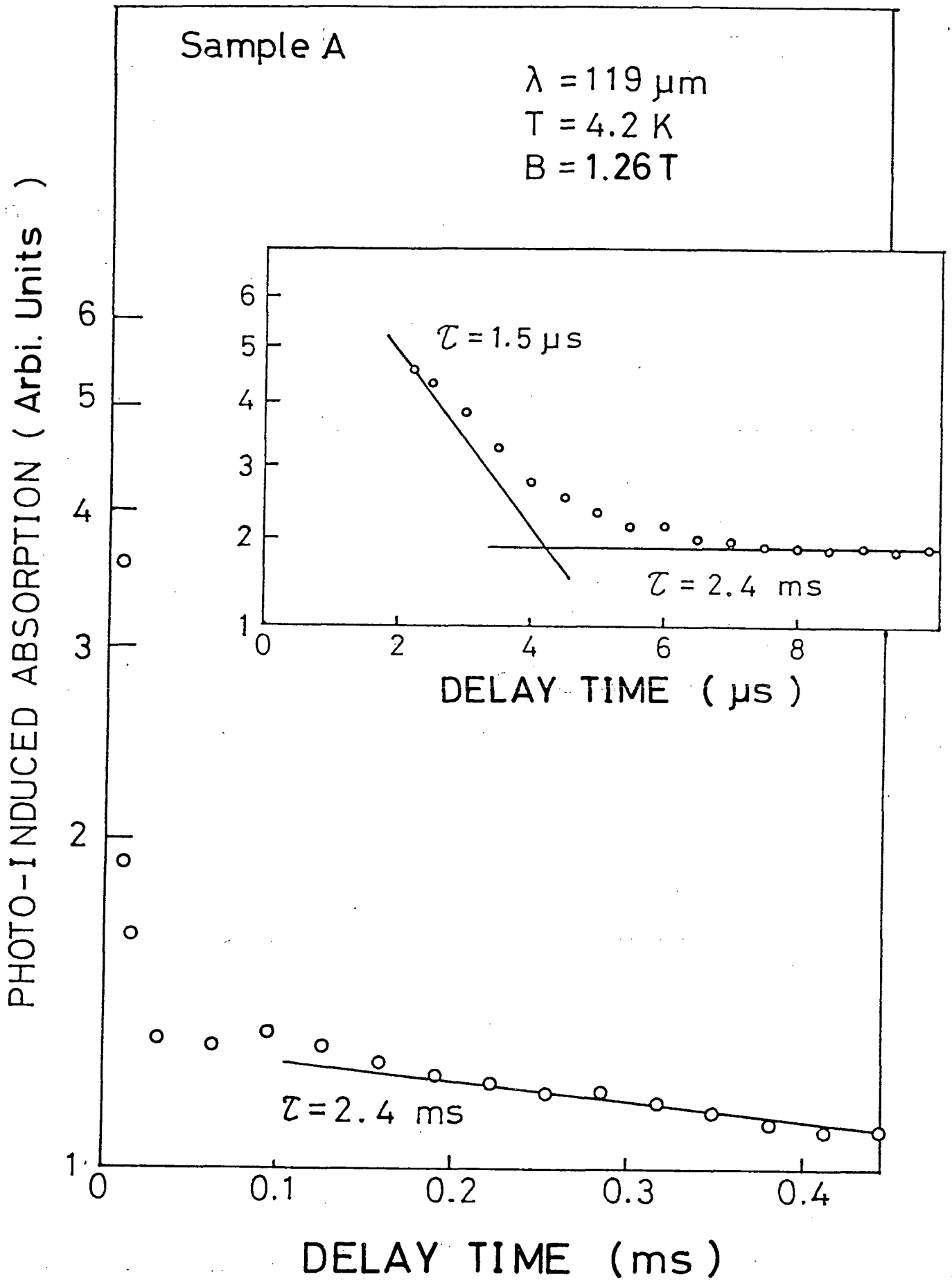
Sample A
λ = 119 μm
T = 4.2 K
B = 1.26 T
PHOTO-INDUCED ABSORPTION (Arbi. Units)
τ = 1.5 μs
τ = 2.4 ms
DELAY TIME (μs)
τ = 2.4 ms
DELAY TIME (ms)

Fig.6

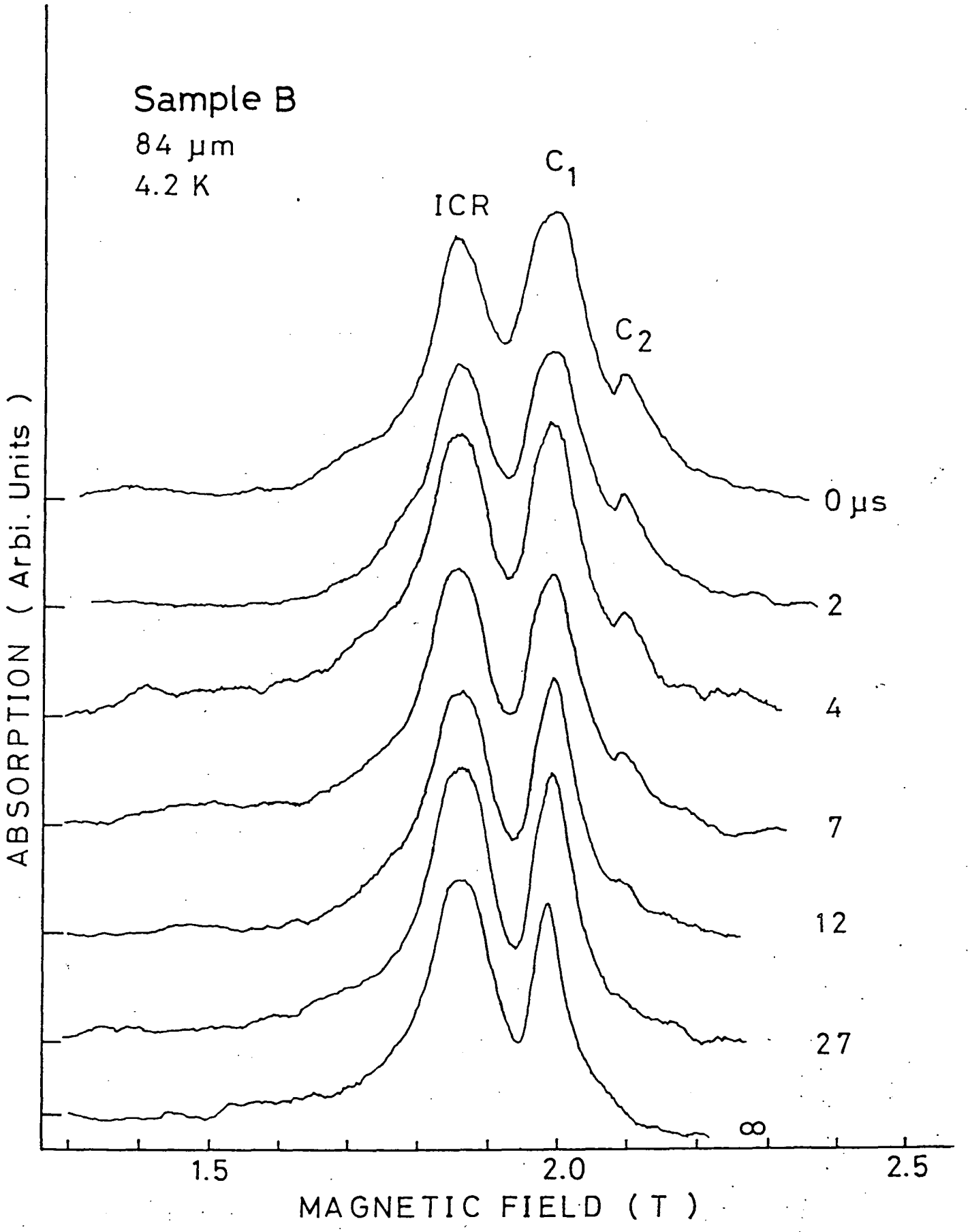
Sample B
84 μm
4.2 K
ICR
C1
C2
0 μs
2
4
7
12
27
∞
ABSORPTION (Arbi. Units)
1.5
2.0
2.5
MAGNETIC FIELD (T)

Fig.7

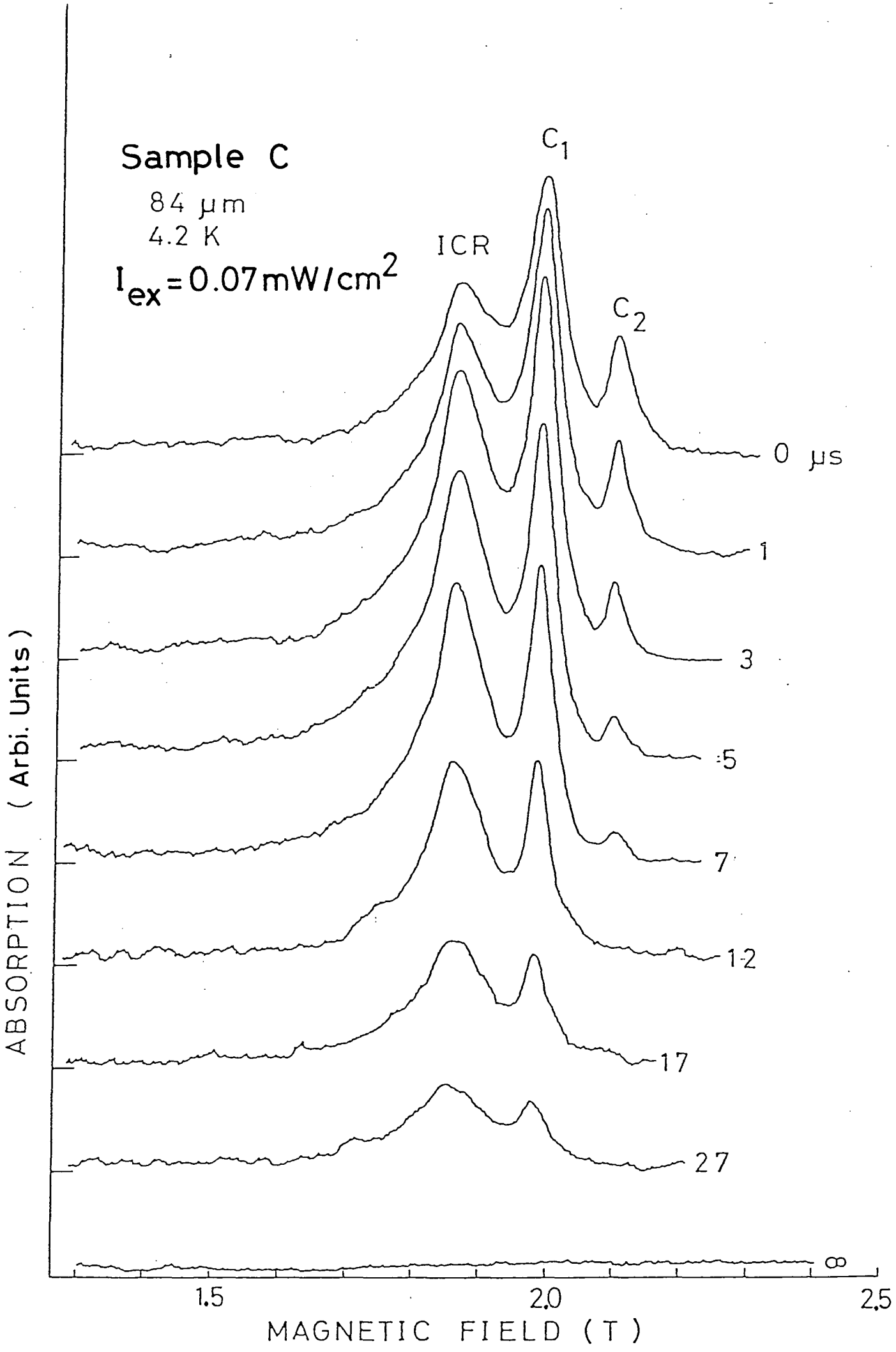
Sample C
84 μm
4.2 K
I_{ex} = 0.07 mW/cm^2
ICR
C_1
C_2
0 μs
1
3
5
7
12
17
27
∞
ABSORPTION (Arbi. Units)
1.5
2.0
2.5
MAGNETIC FIELD (T)

Fig.8

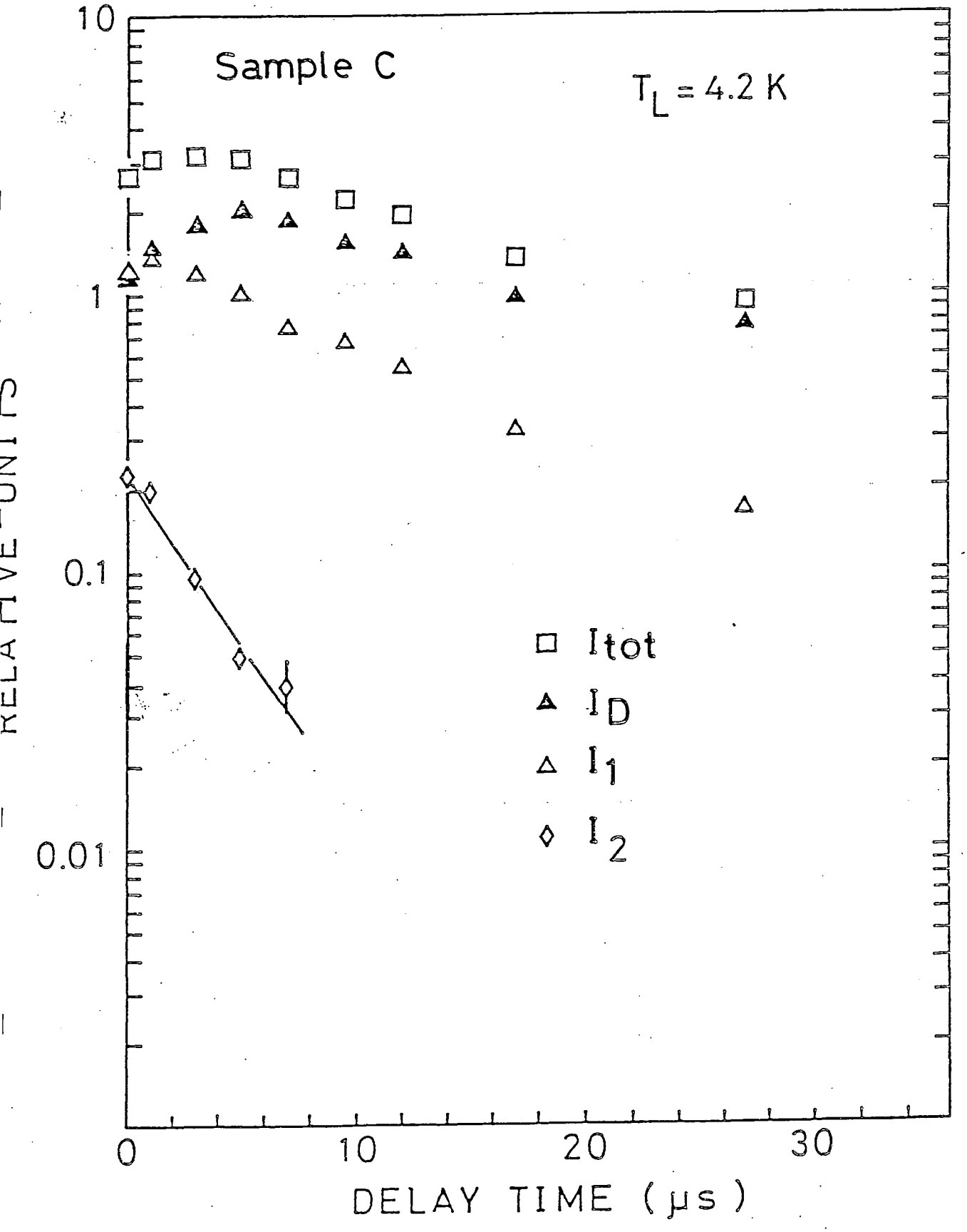
Sample C
$T_L = 4.2$ K
10
1
0.1
0.01
RELATIVE UNITS
Itot
I_D
I_1
I_2
0
10
20
30
DELAY TIME (μs)

Fig.9

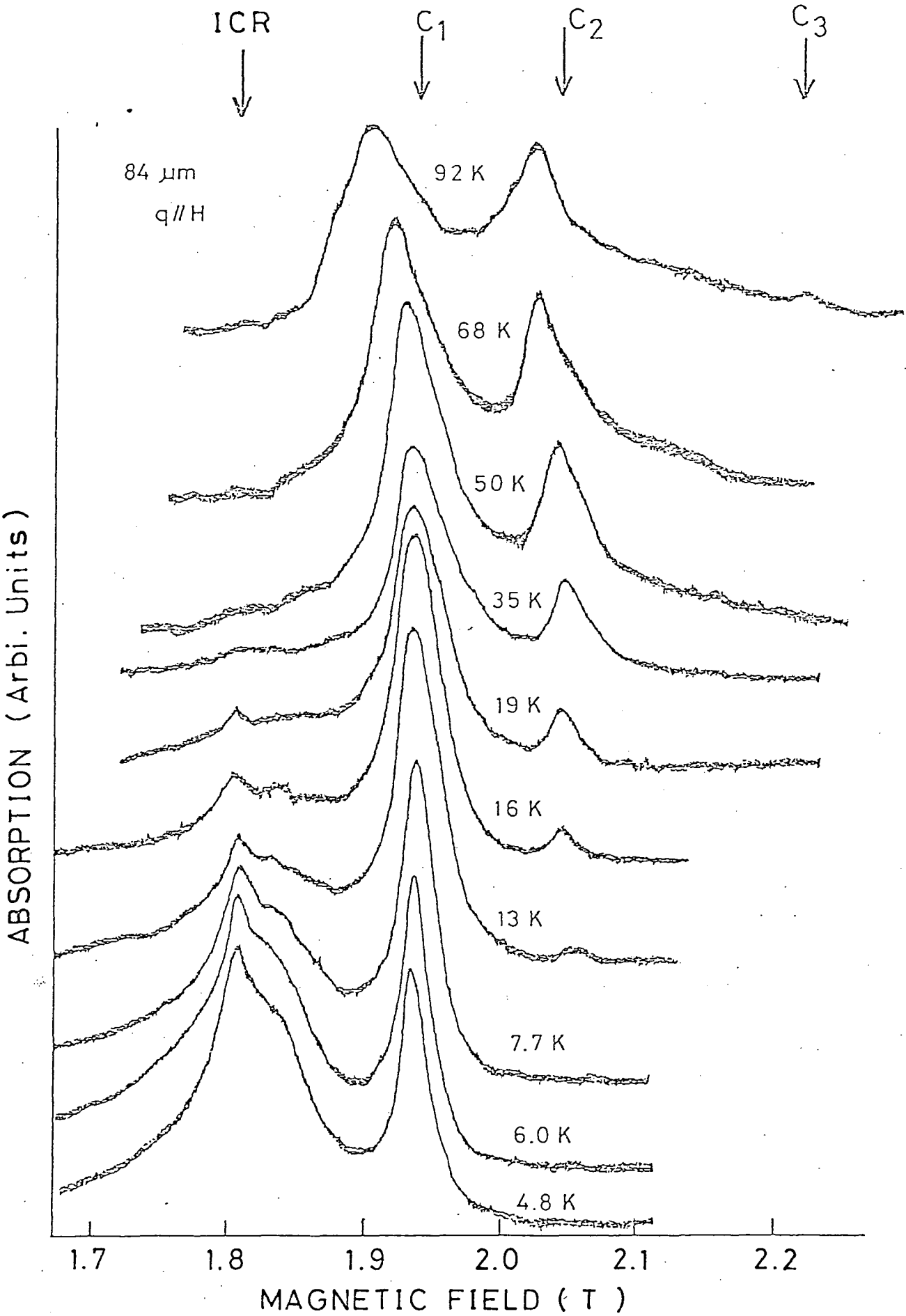
ICR
C1
C2
C3
84 μm
q // H
92 K
68 K
50 K
35 K
19 K
16 K
13 K
7.7 K
6.0 K
4.8 K
ABSORPTION (Arbi. Units)
1.7
1.8
1.9
2.0
2.1
2.2
MAGNETIC FIELD (T)

FIg.10

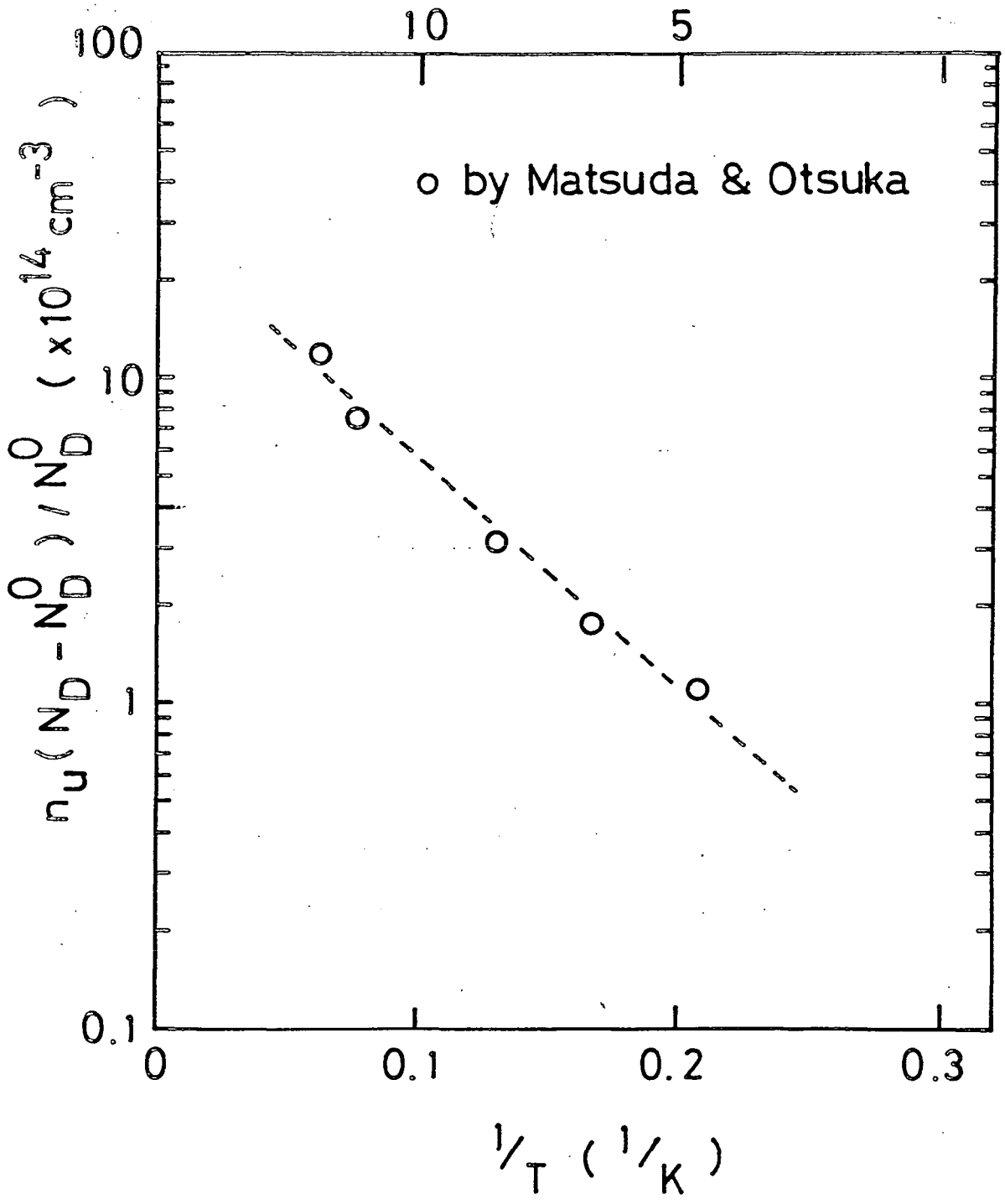
10
5
100
o by Matsuda & Otsuka
10
1
0.1
0
0.1
0.2
0.3
$n_u(N_D - N_D^0)/N_D^0$ ($\times 10^{14}$ cm^{-3})
$1/T$ ($1/K$)

Fig.11

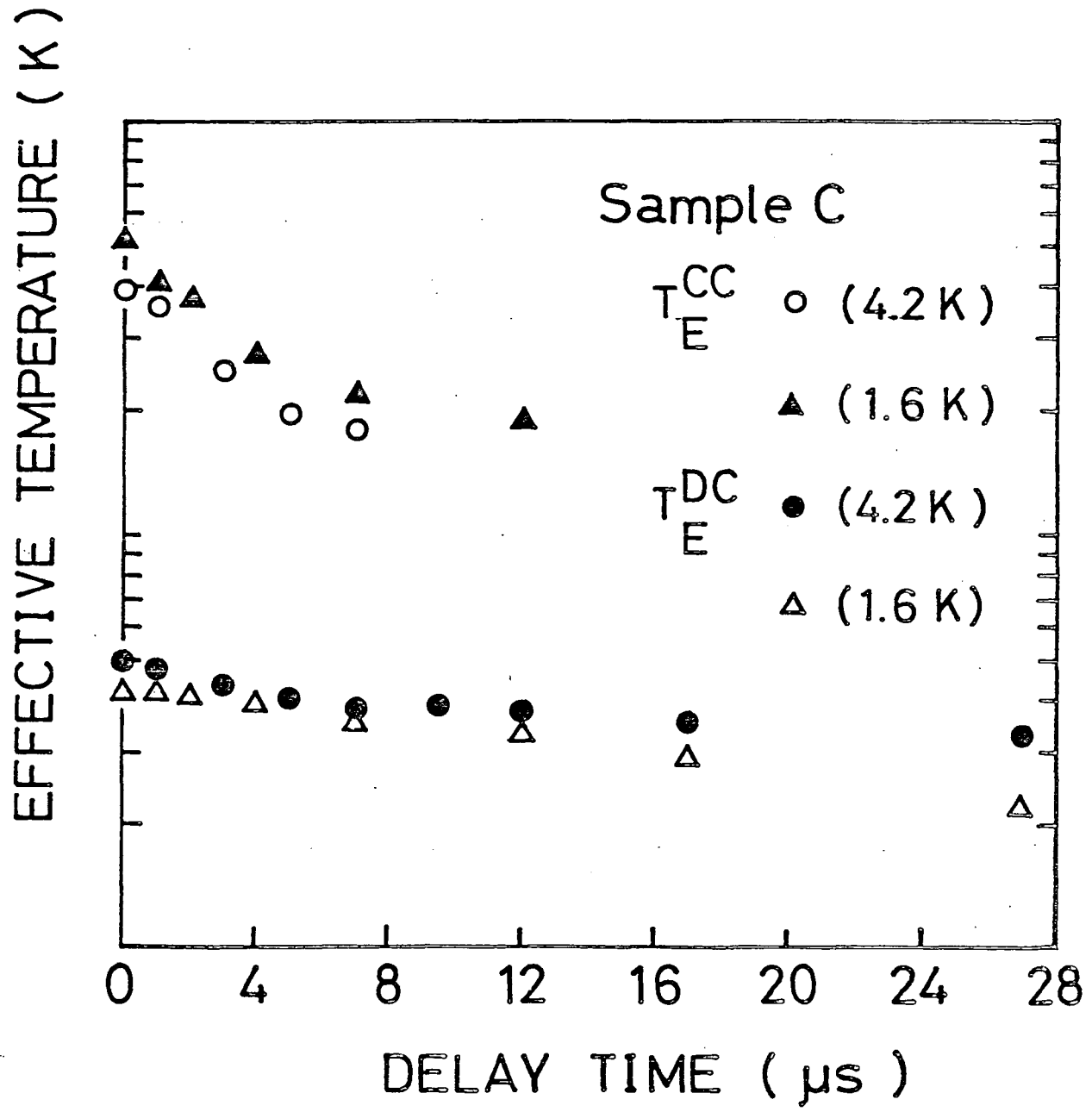
EFFECTIVE TEMPERATURE (K)
Sample C
T_E^{CC} ○ (4.2 K)
▲ (1.6 K)
T_E^{DC} ● (4.2 K)
△ (1.6 K)
0
4
8
12
16
20
24
28
DELAY TIME (μs)

Fig.12

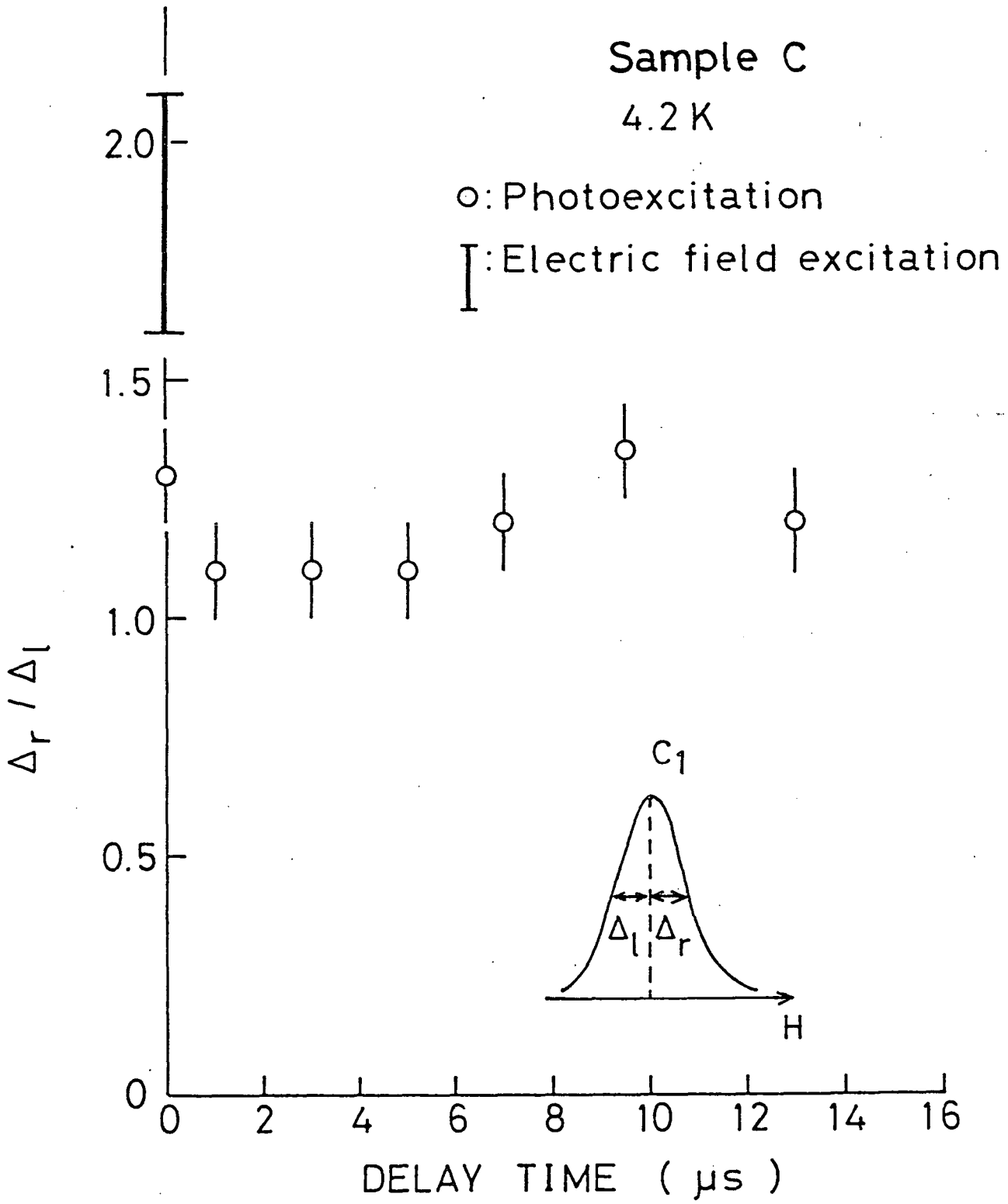
Sample C
4.2 K
o: Photoexcitation
I: Electric field excitation
2.0
1.5
1.0
0.5
0
Δ_r / Δ_l
C_1
Δ_l
Δ_r
H
0
2
4
6
8
10
12
14
16
DELAY TIME (μs)

Fig.13

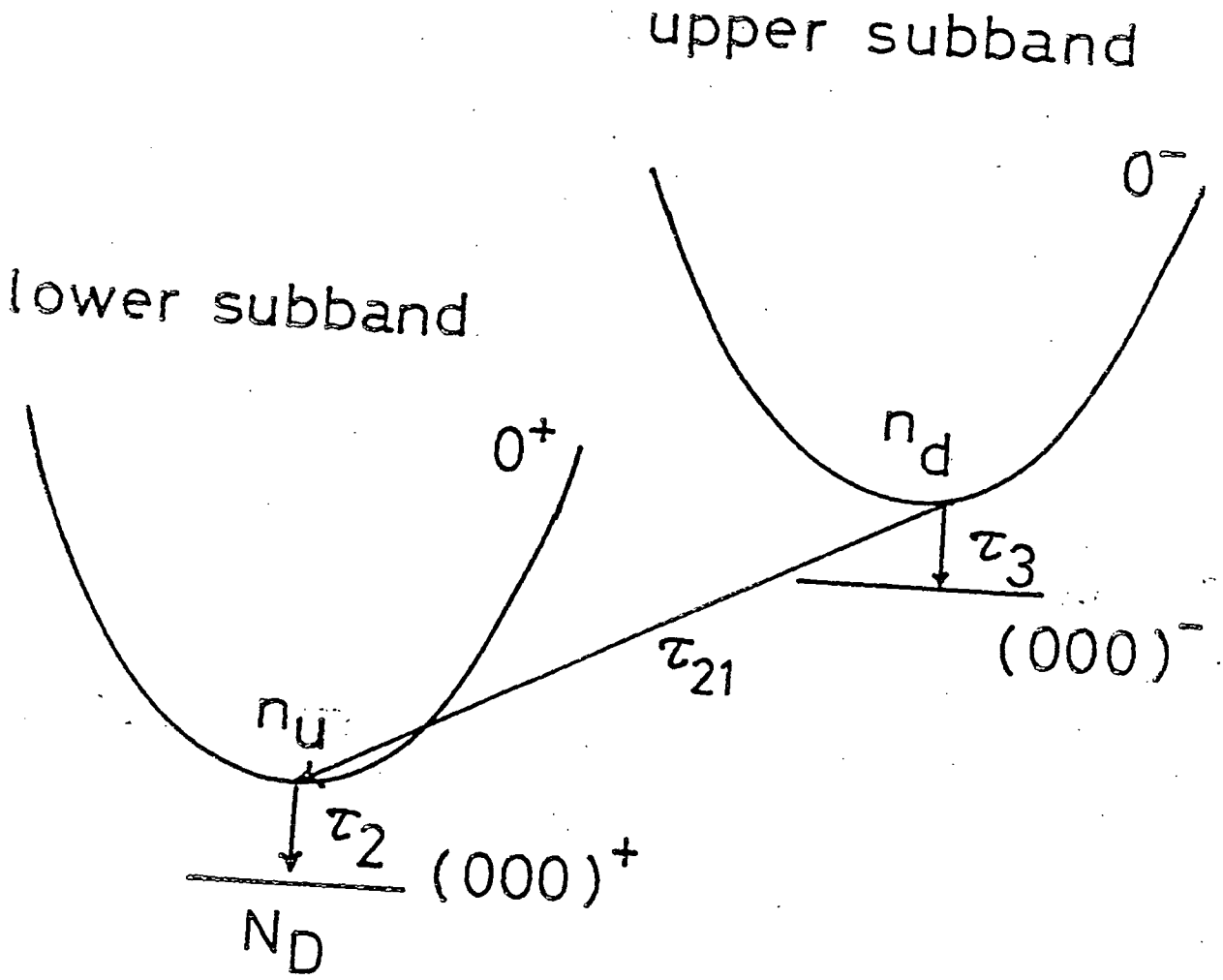
upper subband
0⁻
lower subband
0⁺
n_d
τ_3
τ_{21}
$(000)^-$
n_u
τ_2
$(000)^+$
N_D

Fig.14

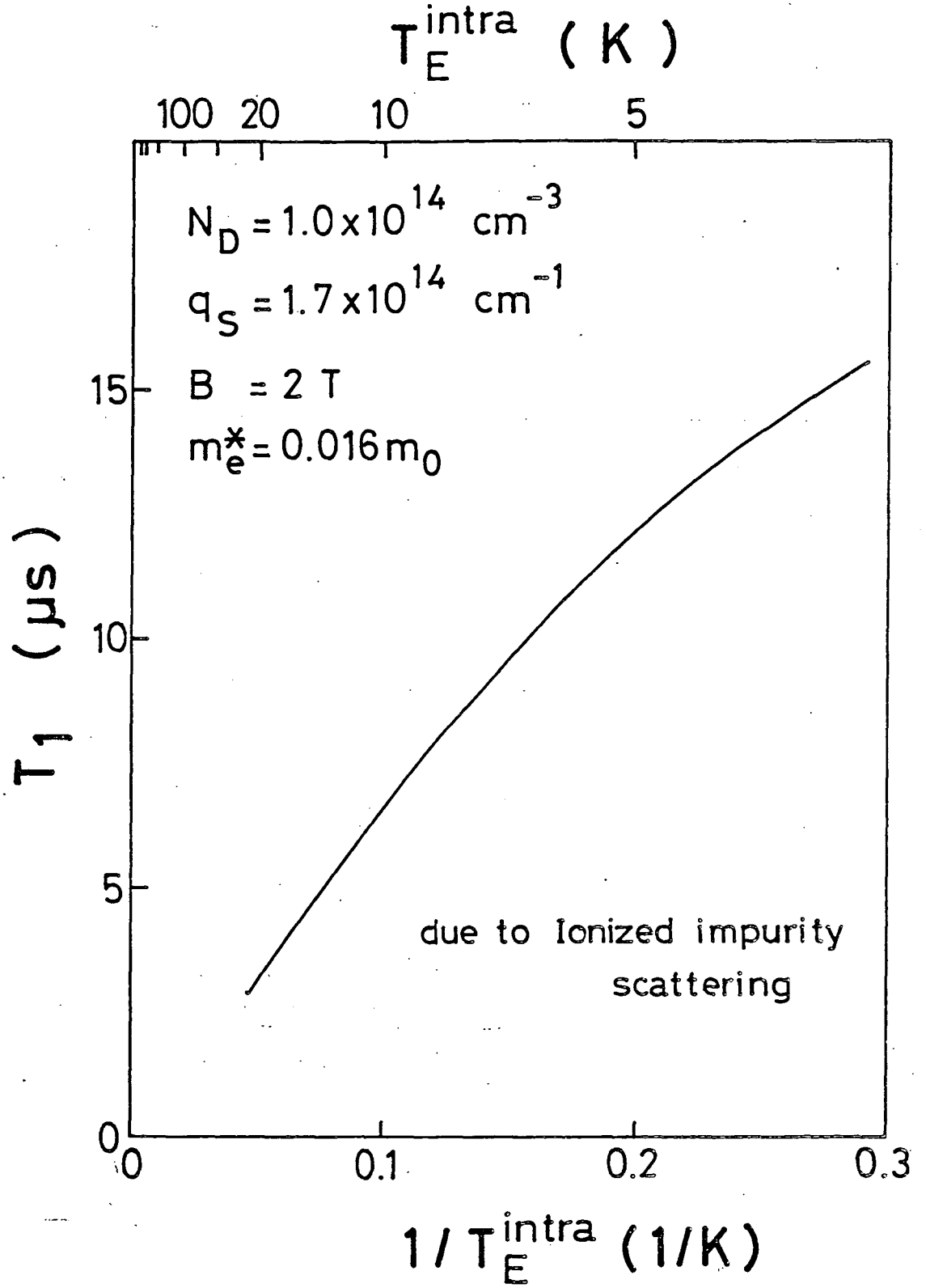
T_E^{intra} (K)
100
20
10
5
$N_D = 1.0 \times 10^{14}$ cm^{-3}
$q_s = 1.7 \times 10^{14}$ cm^{-1}
B = 2 T
$m_e^* = 0.016 m_0$
T_1 (μs)
15
10
5
0
due to Ionized impurity scattering
0
0.1
0.2
0.3
$1 / T_E^{intra}$ (1/K)

Fig.15

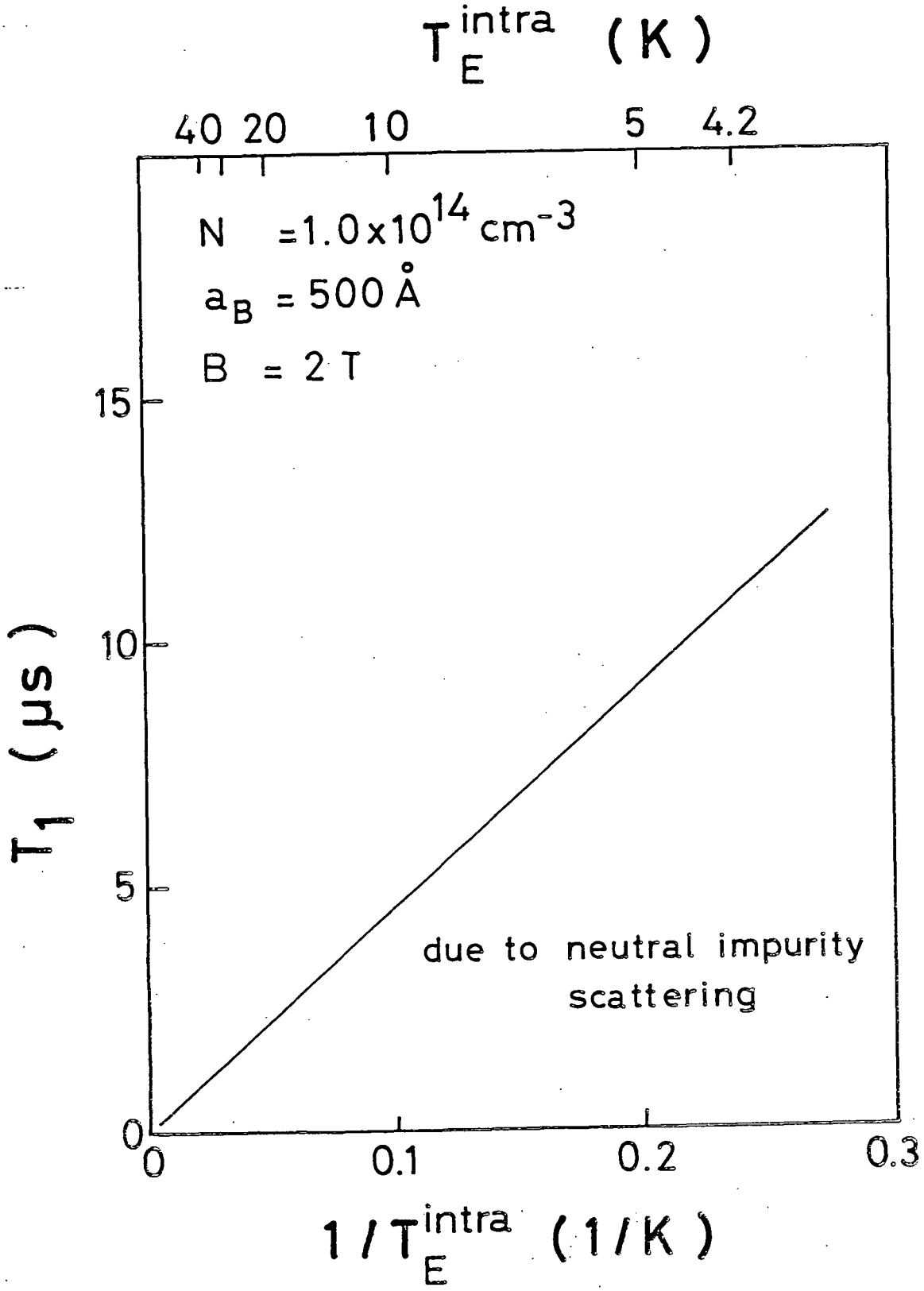
T_E^{intra} (K)
40 20 10 5 4.2
N =1.0x10^{14} cm^{-3}
a_B = 500 Å
B = 2 T
15
10
5
0
T_1 (μs)
due to neutral impurity scattering
0
0.1
0.2
0.3
$1/T_E^{intra}$ (1/K)

Fig.16

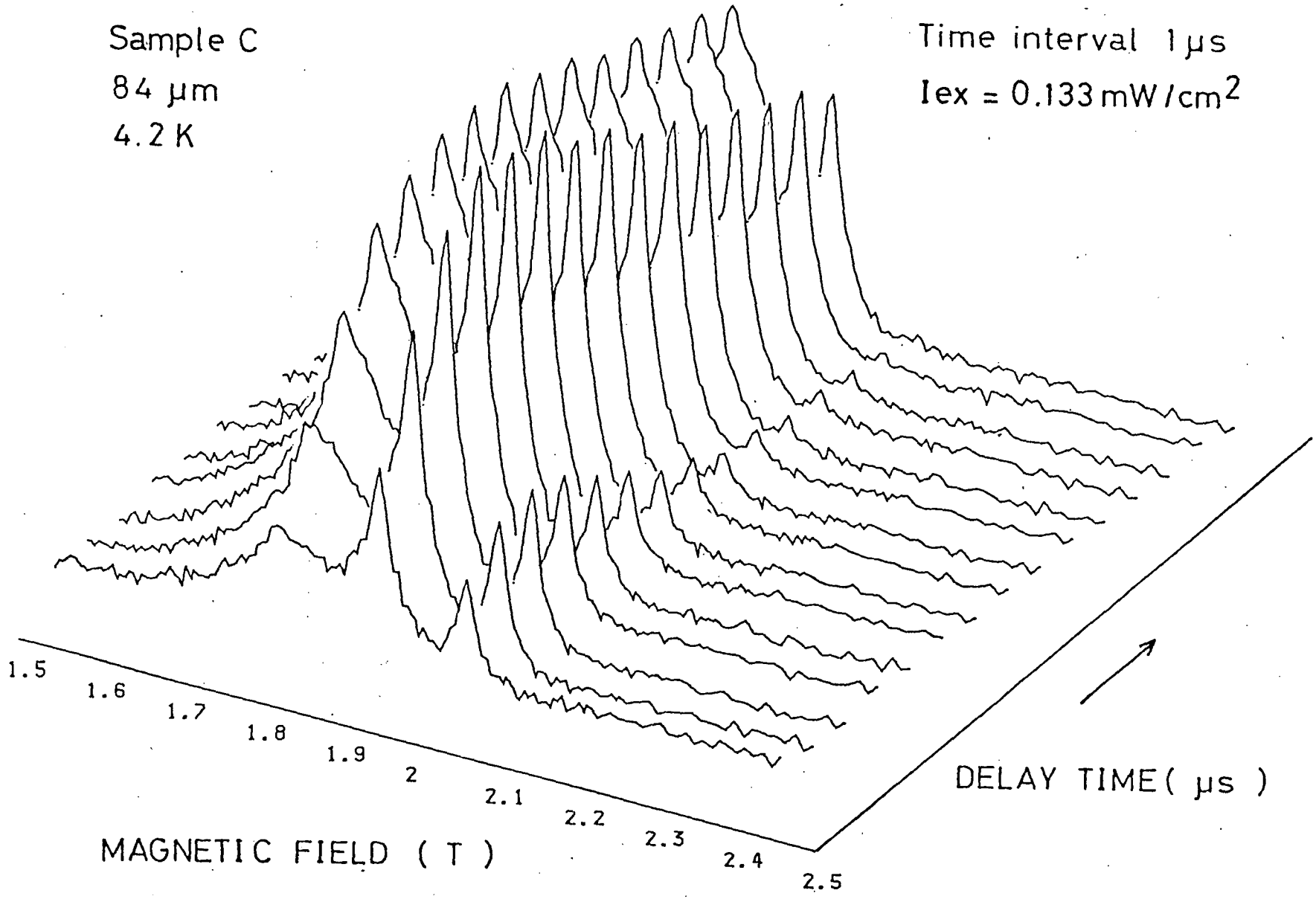
Sample C
84 μm
4.2 K
Time interval 1μs
Iex = 0.133mW/cm2
1.5
1.6
1.7
1.8
1.9
2
2.1
2.2
2.3
2.4
2.5
MAGNETIC FIELD (T)
DELAY TIME(μs)

Fig.17

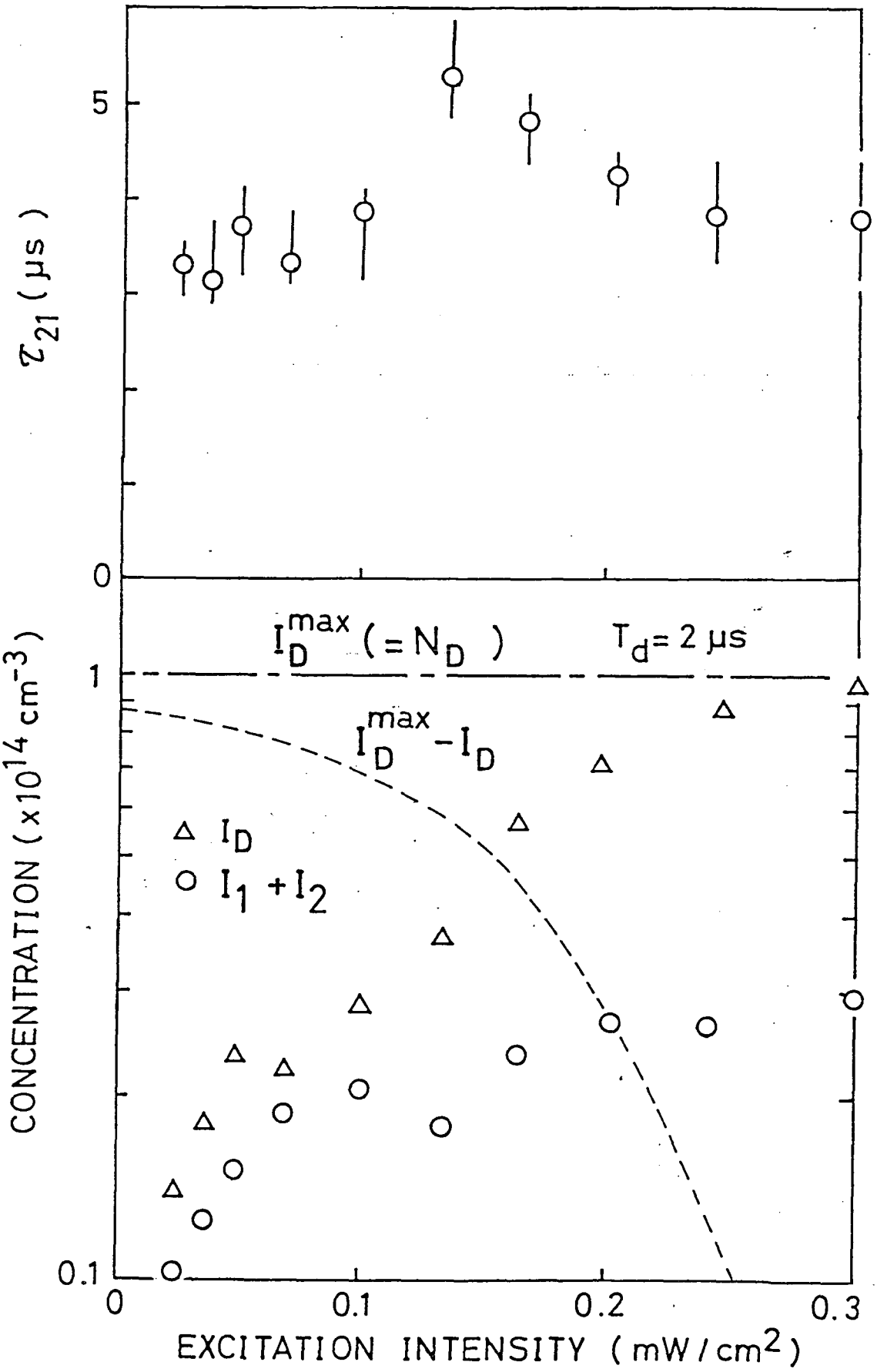
5
0
τ_{21} (μs)
I_D^{max} (= N_D)
T_d = 2 μs
1
$I_D^{max} - I_D$
I_D
$I_1 + I_2$
CONCENTRATION (x10^{14} cm^{-3})
0.1
0
0.1
0.2
0.3
EXCITATION INTENSITY (mW/cm^2)

Fig.18

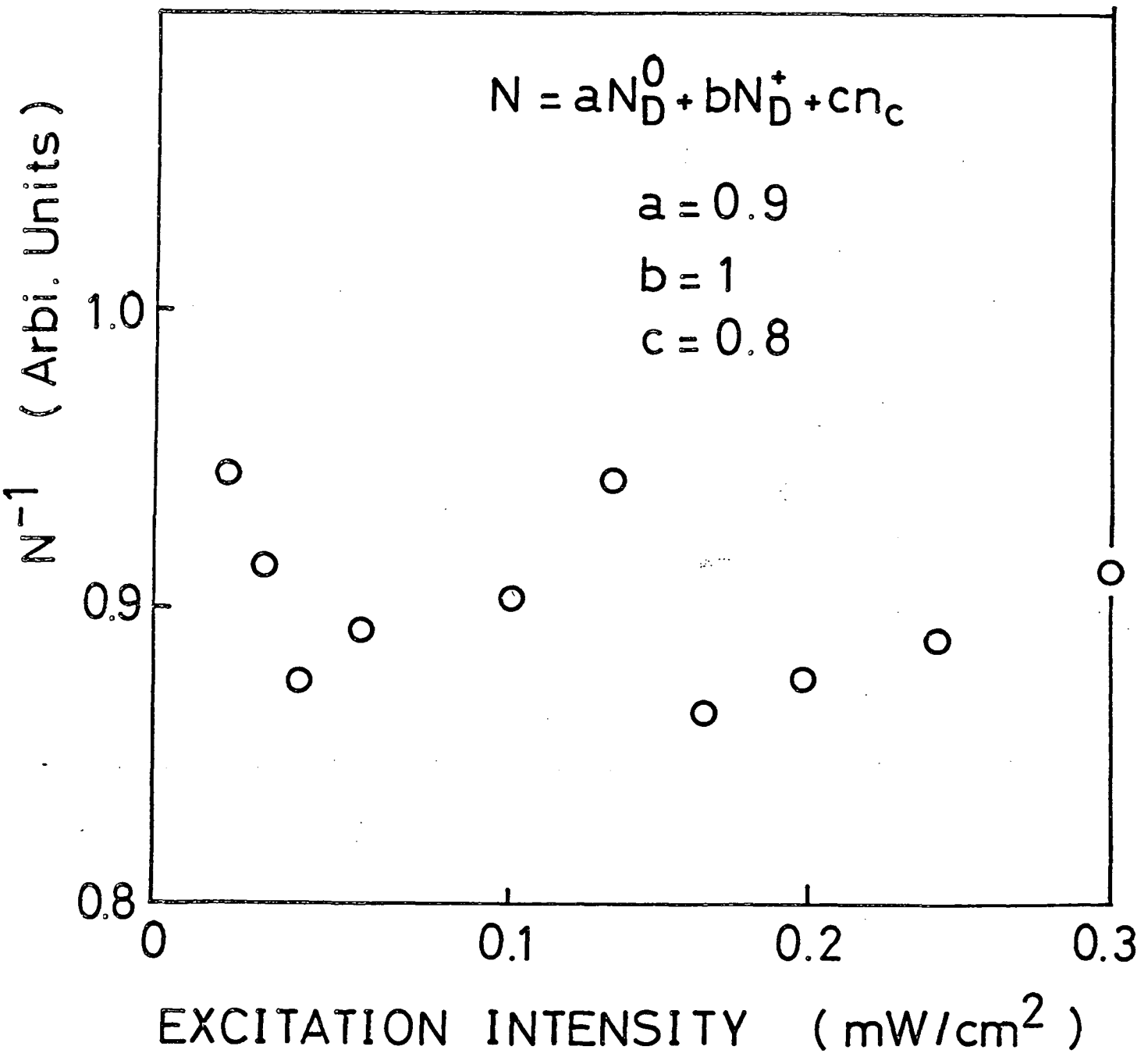
$N = aN_D^0 + bN_D^+ + cn_c$
a = 0.9
b = 1
c = 0.8
N^{-1} (Arbi. Units)
1.0
0.9
0.8
0
0.1
0.2
0.3
EXCITATION INTENSITY (mW/cm^2)

Fig.19

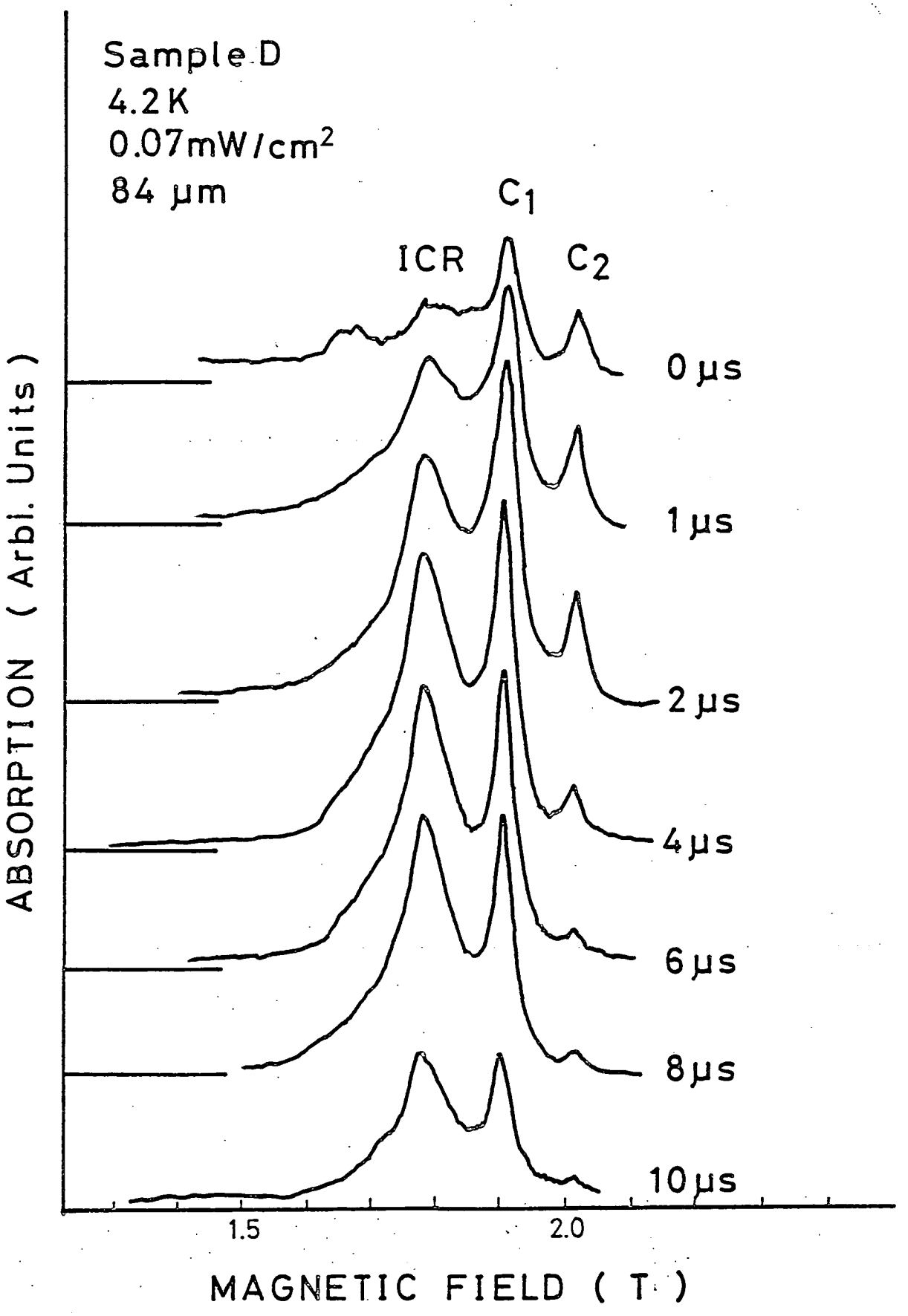
Sample D
4.2 K
0.07mW/cm²
84 μm
C1
ICR
C2
0 μs
1 μs
2 μs
4 μs
6 μs
8 μs
10 μs
ABSORPTION (Arbi. Units)
1.5
2.0
MAGNETIC FIELD (T)

Fig.20

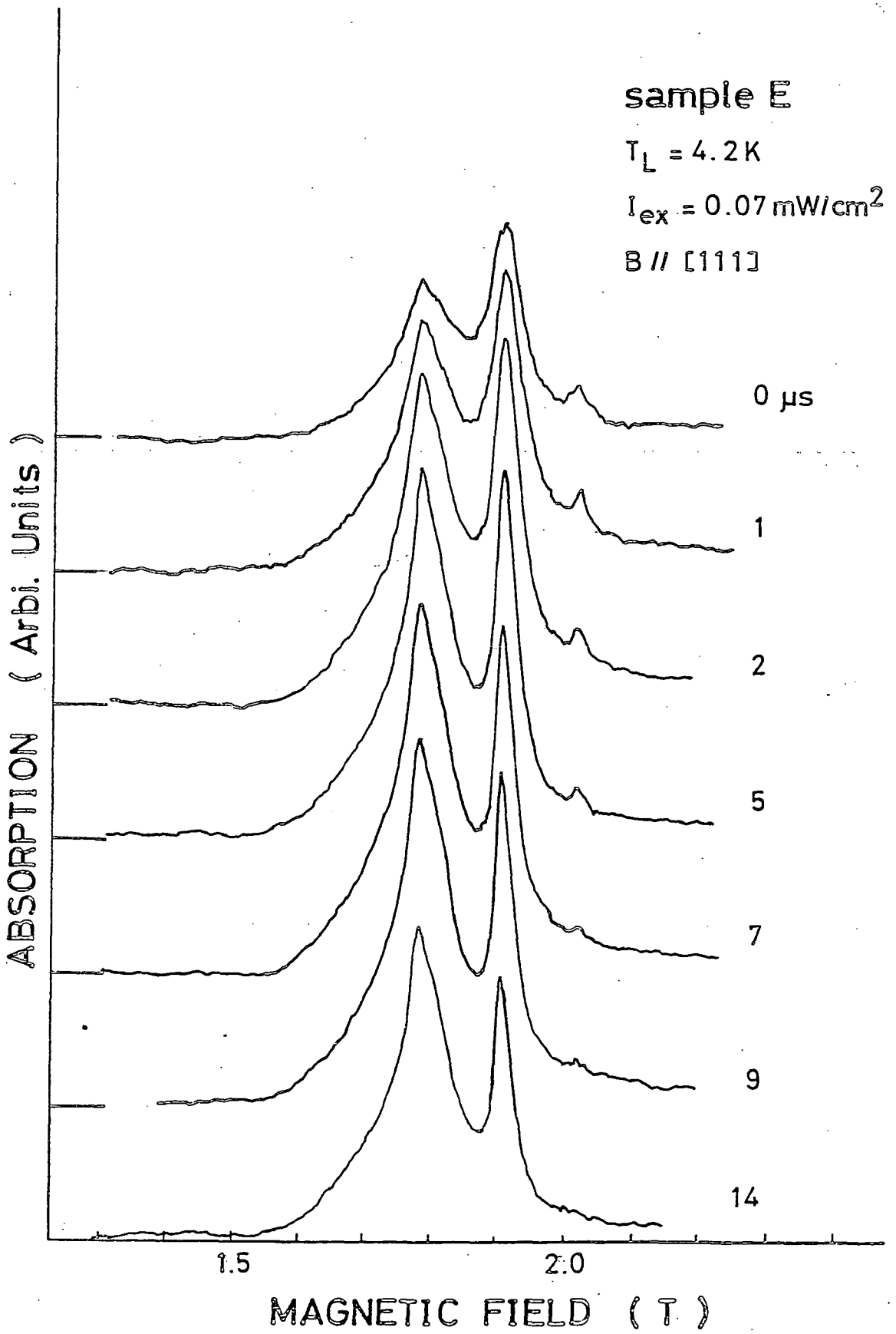
sample E
T_L = 4.2 K
I_{ex} = 0.07 mW/cm^2
B // [111]
0 μs
1
2
5
7
9
14
ABSORPTION (Arbi. Units)
1.5
2.0
MAGNETIC FIELD (T)

Fig.21

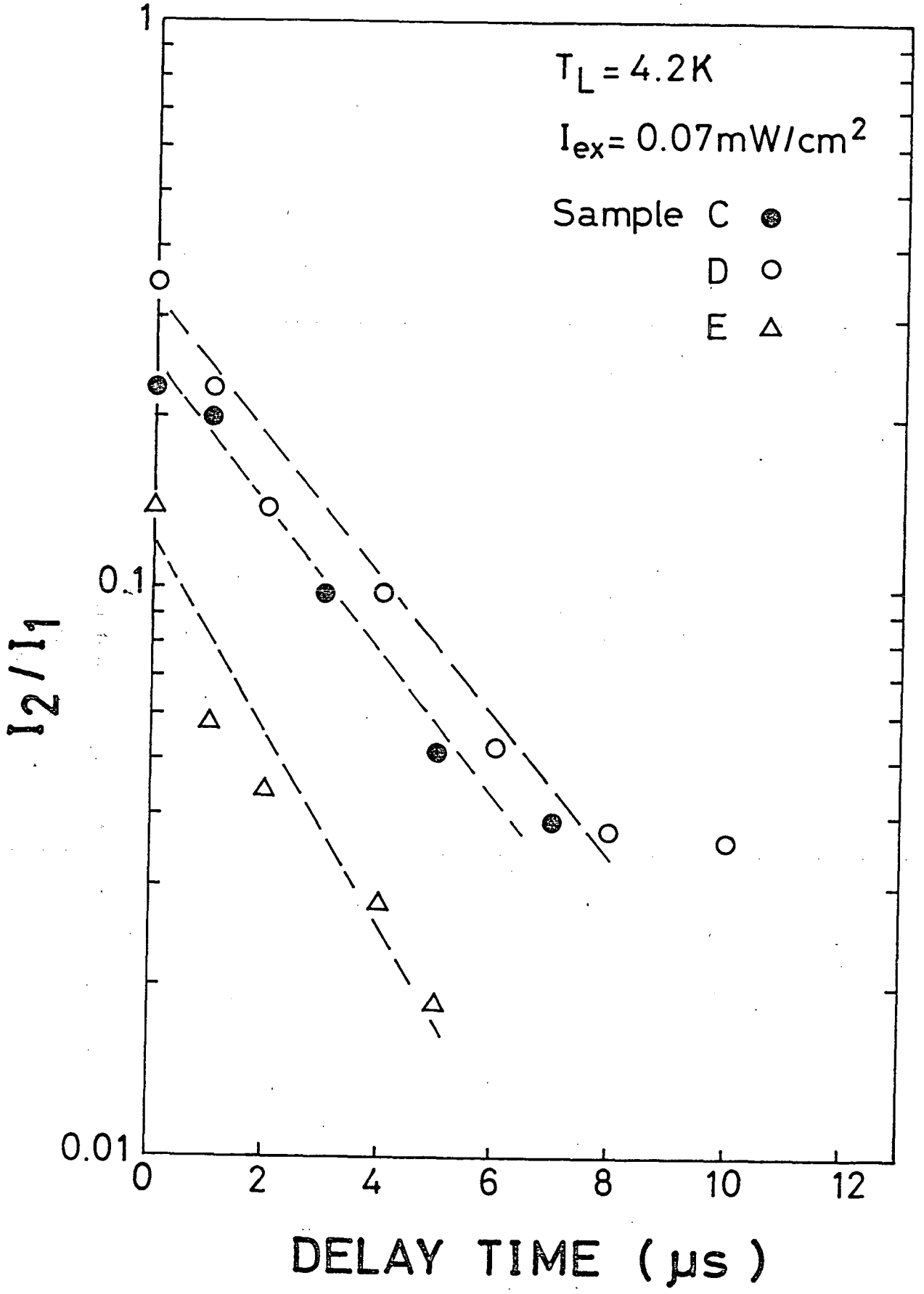
$T_L = 4.2K$
$I_{ex} = 0.07mW/cm^2$
Sample C
D
E
1
0.1
0.01
I_2/I_1
0
2
4
6
8
10
12
DELAY TIME (μs)

Fig.22

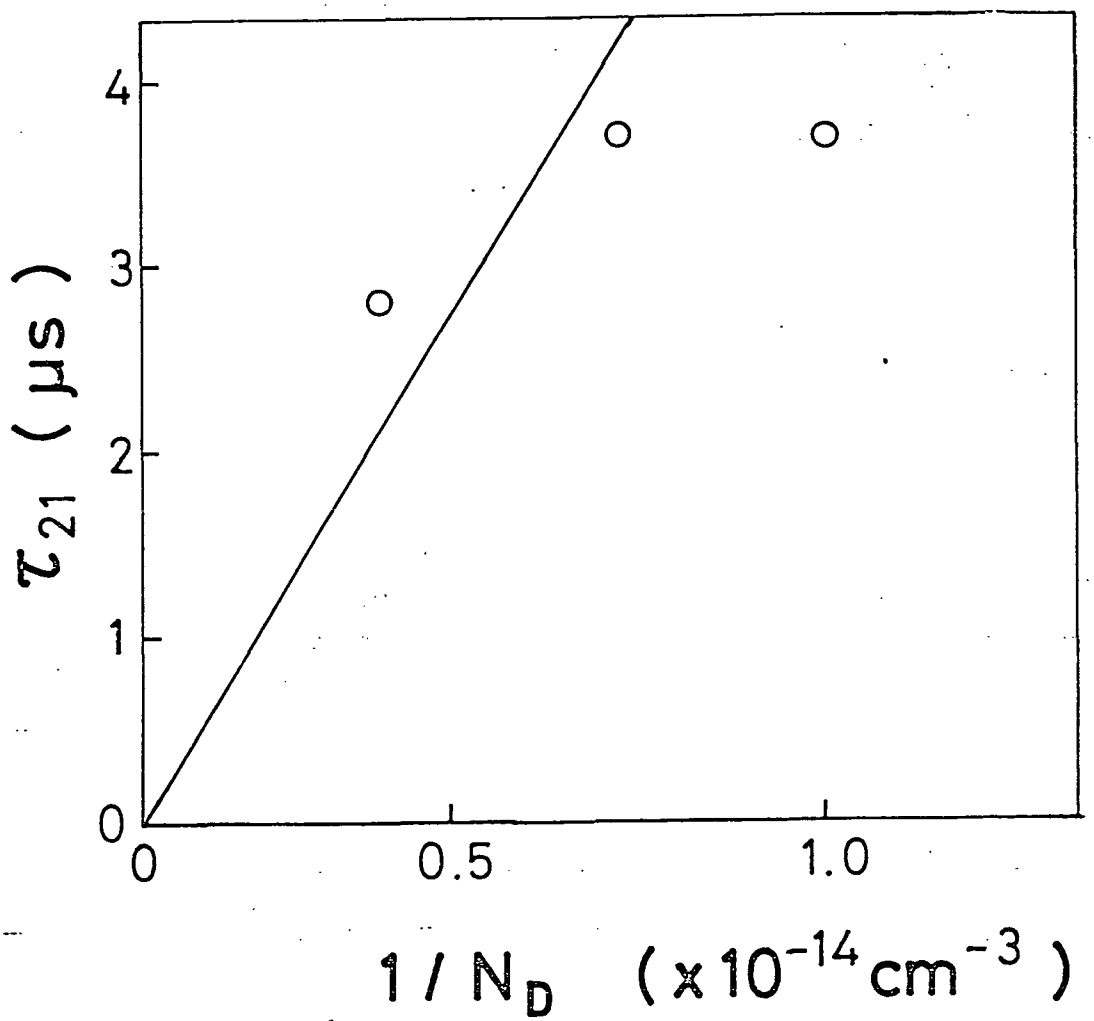

Fig.23

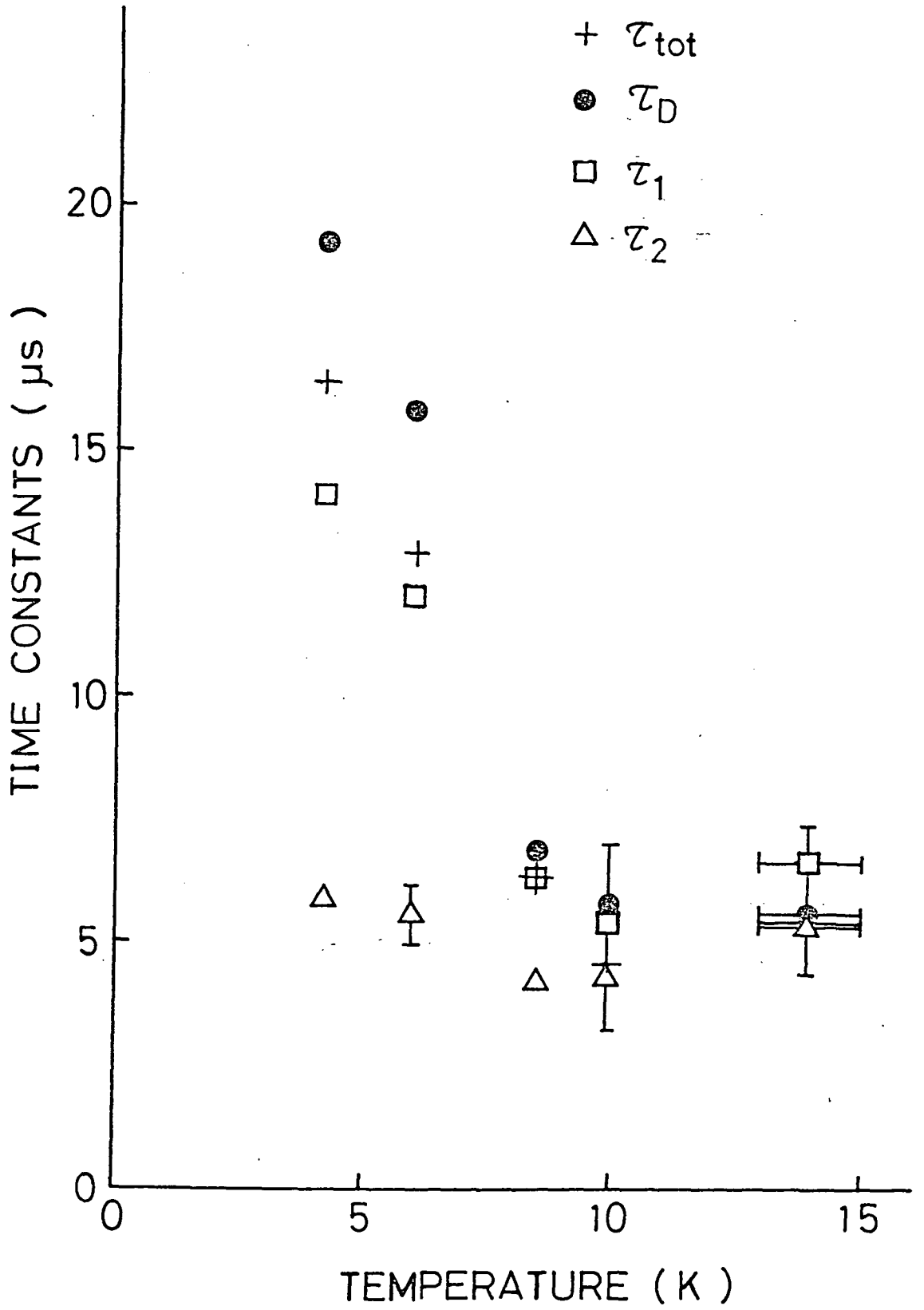
+ τ_{tot}
τ_D
τ_1
τ_2
TIME CONSTANTS (μs)
0
5
10
15
20
0
5
10
15
TEMPERATURE (K)

Fig.24

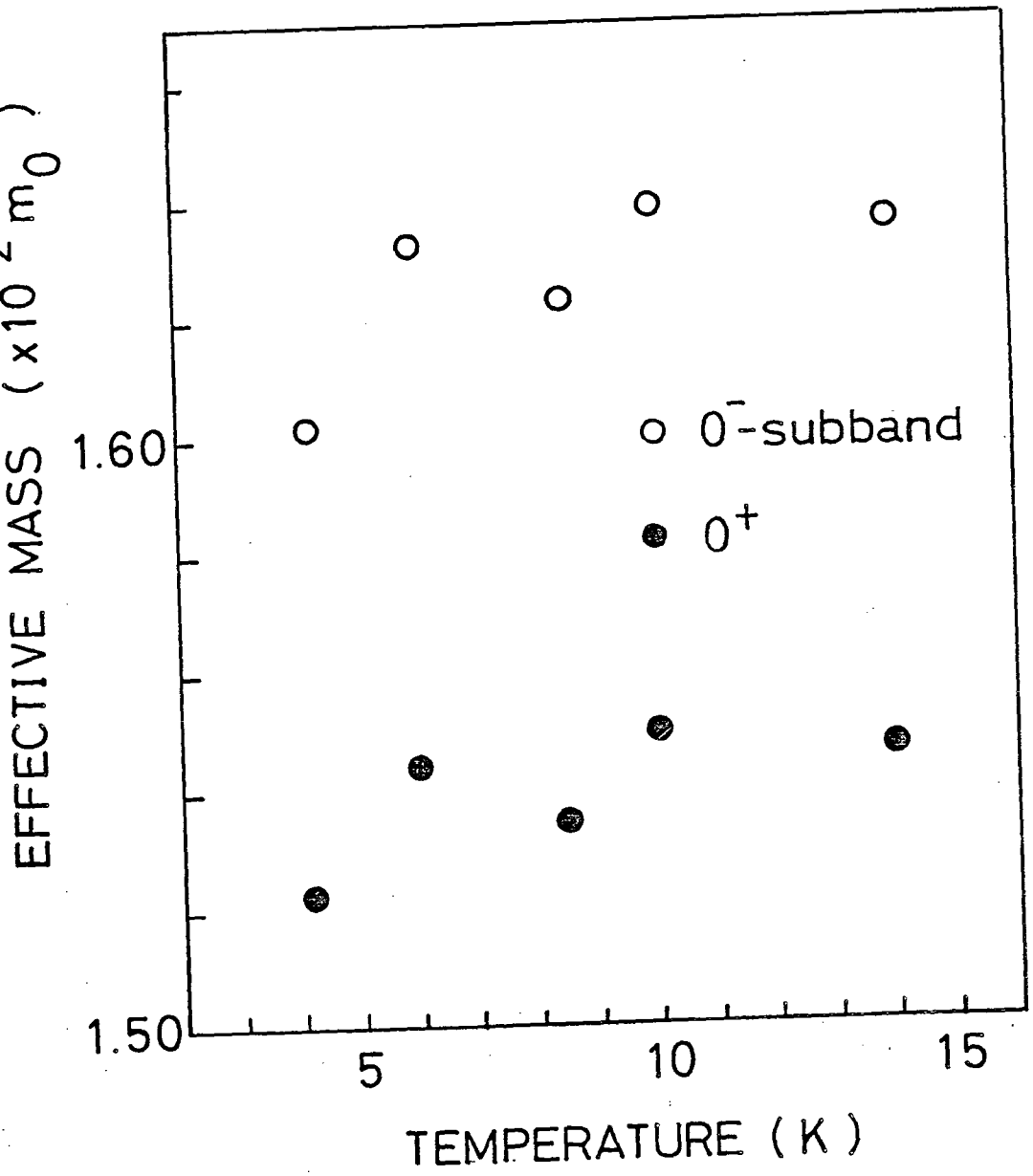
EFFECTIVE MASS (x10^{-2} m$_0$)
1.60
1.50
5
10
15
TEMPERATURE (K)
0$^-$-subband
0$^+$

Fig.25

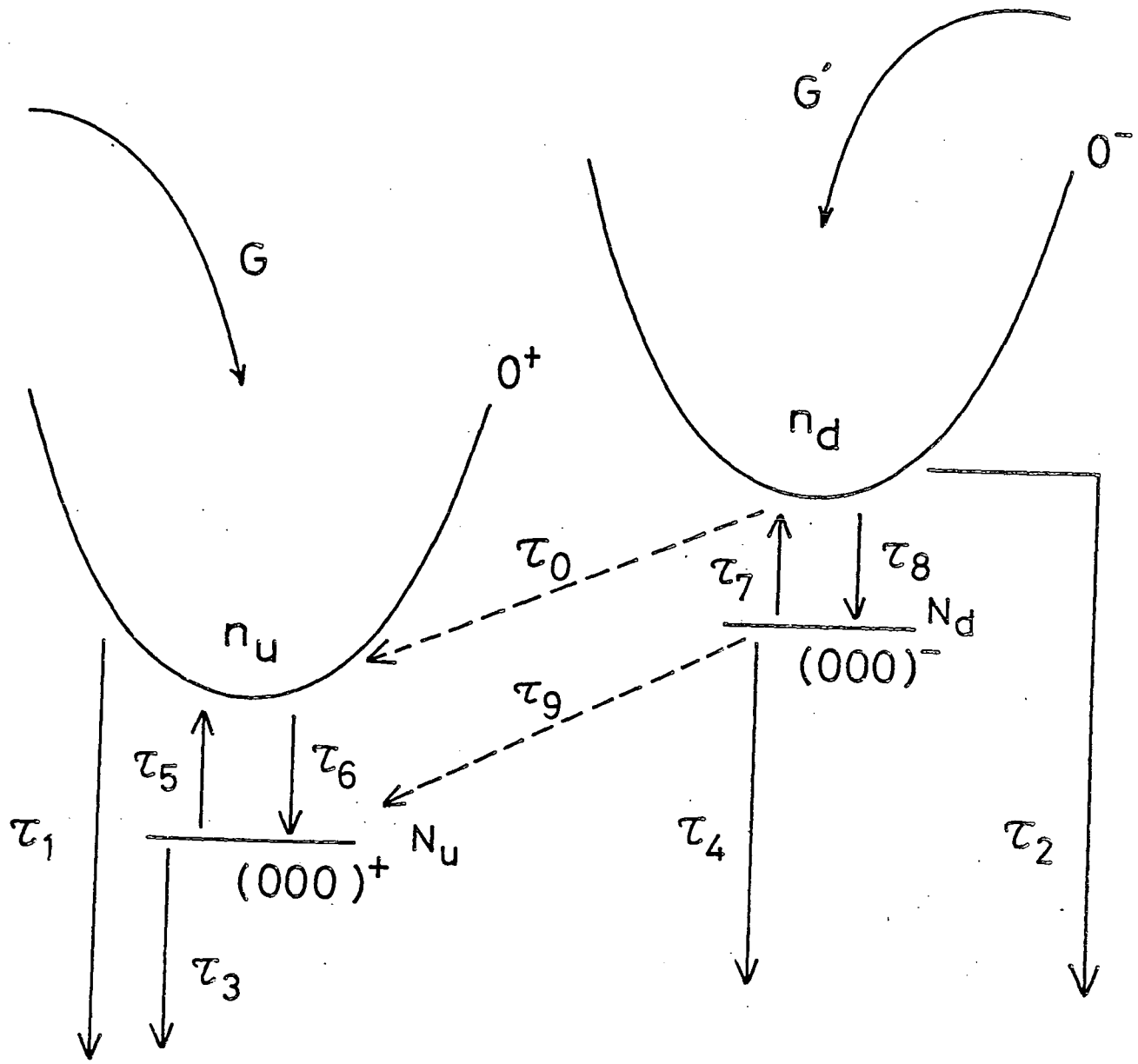
G'
O⁻
G
O⁺
n_d
τ_0
τ_7
τ_8
N_d
n_u
$(000)^-$
τ_9
τ_5
τ_6
τ_1
N_u
τ_4
τ_2
$(000)^+$
τ_3

Fig.26

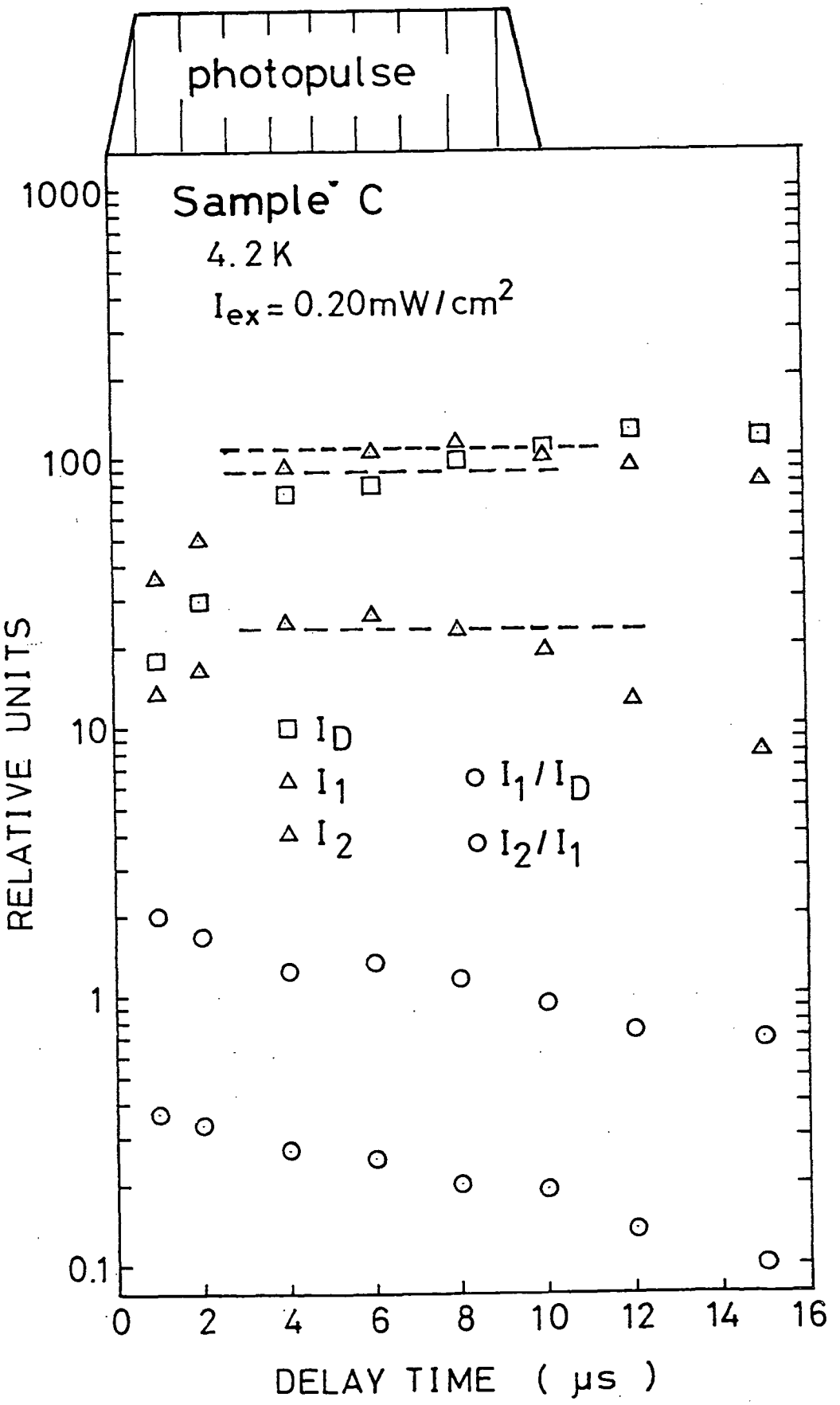
photopulse
Sample C
4.2 K
I_{ex} = 0.20mW/cm^2
1000
100
10
1
0.1
RELATIVE UNITS
I_D
I_1
I_2
I_1/I_D
I_2/I_1
0
2
4
6
8
10
12
14
16
DELAY TIME (μs)

Fig.27

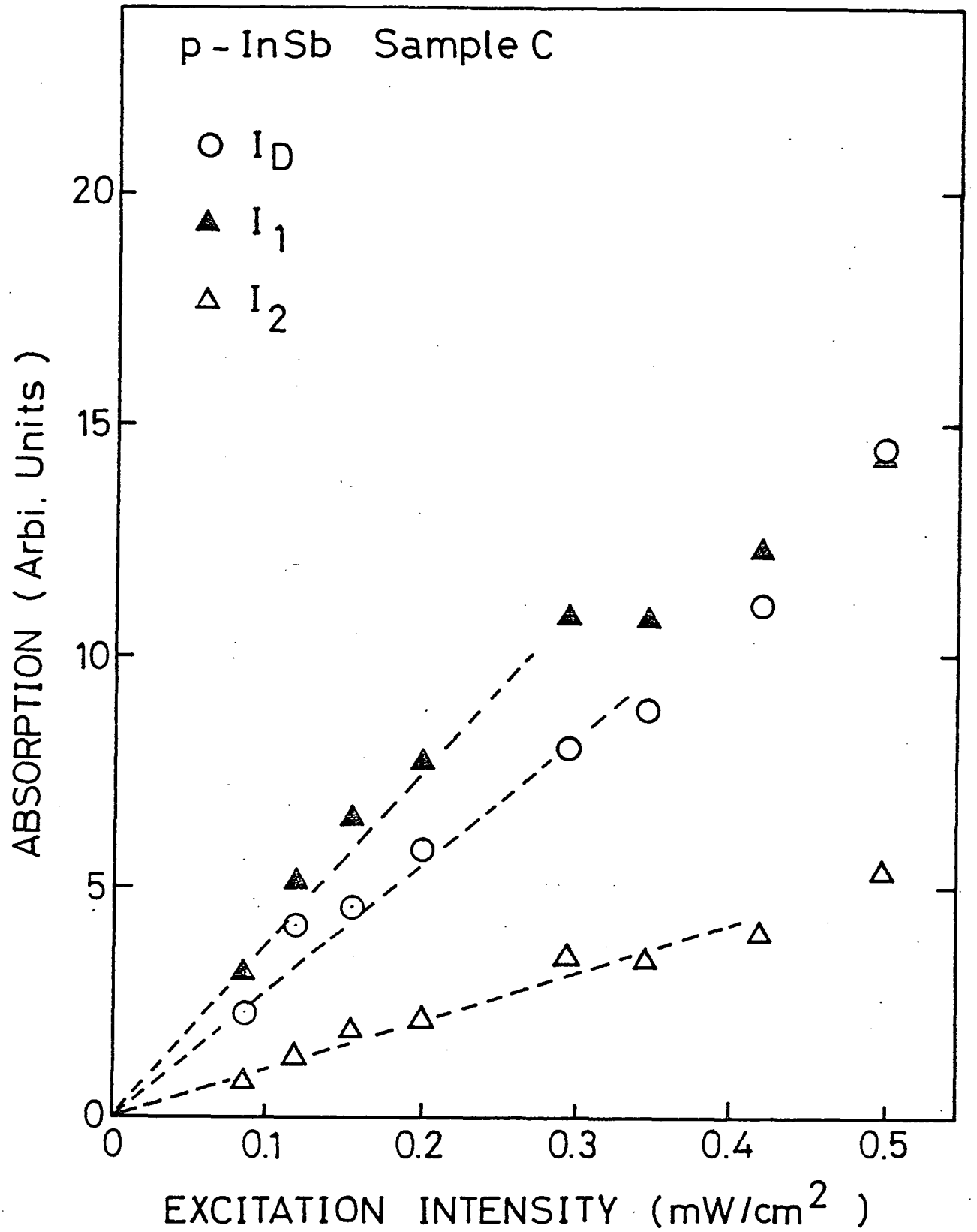
p - InSb Sample C
O I_D
▲ I_1
△ I_2
ABSORPTION (Arbi. Units)
0
5
10
15
20
0
0.1
0.2
0.3
0.4
0.5
EXCITATION INTENSITY (mW/cm^2)

Fig.28

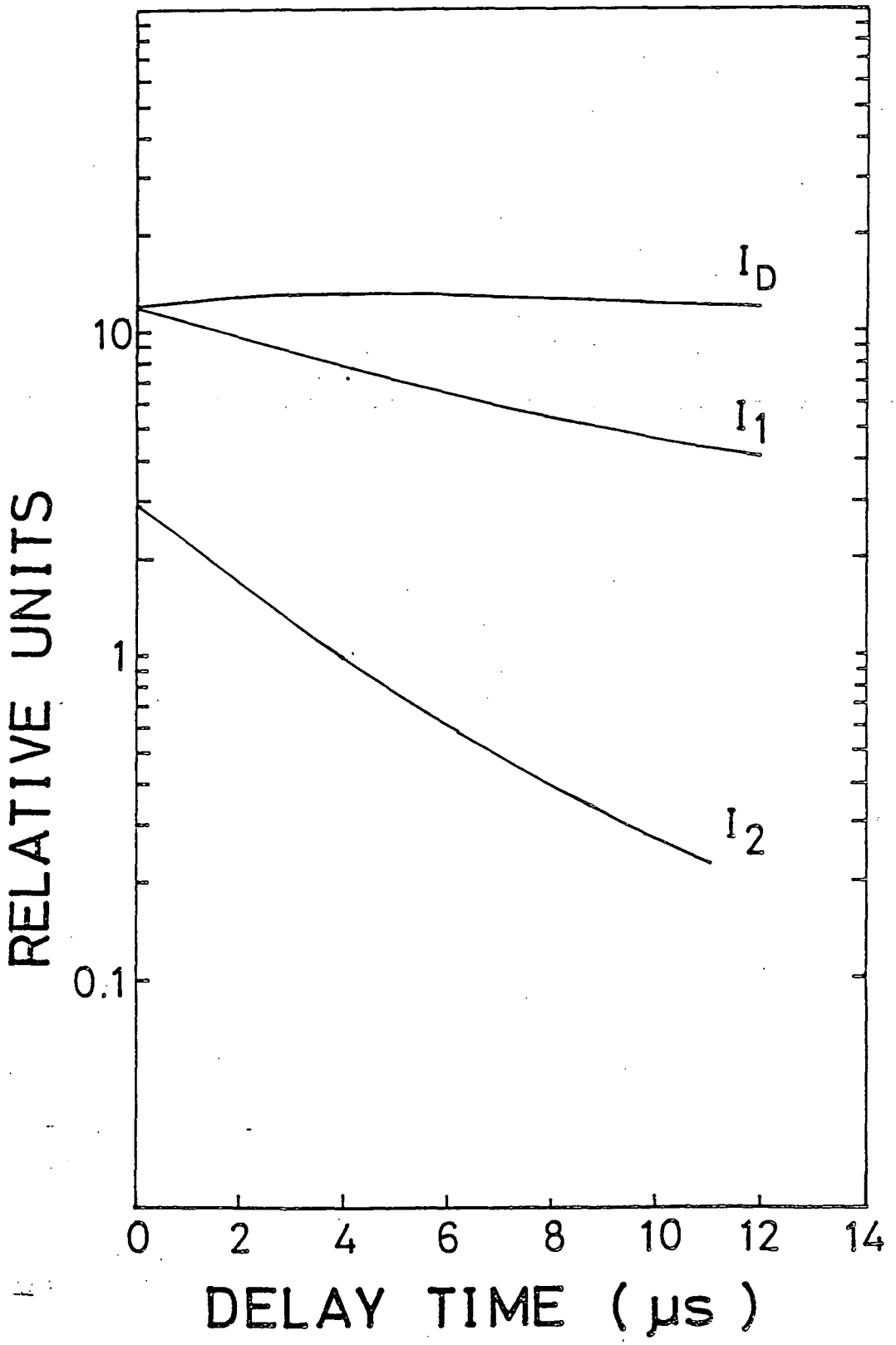

Fig.29

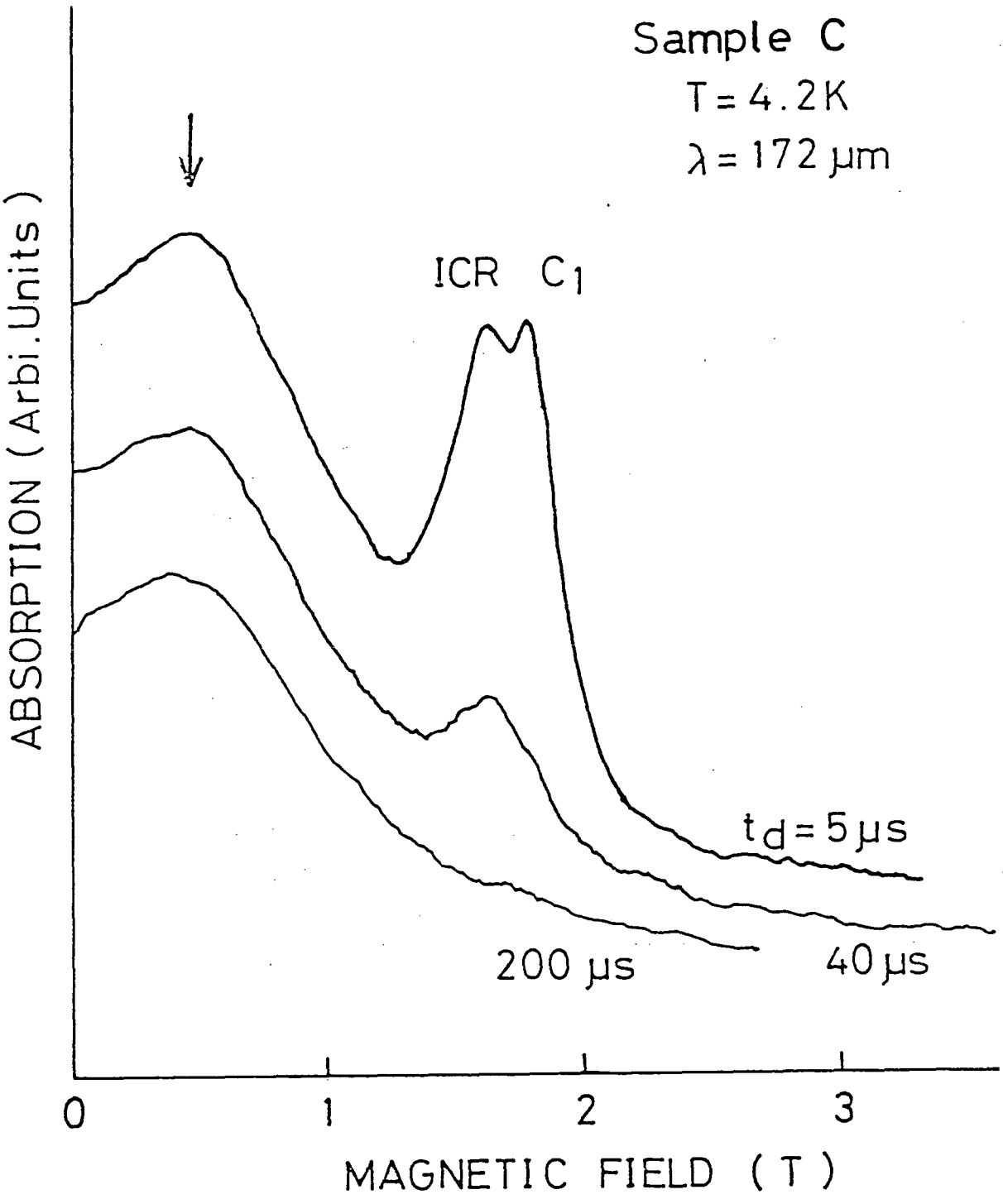
Sample C
T = 4.2K
λ = 172 μm
ICR C1
ABSORPTION (Arbi.Units)
td = 5 μs
200 μs
40 μs
0
1
2
3
MAGNETIC FIELD (T)

Fig.30

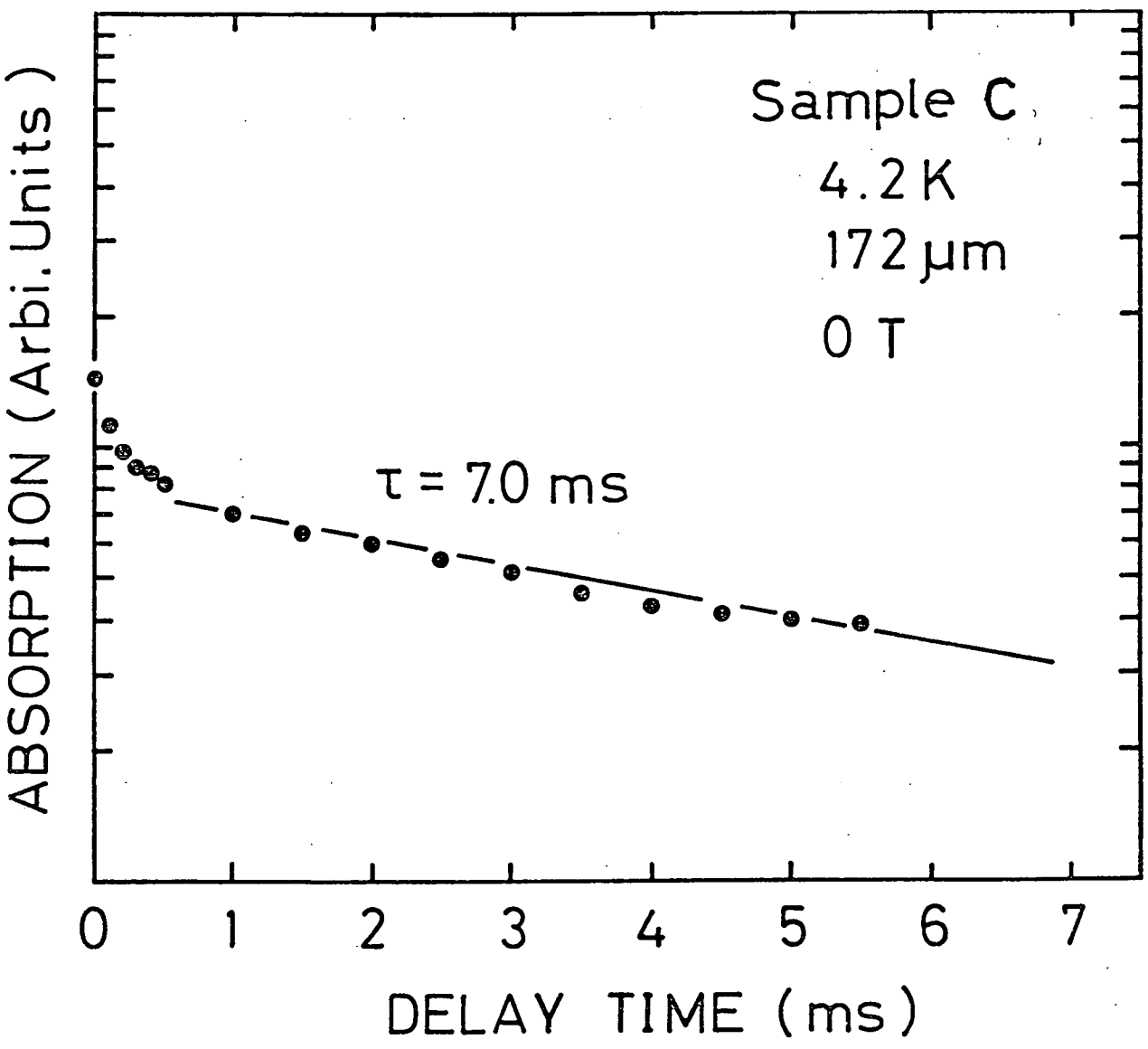
Sample C
4.2 K
172 μm
0 T
τ = 7.0 ms
ABSORPTION (Arbi. Units)
0
1
2
3
4
5
6
7
DELAY TIME (ms)

Fig.31

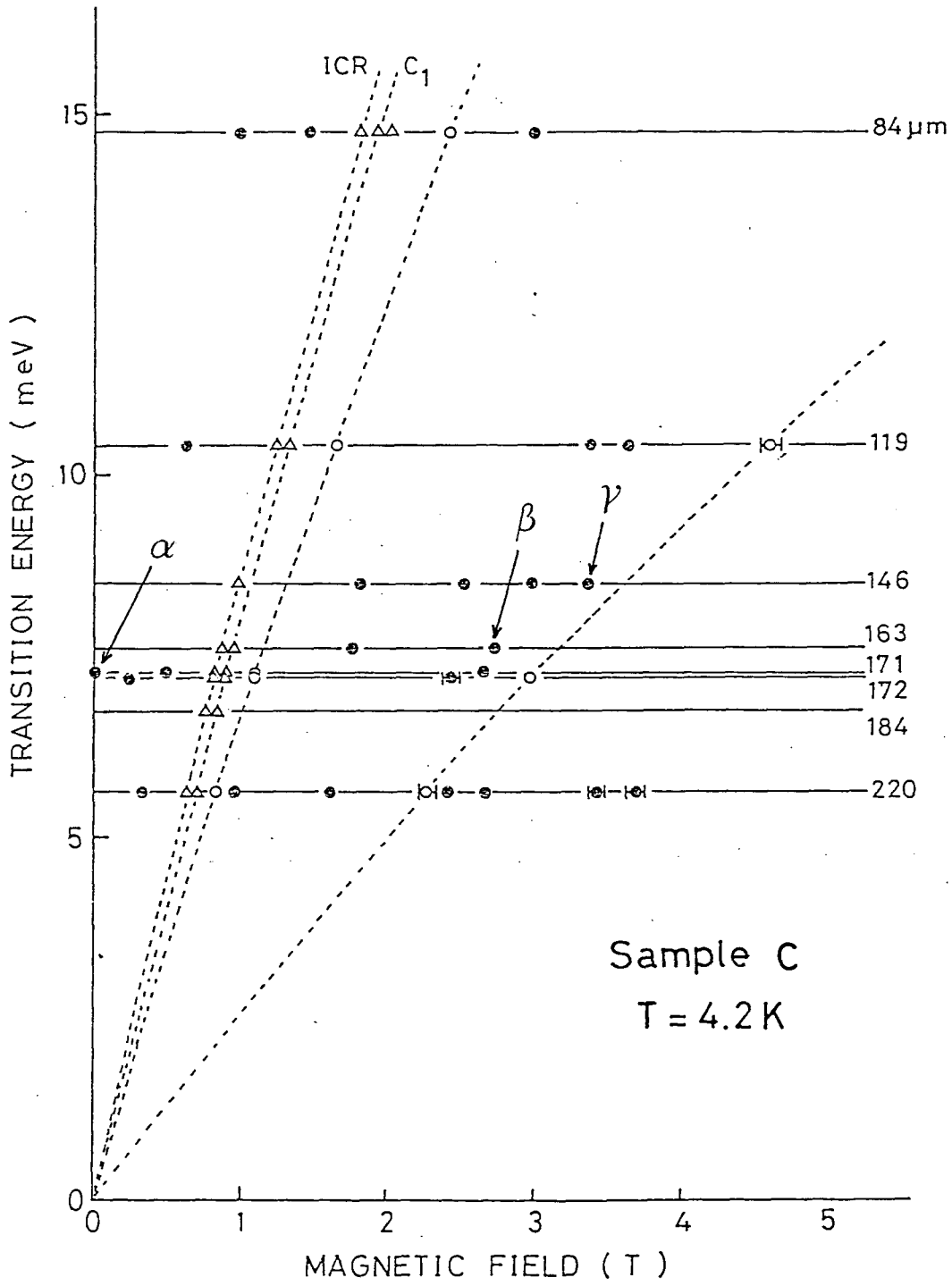
ICR
C_1
84 μm
119
146
163
171
172
184
220
α
β
γ
Sample C
T = 4.2 K
TRANSITION ENERGY (meV)
MAGNETIC FIELD (T)
0
5
10
15
0
1
2
3
4
5

Fig.32

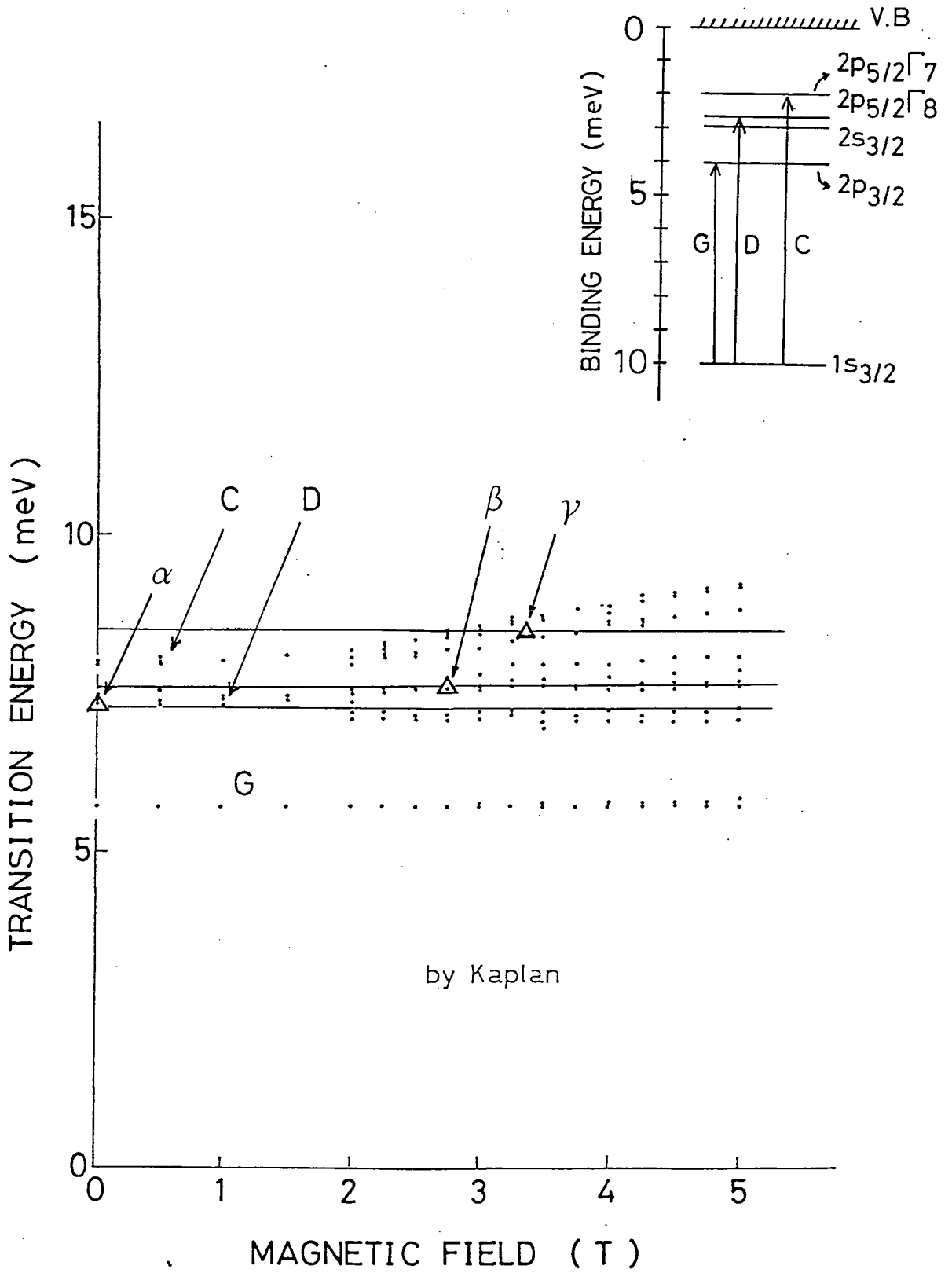
BINDING ENERGY (meV)
0
5
10
V.B
2p5/2Γ7
2p5/2Γ8
2s3/2
2p3/2
1s3/2
G
D
C
TRANSITION ENERGY (meV)
15
10
5
0
C
D
β
γ
α
G
by Kaplan
0
1
2
3
4
5
MAGNETIC FIELD (T)

Fig.33

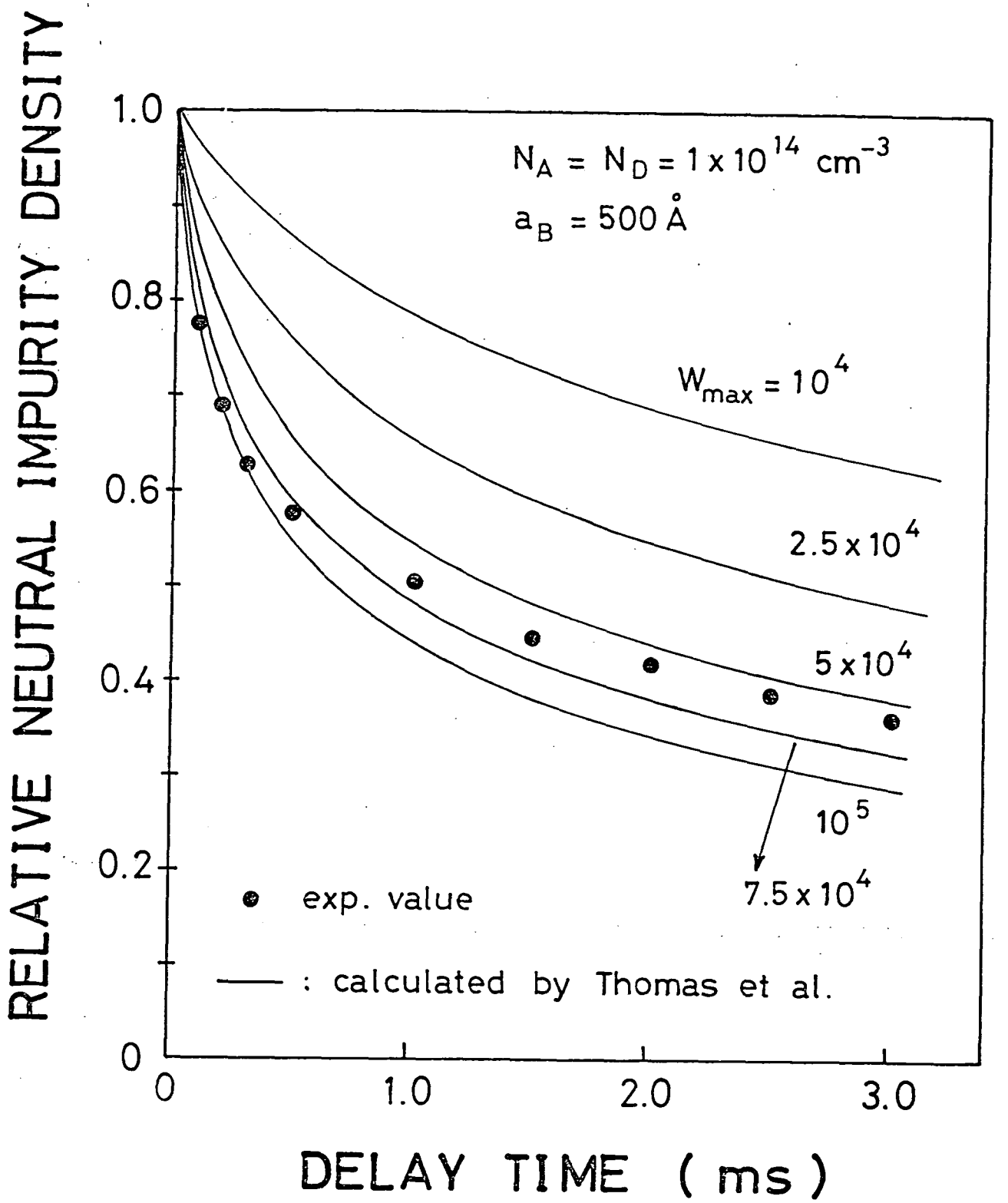
RELATIVE NEUTRAL IMPURITY DENSITY
1.0
0.8
0.6
0.4
0.2
0
0
1.0
2.0
3.0
DELAY TIME (ms)
$N_A = N_D = 1 \times 10^{14}$ cm^{-3}
$a_B = 500$ Å
$W_{max} = 10^4$
2.5×10^4
5×10^4
10^5
7.5×10^4
exp. value
: calculated by Thomas et al.

Fig.34

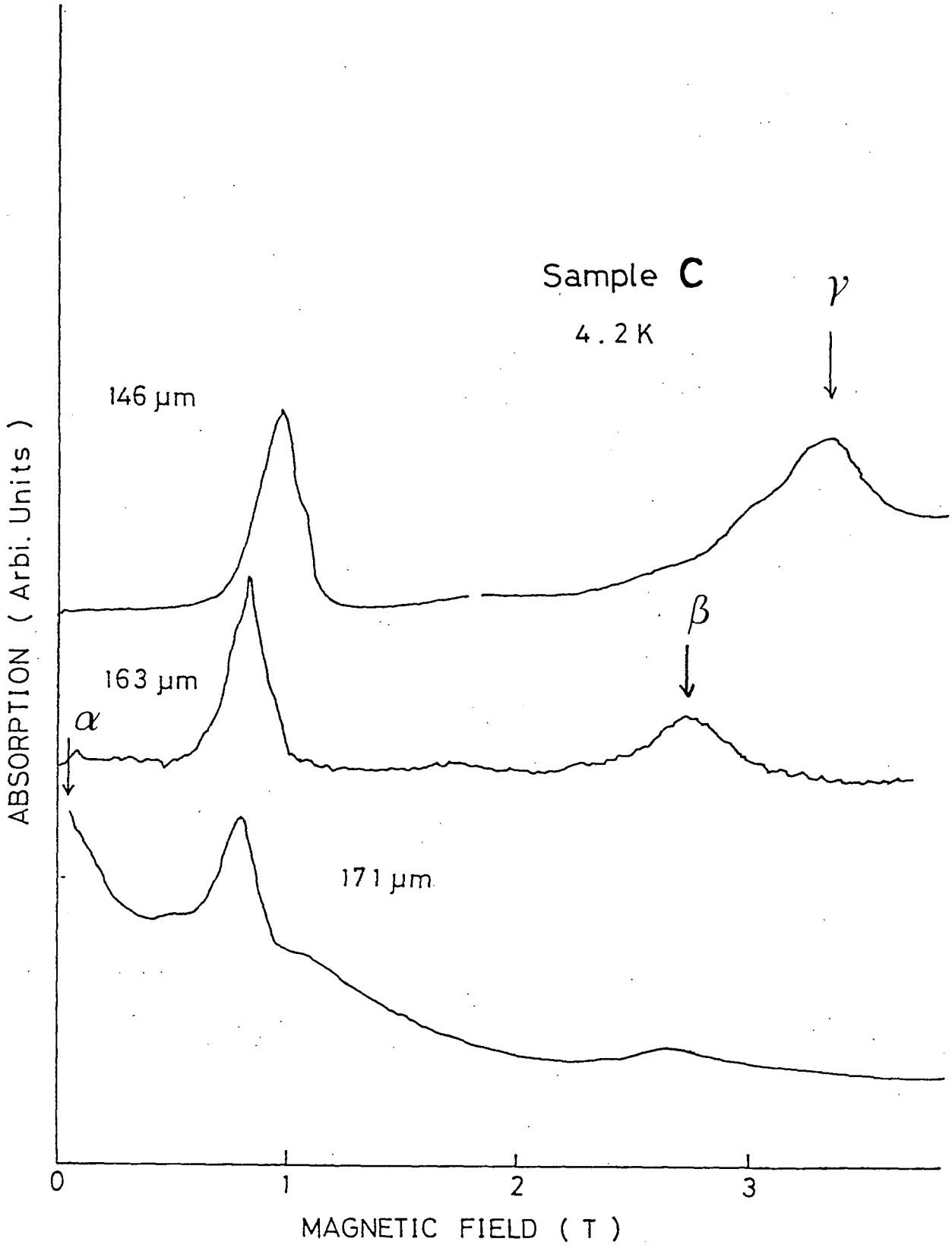
Sample C
4.2 K
γ
146 μm
β
163 μm
α
171 μm
ABSORPTION (Arbi. Units)
0
1
2
3
MAGNETIC FIELD (T)

Fig.35

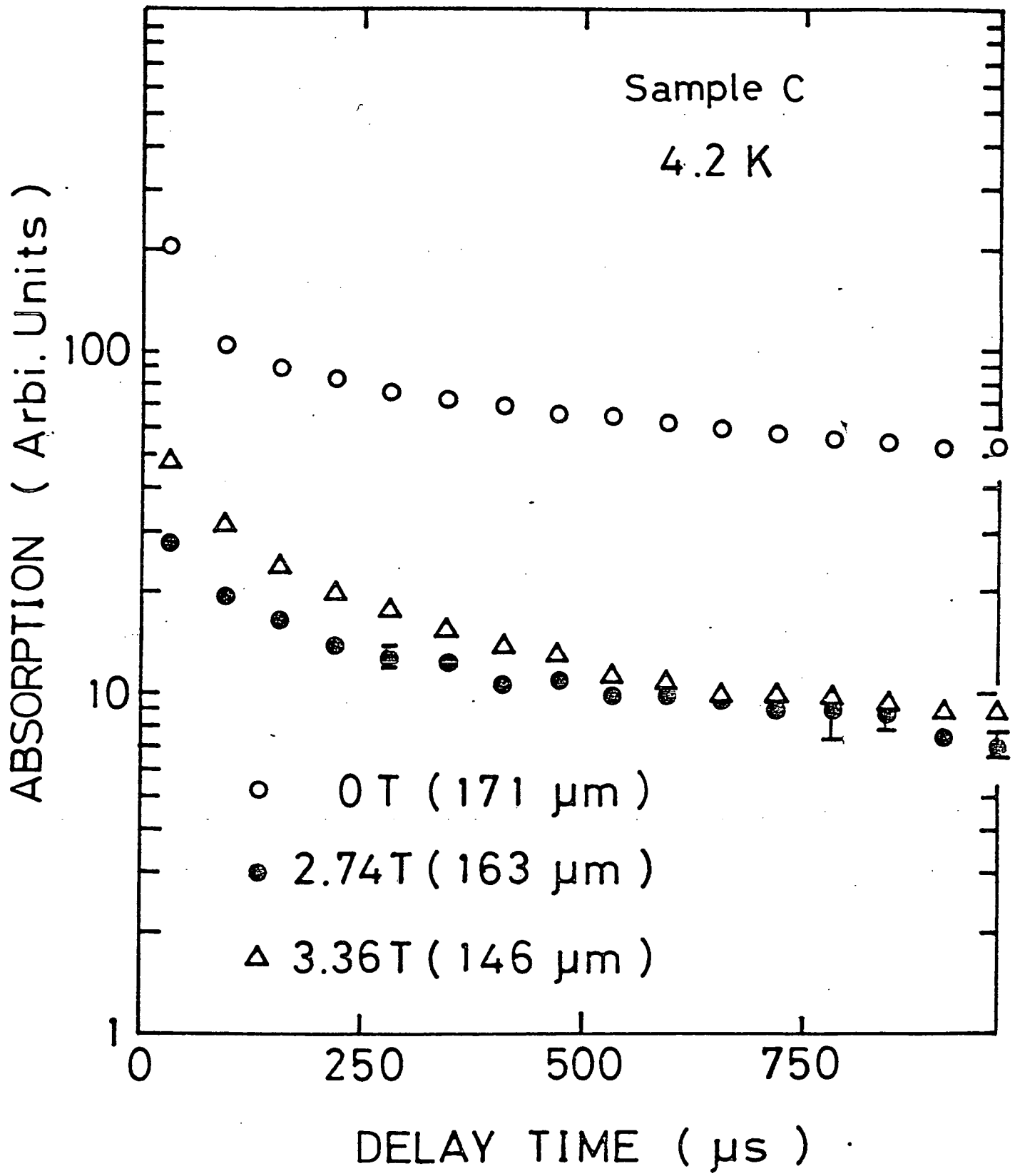
Sample C
4.2 K
ABSORPTION (Arbi. Units)
100
10
1
0
250
500
750
DELAY TIME (μs)
0 T (171 μm)
2.74T (163 μm)
3.36T (146 μm)

Fig. 36

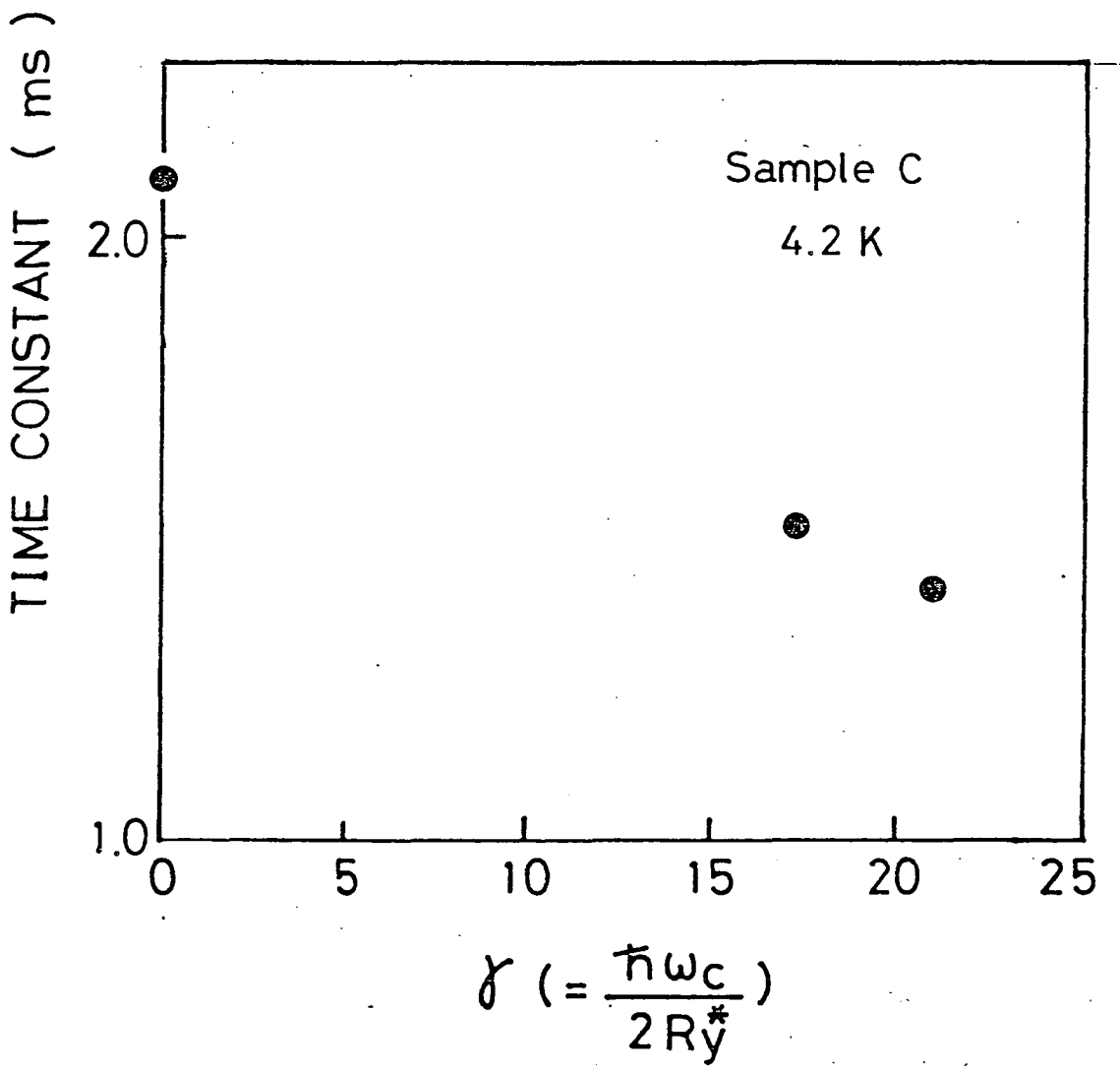

Fig. 37

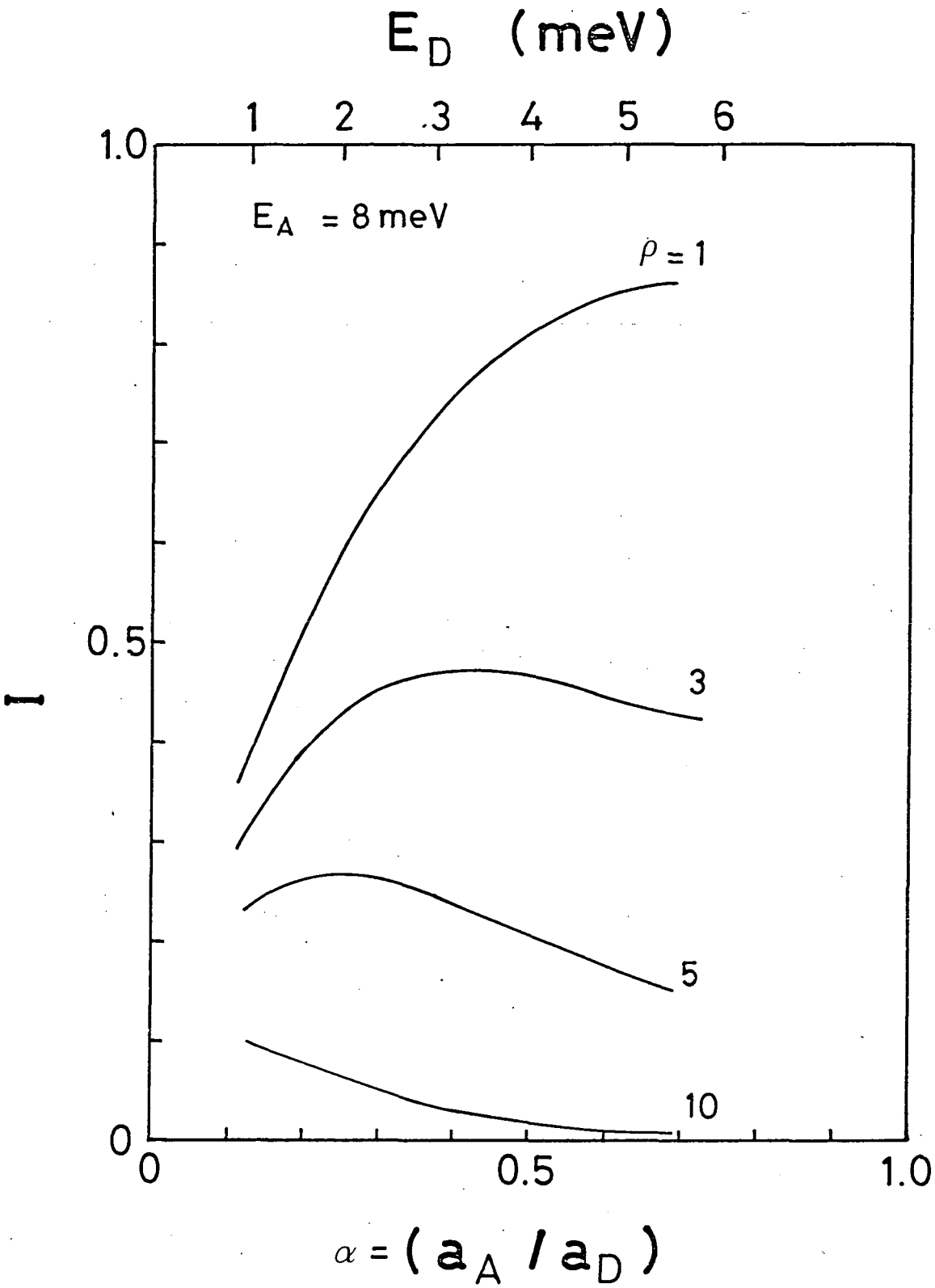

Fig.38

Table Captions

Table 1 Sample characteristics employed in the experiment. The donor concentrations were derived from the cyclotron absorption measurement.

Table 2 Wavefunction parameters of the free carrier Landau levels calculated by Pidgeon and Brown at B = 2 T.

Table 3 The same parameters as in Table 2 calculated by Lin-Chung and Henvis at B = 5 T.

Table 4 The values of $f_{sn}^{c*} f_{sN}^{lh}$ for the transition from conduction band to light hole like acceptor level. These values are regarded as measures of transition probability. The superscripts c and lh mean the conduction band and light hole band. The subscript s can be taken either a or b and that means the spin state of the conduction electron. The subscripts n and N indicate the Landau quantum number of the conduction electron and the quantum state of the light hole like acceptor hole, respectively.

Table 5 The fitting parameters of the coupled rate equations (4-41)-(4.44) to fit the experimental result of sample C under weak excitation at 4.2 K (Fig. 29).

Table 6 The time constants of the spin flip transition between 0^- and 0^+ Landau subbands in the conduction band. Comparison is made between previous experiments and ours.

Sample Characteristics

Sample Name	Type	$N_A (cm^{-3})$	$N_D (cm^{-3})$	$\lvert N_A - N_D \rvert (cm^{-3})$
A	n	1.8×10^{14}	1.9×10^{14}	1×10^{13}
B	n	1.7×10^{14}	3.8×10^{14}	2.1×10^{14}
C	p	1.1×10^{14}	1.0×10^{14}	5.8×10^{12}
D	p	2.6×10^{14}	1.3×10^{14}	1.3×10^{14}
E	p	3.4×10^{14}	2.6×10^{14}	8×10^{13}

Table 1

Parameters at 2 T by Pidgeon & Brown

Conduction band

N	A_1	A_3	A_5	A_7	A_2	A_6	A_4	A_8
0	0.992	0	-0.120	0.036	0.880	0	-0.200	0
1	0.968	-0.192	-0.155	0.049	0.959	-0.108	-0.262	0.034
2	0.949	-0.252	-0.177	0.058	0.942	-0.143	-0.300	0.047

Light hole band

N	A_1	A_3	A_5	A_7	A_2	A_6	A_4	A_8
-1	0	0	1.00	0	0	0	1	0
0	0.119	0	0.993	0.0058	0.200	0	0.980	0
1	0.246	0.719	0.650	0.016	0.282	0.334	0.899	0.013
2	0.307	0.762	0.569	0.025	0.331	0.380	0.863	0.0220

Table 2

Parameters at 5 T by Lin-Chung and Henvis

Conduction band

N	A_1	A_3	A_5	A_7	A_2	A_6	A_4	A_8
0	0.983	0	0.175	0.059	0.959	0	0.285	o
1	0.939	0.261	0.209	0.077	0.925	0.144	0.347	0.053
2	0.914	0.326	0.226	0.090	0.904	0.188	0.380	0.072

Light hole band

N	A_1	A_3	A_5	A_7	A_2	A_6	A_4	A_8
-1	0	0	1	0	0	0	1	0
0	-0.175	0	0.984	-0.013	-0.285	0	0.959	0
1	-0.331	0.679	0.655	-0.037	-0.374	0.328	0.867	-0.031
2	-0.392	0.719	0.571	-0.056	-0.418	0.373	0.826	-0.051

Table 3

$$f^{c*}_{sn} \cdot f^{lh}_{sN}$$

$s = a,b$

$n = 0$

$N = -1,0,1$

PB

Transition $n=0 \rightarrow N$	$s = a$ (up-spin)	$s = b$ (down-spin)
$0 \rightarrow -1$	-0.120	-0.200
$0 \rightarrow 0$	-9.03×10^{-4}	0
$0 \rightarrow 1$	0.167	0.0966

LH

Transition $n=0 \rightarrow N$	$s = a$ (up-spin)	$s = b$ (down-spin)
$0 \rightarrow -1$	0.175	0.285
$0 \rightarrow 0$	9.42×10^{-4}	0
$0 \rightarrow 1$	-0.213	-0.112

Table 4

The values of the time constants for sample C at 4.2 K

$\tau_0 = 3.5\ \mu s$

$\tau_1 = 6.5\ \mu s$

$\tau_5 = \tau_7 = 15\ \mu s$

$\tau_6 = \tau_8 = 20\ \mu s$

$\tau_9 = 10\ \mu s$

$\tau_2 = \tau_3 = \tau_4 = \infty$

Table 5

	T_1 (μs)	T(K)	B(T)	type	$\lvert N_D - N_A \rvert$ cm^{-3}
A	0.001	2	5	n	10^{15}
B	0.110 ± 0.020	1.8	1.0	n	1.35×10^{15}
B	0.100 ± 0.020	1.8	2.0	n	3.00×10^{15}
B	0.185 ± 0.020	1.8	1.3	n	3.00×10^{15}
C	0.250 ± 0.050	24.0	5.0	n	1.60×10^{16}
C	0.150	24.0	13.5	n	1.60×10^{16}
D	0.060 ± 0.020	20.0	6.0	n	1.20×10^{16}
E	3.5 ± 0.2	1.6 - 4.2	2.0	p	5.8×10^{12}

A) Nguyen et al.[72)]

B) Pascher et al.[73)]

C) Brueck and Mooradian[75)]

D) Grisar et al.[74)]

E) Ours

Table 6